ADAM MICKIEWICZ
UNIVERSITY
POZNAŃ

AMOTL2 role in pluripotency and human stem cell differentiation

Anna Paulina Jędrzejak

PhD thesis prepared under supervision
of dr hab. Małgorzata Borowiak, prof. AMU

Adam Mickiewicz University in Poznań, Poland
Faculty of Biology
Institute of Molecular Biology and Biotechnology
Department of Gene Expression
Stem Cell Laboratory

Poznań, 2024

ADAM MICKIEWICZ
UNIVERSITY
POZNAŃ

Rola genu AMOTL2 w pluripotencji i różnicowaniu ludzkich komórek macierzystych

Anna Paulina Jędrzejak

Rozprawa doktorska przygotowana pod opieką
dr hab. Małgorzaty Borowiak, prof. UAM

Uniwersytet im. Adama Mickiewicza w Poznaniu
Wydział Biologii
Instytut Biologii Molekularnej i Biotechnologii
Zakład Ekspresji Genów
Laboratorium Komórek Macierzystych

Poznań, 2024

With all my heart, I would like to thank:

Prof. Małgorzata Borowiak for an opportunity to learn multiple skills
and top-notch techniques, for sharing her knowledge and scientific advice.

The one and only ***AMOTL2 Dream Team***, aka ***Amotlówki***,
aka ***Dr. Marta Orlicka-Płocka*** and ***Dr. Małgorzata Grabowska***,
with whom I worked on the AMOTL2 project, for constant reassurance, patience,
encouragement, support and crazy ideas. I'm grateful I had a chance to work with you.

Dr. Wojciech Szlachcic for guidance, emotional and scientific support,
book recommendations, and always providing me with COFFEE.

MSc Ekaterina Shcheglova for being able to eat a whole bag of pistachio
at once with me and recommending the best pistachio source, sharing chocolate,
wicked sense of humor, and company at the dancing course.

The entire team of Stem Cell Laboratory, ***Dr. hab. Maciej Łałowski***, ***Dr. Katarzyna Błaszczyk***,
Dr. Artur Jankowski, ***Dr. Natalia Ziojła***, ***Dr. Joanna Szpotkowska***, ***Dr. Magdalena Socha***,
MSc Sara Henry, ***MSc Edyta Urbaniak***, ***MSc Dorota Kiżewska, MSc. Maroua Rami,***
and MSc. Jadwiga Waśko, for all the lunches, coffee breaks, long conversations and company
during weekends in the lab. For your genuine care, sense of humor, and being
the best team I could hope for.

My Mom, for everlasting and unconditional love and support, being my safest person
in the world, and valuing my wellbeing more than my carrier.
Also, for translating all the paperwork from black magic into polish language.

Sara Pieczyńska and ***Ewa Michalak***, for being amazing friends, supporting me
through good and bad times and always believing in me, even when I didn't.

All my friends and kindred spirits who cheered for me, believed in me,
and were there to be happy with me when I laughed and to support me when I cried.

ACADEMIC ACHIEVEMENTS

During the PhD programme I was a co-author of the following publications and conference reports:

Articles:

- **Anna P. Jędrzejak**, Edyta Urbaniak, Jadwiga Waśko, Natalia Ziojła, Małgorzata Borowiak; *Diabetes and SARS-CoV-2 – is there a mutual connection?;* Frontiers in Cell and Developmental Biology, 06.2022, DOI: 10.3389/fcell.2022.913305 impact factor: 5.5

- IN REVISION in Experimental & Molecular Medicine: Katarzyna Blaszczyk*, **Anna P. Jedrzejak***, Natalia Ziojla, Ekaterina Shcheglova, Karolina Szarafin, Artur Jankowski, Christine A. Beamish, Jolanta Chmielowiec, Omaima M. Sabek, Ashok Balasubramanyam, Sanjeet Patel, Malgorzata Borowiak, *SPOCK2 controls the proliferation and function of immature pancreatic β-cells through MMP2;* * co-first authors impact factor: 12.8

Conference reports:

- **Anna Jędrzejak**, Małgorzata Borowiak, poster: *AMOTL2 regulates nucleus size in human pluripotent stem cells*, conference BioLOGIES: Bioinspiration, Inventions and Breakthrough technologies, 22– 24 September 2020, Poznań, Poland

- **Anna Jędrzejak**, oral presentation: Shape-shifters: *How AMOTL2 influences cell and colony morphology in human pluripotent stem cells and early pancreatic differentiation*; conference COMPASS: the future of interdisciplinary science, 22–24 September 2021, Poznań, Poland

- **Anna Jędrzejak**, Sara Henry, Małgorzata Borowiak; poster*: Shaping the future: AMOTL2 in delamination and cell fate determination of pancreatic endocrine progenitors*; 8th Central European Congress of Life Sciences EUROBIOTECH, 20-22 June 2022, Kraków, Poland

- Marta Orlicka-Płocka, Małgorzata Grabowska, **Anna Jędrzejak**, Małgorzata Borowiak; poster: *The role of angiomotin-like 2 (AMOTL2) in human pluripotent stem cells and its effects on the Hippo signaling pathway*; 5th BIO Congress, 13-16 September 2023, Szczecin, Poland

- Małgorzata Grabowska, Marta Orlicka-Płocka, **Anna Jędrzejak**, Małgorzata Borowiak; oral presentation: *AMOTL2 protein as an example of the cell fate determinant*; 9th Central European Congress of Life Sciences EUROBIOTECH, 27-28 June 2024, Kraków, Poland

FUNDING

The research work included in the dissertation was supported by the following funding:

- Faculty of Biology Dean's Grant (GDWB-03/2020) to **Anna Jędrzejak**
- MINIGRANT MG/POWER17/2021/12 to **Anna Jędrzejak**, within the project Passport to the future - Interdisciplinary doctoral studies at the Faculty of Biology AMU, POWR.03.02.00-00-I006/17
- National Science Centre (NCN) Preludium grant 2021/41/NZ4/02626 to **Anna Jędrzejak**

- Foundation for Polish Science (FNP) grant POIR.04.04.00-00-20C5/16-00 (TEAM.2016-2/10) to **Małgorzata Borowiak**
- Polish National Science Centre (NCN) grant 2019/33/B/NZ3/01226 to **Małgorzata Borowiak**

Due to major health issues, I was on sick leave from July to December 2022. During this time Dr. Marta Orlicka-Płocka and Dr. Małgorzata Grabowska started working on the AMOTL2 project. Since January 2023 we have all been working together on the project.

In consequence, some of the experiments here were performed by Dr. Marta Orlicka-Płocka and Dr. Małgorzata Grabowska. This includes:

- Fig. 27D-F – N=1 performed by Dr. Marta Orlicka-Płocka
- Fig. 35A, B – staining repeated after Dr. Marta Orlicka-Płocka
- RNA isolation and RT-qPCRs – Dr. Małgorzata Grabowska
- F-actin fiber organization (chapter 3.8, data not shown) – Dr. Marta Orlicka-Płocka & MSc Wojciech Kwiatkowski
- Adhesion protein staining (data not shown; mentioned in discussion as summarizing cartoon, Fig. 36) – Dr. Marta Orlicka-Płocka

Whenever important for the logical reasoning, I will mention those experiments in the results section. Some will be mentioned in the discussion, as an additional background. All the experiments were included with the permission of Dr. Małgorzata Grabowska and Dr. Marta Orlicka-Płocka.

Contents

Abbreviations

2D	two-dimensional
3D	3-dimensional
aa	amino acid
ALL	allele
ATAC	assay for transposase-accessible chromatin
AU	arbitrary unit
BPs	bipotent progenitors
BSA	bovine serum albumin
CHIR	CHIR99021
C-PEP	c-peptide
CPM	count per million mapped reads
CRISPR	clustered regularly interspaced short palindromic repeats
ctrl	control
d	day
DE	definitive endoderm
DEGs	differentially expressed genes
DMSO	dimethyl sulfoxide
DNA	deoxyribonucleic acid
dpc	day post conception
e	embryonic day
EBs	embryoid bodies
ECM	extracellular matrix
EDTA	ethylenediaminetetraacetic acid
EMT	epithelial-mesenchymal transition
EP1 (2, 3, 4)	endocrine progenitor subtype 1 (2, 3, 4)
EPs	endocrine progenitors
ESCs	embryonic stem cells
F-ACT	F-actin
FBS	fetal bovine serum
FBS	fetal bovine serum
FC	flow cytometry
FDR	false discovery rate
FG	foregut
FPKM	fragments per kilobase million
GO	gene ontology
GPRC	G-protein-coupled receptor
hESCs	human embryonic stem cells
hPSCs	human pluripotent stem cells

Hu	human
ICE	interference of CRISPR edits
ICM	inner cell mass
IF	immunofluorescence
incl.	including
indel	insertion-deletion
iPSCs	induced pluripotent stem cells
KD	knockdown
KO	knockout
KOSR	knockout serum replacement
LDN	LDN193189
ME	mesendoderm
MES	mesenchyme
MITO	mitochondrial
Mk	monkey
MPPs	multipotent pancreatic progenitors
mRNA	messenger ribonucleic acid
Mus	mouse
NDS	normal donkey serum
NEAA	non-essential amino acids
nt	nucleotide
PBS	phosphate buffered saline
PC	principal component
PCA	principal component analysis
PCR	polymerase chain reaction
pen/strep	penicillin/streptomycin
PFA	paraformaldehyde
PGT	primitive gut tube
pHH3	phosphorylated histone H3
PP-cells	pancreatic polypeptide cells
PPs	pancreatic progenitors
PSCs	pluripotent stem cells
p-val	p-value
p-val adj	p-value adjusted
RNA	ribonucleic acid
RNA-seq	RNA-sequencing (ribonucleic acid-sequencing)
ROCKi	ROCK inhibitor
RT	room temperature
RT-qPCR	real time quantitative polymerase chain reaction
SB	SB431542
SBP	saponin-BSA-PBS solution

scRNA-seq	single cell RNA-sequencing
sgRNAs	single guide RNAs (single guide ribonucleic acids)
TALEN	transcription activator-like effector nucleases
TE	trophectoderm
tSNE	t-distributed stochastic neighbor embedding
UMAP	uniform manifold approximation and projection
VEGF	vascular endothelial growth factor
wpc	week post conception
WT	wild type
α-cells	alpha-cells
β-cells	beta-cells
γ-cells	epsilon-cells
δ-cells	delta-cells

Abbreviations – gene names

ACTA1	Actin Alpha 1
ACTB	Actin Beta
ADORA1	Adenosine A1 Receptor
AKNA	AT-Hook Transcription Factor
AKT	AKT Serine/Threonine Kinase
AMOT	Angiomotin
AMOTL1	Angiomotin Like 1
AMOTL2	Angiomotin Like 2
ANXA1	Annexin A1
APC	APC Regulator Of WNT Signaling Pathway
AXIN1	Axin 1
BHLHE40	Basic Helix-Loop-Helix Family Member E40
BIN1	Bridging Integrator 1
BMP	Bone Morphogenetic Protein
BMP4	Bone Morphogenetic Protein 4
BOK	BCL2 Family Apoptosis Regulator BOK
BST2	Bone Marrow Stromal Cell Antigen 2
BTBD3	BTB Domain Containing 3
CACNA1A	Calcium Voltage-Gated Channel Subunit Alpha1 A
CASP3	Caspase 3
CASP8	Caspase 8
CAV1	Caveolin1
CBFA2T2	CBFA2/RUNX1 Partner Transcriptional Co-Repressor 2
CBR3	Carbonyl Reductase 3
CDH1	Cadherin 1 (E-cadherin)
CDH2	Cadherin 2 (N-cadherin)
CDH7	Cadherin 7
CDX2	Caudal Type Homeobox 2
CENPF	Centromere Protein F
CHGA	Chromogranin A
CK1 (CSNK1A1)	Casein Kinase 1 Alpha 1
c-MYC	MYC Proto-Oncogene, BHLH Transcription Factor
CNTN1	Contactin 1
COL1A1	Collagen Type I Alpha 1 Chain
COL1A2	Collagen Type I Alpha 2 Chain
COL6A1	Collagen Type VI Alpha 1 Chain
COL7A1	Collagen Type VII Alpha 1 Chain
COTL1	Coactosin Like F-Actin Binding Protein 1

c-SRC	SRC Proto-Oncogene, Non-Receptor Tyrosine Kinase
CXCR4	C-X-C Motif Chemokine Receptor 4
CYP1B1	Cytochrome P450 Family 1 Subfamily B Member 1
DDC	Dopa Decarboxylase
DGKB	Diacylglycerol Kinase Beta
DMTN	Dematin Actin Binding Protein
DPYSL4	Dihydropyrimidinase Like 4
DPYSL5	Dihydropyrimidinase Like 5
DVL	Dishevelled Segment Polarity Protein
EFB41L3	Erythrocyte Membrane Protein Band 4.1 Like 3
EPHA7	EPH Receptor A7
ERBB4	Erb-B2 Receptor Tyrosine Kinase 4
ERK1/2 (MAPK3)	Extracellular Signal-Regulated Kinase 1/2 (Mitogen-Activated Protein Kinase 3/1)
ETS1	ETS Proto-Oncogene 1, Transcription Factor
FEV	FEV Transcription Factor, ETS Family Member
FEZ1	Fasciculation And Elongation Protein Zeta 1
FEZF1	FEZ Family Zinc Finger 1
FGF	Fibroblast Growth Factor
FGF8	Fibroblast Growth Factor 8
FN1	Fibronectin 1
FOXA2	Forkhead Box A2
FOXC1	Forkhead Box C1
FRAS1	Fraser Extracellular Matrix Complex Subunit 1
FZD1	Frizzled Class Receptor 1
FZD10	Frizzled Class Receptor 10
FZD5	Frizzled Class Receptor 5
GAP43	Growth Associated Protein 43
GAPDH	Glyceraldehyde-3-Phosphate Dehydrogenase
GAS2L1	Growth Arrest Specific 2 Like 1
GAS7	Growth Arrest Specific 7
GATA3	GATA Binding Protein 3
GATA4	GATA Binding Protein 4
GCG	Glucagon
GDF3	Growth Differentiation Factor 3
GLIS3	GLIS Family Zinc Finger 3
GPC3	Glypican 3
GRHL3	Grainyhead Like Transcription Factor 3
GSK3	Glycogen Synthase Kinase 3
HNF1B	HNF1 Homeobox B
IGF	Insulin Like Growth Factor

IGF2BP3	Insulin Like Growth Factor 2 MRNA Binding Protein 3
INS	Insulin
INSM1	INSM Transcriptional Repressor 1
ITGA5	Integrin Subunit Alpha 5
ITGB5	Integrin Subunit Beta 5
KCNIP4	Potassium Voltage-Gated Channel Interacting Protein 4
KCTD12	Potassium Channel Tetramerization Domain Containing 12
KLF4	Kruppel-Like Factor 4
KLF5	Kruppel-Like Factor 5
LAPTM4B	Lysosomal Protein Transmembrane 4 Beta
LATS1/2	Large Tumor Suppressor Kinase 1/2
LCP1	Lymphocyte Cytosolic Protein 1
LEFTY1	Left-Right Determination Factor 1
LEFTY2	Left-Right Determination Factor 2
LIN28	Lin-28 Homolog A
LINC00907	Long Intergenic Non-Protein Coding RNA 907
LRP	LDL Receptor Related Protein
LRP2	LDL Receptor Related Protein 2
MAGI1	Membrane Associated Guanylate Kinase, WW And PDZ Domain Containing 1
MAGI2	Membrane Associated Guanylate Kinase, WW And PDZ Domain Containing 2
MAML2	Mastermind Like Transcriptional Coactivator 2
MAPK	Mitogen-Activated Protein Kinase
MCC	MCC Regulator Of WNT Signaling Pathway
MEIS2	Meis Homeobox 2
MEK1/2 (MAPK2K1/2)	Mitogen-Activated Protein Kinase Kinase 1/2
MIR7-3HG	MIR7-3 Host Gene
MIXL1	Mix Paired-Like Homeobox
MMP2	Matrix Metallopeptidase 2
MMP9	Matrix Metallopeptidase 9
MST1/2	Macrophage Stimulating 1/2
mTORC2	Mechanistic Target Of Rapamycin Kinase Complex2
MYLIP	Myosin Regulatory Light Chain Interacting Protein
NANOG	Nanog Homeobox
NEDD4	NEDD4 E3 Ubiquitin Protein Ligase
NEURL1	Neuralized E3 Ubiquitin Protein Ligase 1
NEUROD1	Neuronal Differentiation 1
NGN3 (NEUROG3)	Neurogenin 3
NKX6.1	NK6 Homeobox 1
NMI	N-Myc And STAT Interactor

NODAL	Nodal Growth Differentiation Factor
NOVA2	NOVA Alternative Splicing Regulator 2
NRG3	Neuregulin 3
NRP2	Neuropilin 2
OCT3/4	Octamer-Binding Transcription Factor 3/4;
OTX2	Orthodenticle Homeobox 2
PAR3	Par-3 Family Cell Polarity Regulator
PAX6	Paired Box 6
PCDHB5	Protocadherin Beta 5
PDGFRA	Platelet Derived Growth Factor Receptor Alpha
PDK1	Pyruvate Dehydrogenase Kinase 1
PDX1	Pancreatic And Duodenal Homeobox 1
PI3K	Phosphatidylinositol 3-Kinase
PIP2	Phosphatidylinositol 4,5-Bisphosphate
PITX2	Paired Like Homeodomain 2
PPP2R2A	Protein Phosphatase 2 Regulatory Subunit Balpha
PRKD1	Protein Kinase D1
PTN	Pleiotrophin
PXN	Paxillin
RAF	RAF proto-oncogene serine/threonine-protein kinase
RAP1	RAP1 GTPase Activating Protein
RAPGEFL1	Rap Guanine Nucleotide Exchange Factor Like 1
RAS	Rat Sarcoma Virus, GTPase
RGS2	Regulator Of G Protein Signaling 2
RHOB	Ras Homolog Family Member B
RHOBTB1	Rho Related BTB Domain Containing 1
RHOBTB3	Rho Related BTB Domain Containing 3
RICTOR	RPTOR Independent Companion Of MTOR Complex 2
RIPPLY3	Ripply Transcriptional Repressor 3
RNF146	Ring Finger Protein 146
S100A11	S100 Calcium Binding Protein A11
SCN8A	Sodium Voltage-Gated Channel Alpha Subunit 8
SEMA3C	Semaphorin 3C
SEMA3D	Semaphorin 3D
SEMA5B	Semaphorin 5B
SEMA6C	Semaphorin 6C
SERPINE2	Serpin Family E Member 2
SLC4A4	Solute Carrier Family 4 Member 4
SLIT3	Slit Guidance Ligand 3
SMAD1/5/8	Mothers Against Decapentaplegic Homolog 1/5/8
SMAD2/3	Mothers Against Decapentaplegic Homolog 2/3

SMAD4	Mothers Against Decapentaplegic Homolog 4
SOX1	SRY-Box Transcription Factor 1
SOX17	SRY-Box Transcription Factor 17
SOX2	SRY-Box Transcription Factor 2
SOX7	SRY-Box Transcription Factor 7
SOX9	SRY-Box Transcription Factor 9
SPRY2	Sprouty RTK Signaling Antagonist 2
SST	Somatostatin
TAZ (WWTR1)	WW Domain Containing Transcription Regulator 1
TCF	T-Cell Factor
TEAD	TEA Domain Transcription Factor 1
TGFβ	Transforming Growth Factor β
TNKS1	Tankyrase 1
TNKS2	Tankyrase 2
TNNT2	Troponin T2, Cardiac Type
TOP2A	DNA Topoisomerase II Alpha
TRAPPC9	Trafficking Protein Particle Complex Subunit 9
TXNIP	Thioredoxin Interacting Protein
UTRN	Utrophin
VCL	Vinculin
VIM	Vimentin
WNT	Wingless-Type MMTV Integration Site
WNT3	Wingless-Type MMTV Integration Site 3
WNT9A	Wingless-Type MMTV Integration Site 9A
WWC2	WW And C2 Domain Containing 2
WWP1	WW Domain Containing E3 Ubiquitin Protein Ligase 1
YAP	Yes Associated Transcriptional Regulator
ZFP36L1	ZFP36 Ring Finger Protein Like 1
ZIC1	Zic Family Member 1
β-CAT (CTNNB1)	Catenin Beta 1
δ-CAT (CTNND1)	Catenin Delta 1

Marker table

GENE	MARKER OF
CHGA	endocrine cells
COL1A1	mesenchyme
C-PEP	β-cells
FOXA2	definitive endoderm
GCG	α-cells
INS	β-cells
NANOG	pluripotency
NEUROD1	endocrine progenitors/late endocrine progenitors (downstream of NGN3)
NGN3 (NEUROG3)	endocrine progenitors
NKX6.1	pancreatic progenitors; β-cells
OCT3/4	pluripotency
OTX2	ectoderm
PDX1	pancreatic progenitors; β-cells
SOX1	ectoderm
SOX17	definitive endoderm
SOX2	pluripotency; ectoderm
SST	δ-cells
VIM	mesenchyme

Abstract

The transcriptional regulation of developmental processes was extensively studied over the last years, yet there is still a considerable gap of knowledge concerning the mechanistic and metabolic cues, and underlying morphological events that accompany human pluripotent stem cell (hPSC) differentiation. In search of such signals, I first identified the *Amotl2* gene in the single-cell RNA-sequencing (scRNA-seq) data of the developing murine pancreata from embryonic days 14.5 (e14.5) and 16.5 (e16.5). Interestingly, despite conserved canonical markers, the endocrine progenitor (EP) populations from these timepoints differed significantly in their transcriptomes, with e16.5 EPs being more prone to form pancreatic β-cells, and e14.5 EPs preferentially forming α-cells. *Amotl2* was specifically expressed in the subtype of e16.5 EPs, which reflected EPs delamination from epithelial cords, a poorly understood event that might influence endocrine cell fate.

AMOTL2 is a member of the angiomotin family. It is a cytoplasmic protein that resides either in cytosol or at the cellular junctions, facilitating signal transduction, cytoskeleton organization, and modulation of signaling pathways. AMOTL2 in a known regulator of Hippo pathway and its downstream effector YAP. One of the aims of this thesis was identification of *AMOTL2* expression patterns in developing human pancreas *in vivo* and pancreatic differentiation *in vitro* using publicly available scRNA-seq datasets. *AMOTL2* was expressed at the different stages of pancreatic differentiation, including definitive endoderm, pancreatic progenitors, and EPs, *in vitro*, and in EPs, mesenchyme, and acinar cells *in vivo*. *AMOTL2* expression did not persist into mature endocrine cell. Importantly, here, for the first time, is shown the existence of the *NGN3*(+) / *AMOTL2*(+) EP population in human, in both *in vitro* and *in vivo*, which was previously identified only in mice. *AMOTL2* expression was also identified in the preimplantation embryo and hPSCs, suggesting that it might influence also earlier cell fate decisions.

In this thesis, I developed an AMOTL2 knockout (KO) hPSC line using CRISPR/Cas9 approach. During initial characterization, a strong phenotype concerning colony morphology emerged, with AMOTL2 KO hPSC colonies being more irregular and less tightly packed than in wild type (WT). Additionally, AMOTL2 KO hPSCs showed increased confluency compared to WT hPSCs, which was a result of increased proliferation and decreased apoptosis rates.

RNA-sequencing revealed substantial changes in terms connected with cytoskeleton, adhesion, and migration, development, cell metabolism, and signaling pathways. It also shown a potential developmental bias of AMOTL2 KO cells towards ectoderm, at the expense of endoderm and mesoderm, which was confirmed with spontaneous and directed differentiation. In search of the mechanism behind the differentiation bias, the F-actin depolymerization and increased YAP activity were identified as possible culprits. Surprisingly, spontaneous differentiation with F-actin depolymerizing agent, Y-27632, or YAP inhibitor, verteporfin, failed to repeat or rescue AMOTL2 KO developmental phenotype. This indicates that there are other, more potent players in the game,

by which AMOTL2 controls cell fate, which, based on RNA-sequencing and preliminary functional data, might include energy production mechanism or cellular metabolism.

Streszczenie

W ostatnich latach prowadzone były szerokie badania nad regulacją transkrypcji w procesach rozwojowych, jednakże nadal istnieje znaczna luka w wiedzy o mechanistycznych i metabolicznych sygnałach, oraz zdarzeniach morfologicznych towarzyszących różnicowaniu ludzkich pluripotencjalnych komórek macierzystych (ang. human pluripotent stem cells, hPSCs). W poszukiwaniu takich sygnałów po raz pierwszy zidentyfikowałem gen *Amotl2* w danych z sekwencjonowania RNA pojedynczych komórek (ang. single cel RNA-sequencing, scRNA-seq) z rozwijającej się mysiej trzustki z dni embrionalnych 14.5 (e14.5) i 16.5 (e16.5). Co ciekawe, pomimo zachowanych kanonicznych markerów, populacje progenitorów endokrynnych (ang. endocrine progenitors, EP) z tych punktów czasowych różniły się znacząco pod względem transkryptomu, przy czym EP z dnia 16.5 preferencyjnie tworzyły komórki β trzustki, a e14.5 EP preferencyjnie tworzyły komórki α. *Amotl2* ulegał specyficznej ekspresji w podtypie e16.5 EP, który odzwierciedlał wychodzenie EP ze struktury sznurów nabłonkowych, słabo poznane zdarzenie, które z kolei może wpływać na los komórek endokrynnych.

AMOTL2 należy do rodziny angiomotyn. Jest to białko cytoplazmatyczne, które znajduje się w cytozolu lub na połączeniach komórkowych, ułatwiając przekazywanie sygnału, organizację cytoszkieletu, i modulację szlaków sygnalizacyjnych. AMOTL2 jest znanym regulatorem szlaku Hippo i jego efektora – białka YAP. Jednym z celów niniejszej pracy była identyfikacja wzorców ekspresji genu *AMOTL2* w rozwoju ludzkiej trzustki *in vivo* i różnicowaniu trzustki *in vitro* przy użyciu publicznie dostępnych zbiorów danych scRNA-seq. *AMOTL2* ulegał ekspresji na różnych etapach różnicowania trzustki, w tym w endodermie właściwej, komórkach prekursorowych trzustki i EP *in vitro*, ale także w EP, mezenchymie i komórkach pęcherzykowych *in vivo*. Ekspresja genu *AMOTL2*
nie utrzymywała się w dojrzałych komórkach endokrynnych. Co ważne, tutaj po raz pierwszy wykazano istnienie populacji *NGN3*(+) / *AMOTL2*(+) PE u człowieka, zarówno *in vitro*, jak i *in vivo*, którą wcześniej zidentyfikowano jedynie u myszy. Ekspresję *AMOTL2* zidentyfikowano także w zarodku przedimplantacyjnym i hPSCs, co sugeruje, że może on wpływać również na wcześniejsze decyzje dotyczące losu komórki.

W niniejszej pracy wyprowadziłam linię hPSC z wyłączoną ekspresją genu AMOTL2 (ang. knockout, KO) przy użyciu metody CRISPR/Cas9. Podczas wstępnej charakterystyki wyłonił się silny fenotyp dotyczący morfologii kolonii, przy czym kolonie AMOTL2 KO hPSC były bardziej nieregularne i mniej ciasno upakowane niż u typu dzikiego (ang. wild type, WT). Dodatkowo hPSC AMOTL2 KO wykazywały zwiększoną konfluencję w porównaniu z hPSC WT, co było wynikiem ich zwiększonej proliferacji i zmniejszonych szybkości apoptozy.

Sekwencjonowanie RNA ujawniło istotne zmiany w zakresie cytoszkieletu, adhezji oraz migracji, rozwoju, metabolizmu komórkowego i szlaków sygnałowych. Wykazano również potencjalne

tendencje rozwojowe komórek AMOTL2 KO w kierunku ektodermy kosztem endodermy i mezodermy, co zostało potwierdzone spontanicznym i ukierunkowanym różnicowaniem. W poszukiwaniu mechanizmu odpowiedzialnego za takie tendencje w różnicowaniu jako możliwych winowajców zidentyfikowano depolimeryzację F-aktyny i zwiększoną aktywność YAP. Co zaskakujące, spontaniczne różnicowanie z dodatkiem substancji depolimeryzującej F-aktynę, Y-27632 lub inhibitora YAP, werteporfiny, nie powtórzyło ani nie uratowało fenotypu rozwojowego AMOTL2 KO. Oznacza to, że w grze biorą udział inni, silniejsi gracze, za pomocą których AMOTL2 kontroluje los komórek, a którzy w oparciu o sekwencjonowanie RNA i wstępne dane funkcjonalne mogą obejmować mechanizm wytwarzania energii lub metabolizm komórkowy.

1. Introduction

1.1. Pluripotency

1.1.1. Pluripotent stem cell characteristics

The pluripotent stem cells (PSCs) are characterized by their ability to self-renew, meaning that after every cell division at least one descendant cell remains an undifferentiated stem cell. In consequence, under proper culture conditions, PSCs can proliferate indefinitely, providing a potentially unlimited pool of cells. The second characteristic is PSC capacity to differentiate into cells from all three germ layers, namely endoderm, mesoderm, and ectoderm. Due to these features, PSCs constitute a valuable research tool for disease modeling, drug testing and studying the developmental processes, with a potential use in regenerative medicine and cell-based therapies.

Two main subtypes of PSCs can be distinguished - embryonic stem cells (ESC) and induced pluripotent stem cells (iPSC). The former are derived from embryos at the blastocyst stage by isolating the inner cell mass (ICM) where the PSCs reside. However, this procedure raises significant ethical concerns since ESC isolation destroys the embryo. Consequently, working with human ESCs (hESCs) is prohibited in some countries or, if permitted, it is strictly regulated. The development of iPSC derivation provided an answer to this issue. The iPSCs are derived from adult somatic cells by the genetic reprogramming and activation of the set of so-called pluripotency factors. The first hESCs were derived in 1998 (Thomson et al., 1998), while first human iPSCs were derived in 2007 independently by two teams by introducing *OCT3/4*, *SOX2*, *KLF4*, and *c-MYC* (Octamer-Binding Transcription Factor 3/4, SRY-Box Transcription Factor 2, Kruppel-Like Factor 4, and MYC Proto-Oncogene, BHLH Transcription Factor) (Takahashi et al., 2007) or *OCT3/4*, *SOX2*, *NANOG*, and *LIN28* (Nanog Homeobox and Lin-28 Homolog A) (Yu et al., 2007) to human fibroblasts.

1.1.2. Regulation of hPSC pluripotency

Pluripotency maintenance is crucial for the successful use of PSCs in research and medicine. Self-renewal and pluripotency of PSCs are governed by the intricate, highly interconnected network of the extrinsic signals and pluripotency-related pathways which regulate the core pluripotency factors, OCT3/4, SOX2, and NANOG. On another level, the core pluripotency factors are involved in the auto- and cross-regulatory circuits. Finally, the balance of the pluripotency factors expression decides between the self-renewal and differentiation. An overview on the pluripotency regulatory network in hPSCs is outlined in **Fig. 1**.

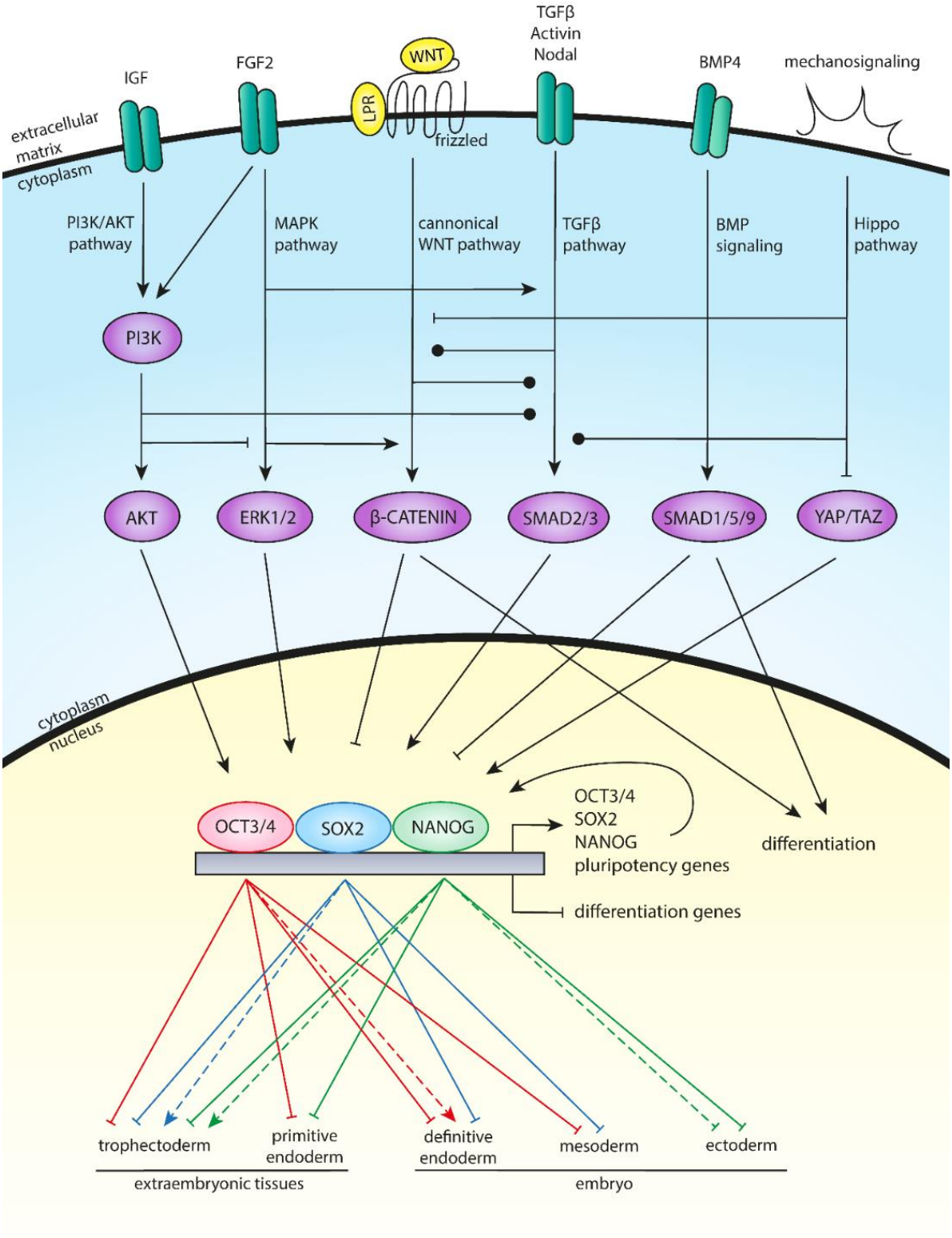

Fig. 1: Regulation of pluripotency in hPSCs. The main signaling pathways involved in pluripotency include PI3K/AKT pathway, MAPK pathway, TGFβ pathway and BMP signaling, canonical WNT pathway, and Hippo pathway. The pathways are highly interconnected and cooperate in pluripotency maintenance. Interplay between the pathways is designated with horizontal lines: arrow - activation, perpendicular line - inhibition, circle - modulation depending on the context. The pathways transduce the extrinsic signals to gene expression of core pluripotency genes, OCT3/4, SOX2, and NANOG, and other pluripotency-related genes. The core pluripotency factors are involved in several auto- and cross-regulatory loops tightly regulating their expression level. Balanced expression of pluripotency genes inhibits differentiation into extraembryonic and embryonic tissues, however overexpression (dashed arrows) might induce differentiation.

1.1.2.1. Signaling pathways involved in hPSC pluripotency

Among the signaling pathways involved in hPSC pluripotency regulation we can distinguish:

1) PI3K/AKT and MAPK pathway governed by IGF/FGF receptor activation
2) TGFβ and BMP signaling pathways
3) canonical WNT pathway
4) Hippo pathway

1.1.2.1.1. PI3K/AKT and MAPK signaling pathways

The PI3K/AKT (Phosphatidylinositol 3-Kinase/AKT Serine/Threonine Kinase) and MAPK (Mitogen-Activated Protein Kinase) are interconnected signaling pathways involved in the hPSC pluripotency maintenance. Both pathways are kinase cascades, meaning that the signal is propagated by phosphorylation and activation of sequential kinases. In the PI3K/AKT pathway, ligand binding to the receptor leads to the phosphorylation of the intracellular domain of the receptor which recruits and activates PI3K kinase. Active PI3K kinase, in turn binds to the PIP2 (Phosphatidylinositol 4,5-Bisphosphate) phospholipid which is a part of the plasma membrane. Phosphorylation by the PI3K kinase forms PIP3 (Phosphatidylinositol (3,4,5)-Trisphosphate) which facilitates the recruitment of PDK1 (Pyruvate Dehydrogenase Kinase 1) to the plasma membrane. PDK1 phosphorylates and activates AKT which can further phosphorylate many targets, including GSK3 (Yu & Cui, 2016).

In MAPK cascade, ligand binding recruits the small GTPase RAS (Rat Sarcoma Virus, GTPase) to the plasma membrane where it is phosphorylated and activated, which in turn recruits and activates RAF (RAF proto-oncogene serine/threonine-protein kinase). The signal is then transmitted to MEK1/2 (Mitogen-Activated Protein Kinase Kinase 1/2) and further to ERK1/2 (Extracellular Signal-Regulated Kinase 1/2). ERK1/2 can phosphorylate multiple cytosolic and nuclear targets, indirectly and directly influencing gene expression (Plotnikov et al., 2011; Haghighi et al., 2018).

1.1.2.1.2. TGFβ and BMP signaling

The TGFβ (Transforming Growth Factor β) signaling pathway is essential for the hPSC self-renewal (Beattie et al., 2005; Xiao et al., 2006). Upon binding of TGFβ/Activin/Nodal signals to TGFβ receptors, SMAD2/3 (Mothers Against Decapentaplegic Homolog 2/3) proteins are activated by phosphorylation, which allows them to form a complex with SMAD4 (Mothers Against Decapentaplegic Homolog 4). The complex translocates into the nucleus where it regulates gene expression (Mullen & Wrana, 2017).

BMP (Bone Morphogenetic Protein) signaling is closely connected to the TGFβ pathway. The binding of the BMP4 ligand to its receptor results in the phosphorylation and activation of SMAD1/5/8 (Mothers Against Decapentaplegic Homolog 1/5/8), which forms complex with SMAD4 and is translocated into the nucleus to aid gene expression. Contrary to murine PSCs,

where BMP signaling promotes pluripotency, in hPSCs BMP4 inhibits the expression of pluripotency factors and drives differentiation (G. Wang et al., 2005; C. Xu et al., 2005).

1.1.2.1.3. Canonical WNT pathway

In the absence of WNT (Wingless-Type MMTV Integration Site) ligand, β-CAT (β-catenin, CTNNB1, Catenin Beta 1) forms a destruction complex with GSK3, AXIN, CK1 and APC (Glycogen Synthase Kinase 3, Axin, Casein Kinase 1 Alpha 1, and APC Regulator Of WNT Signaling Pathway). This leads to β-CAT phosphorylation by GSK3 and CK1 which targets it for further ubiquitination and proteasomal degradation. As a result, β-CAT cannot enter the nucleus and influence gene expression (Angers & Moon, 2009; Stamos & Weis, 2013). Activation of the canonical WNT pathway begins with binding of the WNT ligand to the LRP (LDL Receptor Related Protein) and FZD (Frizzled Class Receptor) proteins located on the cell membrane. This promotes activation of DVL (Dishevelled Segment Polarity Protein) protein and sequesters AXIN, CK1 and GSK3, preventing formation of the degradation complex. Stabilized β-CAT accumulates in cytoplasm and can be translocated into nucleus where it promotes the gene expression via inhibition of the TCF (T-Cell Factor) repressors (Angers & Moon, 2009). Similar effects to the activation of the canonical WNT pathway can be achieved by pharmacological inhibition of GSK3 (Sato et al., 2004).

1.1.2.1.4. Hippo pathway

Hippo pathway consists of three major levels: upstream regulators, a core kinase cascade, and downstream effectors. Hippo is an inhibitory pathway that transduces mechanical stimuli, such as those resulting from e.g. cell-cell contact to control the activity of YAP (Yes Associated Transcriptional Regulator). Activation of Hippo pathway induces activation of MST1/2 (Macrophage Stimulating 1/2)-mediated phosphorylation and activation of LATS1/2 (Large Tumor Suppressor Kinase 1/2), which subsequently phosphorylates the main Hippo downstream effectors – transcriptional coactivators YAP and TAZ (WW Domain Containing Transcription Regulator 1). Phosphorylated YAP/TAZ are sequestered in the cytoplasm and therefore inactive. Further phosphorylation leads to YAP/TAZ ubiquitination and degradation by the proteasome. In case of inactive Hippo signaling, unphosphorylated YAP/TAZ can be translocated into the nucleus where they bind to TEAD (TEA Domain Transcription Factor 1) and mediate gene expression (Meng et al., 2016).

1.1.2.2. The interplay between the signaling pathways regulating hPSC pluripotency

The signaling pathways involved in the hPSC self-renewal are widely interconnected and they exert mutual regulation (**Fig. 1**). For some pathways, the studies yielded inconclusive results concerning their role in self-renewal vs differentiation, which might stem from the dose-dependent

effects of pathway modification and complex the interplay between different signaling pathways. PI3K/AKT, MAPK/ERK and TGFβ pathways appear to be the dominant signaling pathways ensuring the pluripotency maintenance, with PI3K/AKT exerting regulatory control over many pathways involved in pluripotency.

PI3K/AKT pathway is necessary for hPSC pluripotency maintenance (Armstrong et al., 2006) and its activation leads to the upregulation of NANOG and OCT3/4 expression (Alva et al., 2011; Madsen, 2020). Pharmacological inhibition of the PI3K/AKT pathway results in the loss of pluripotency in hPSCs (Bendall et al., 2007; McLean et al., 2007). MAPK/ERK signaling is highly active in hPSCs and it enhances self-renewal and inhibits differentiation towards trophectoderm, primitive endoderm and ectoderm, both directly and by the induction of the TGFβ pathway (Armstrong et al., 2006; Eiselleova et al., 2009; Haghighi et al., 2018; J. Li et al., 2007). PI3K/AKT is primarily activated by IGF (Insulin Like Growth Factor) ligand, while MAPK responds to FGF2 (Fibroblast Growth Factor 2), however high concentrations of FGF2 also activate PI3K/AKT pathway (J. Li et al., 2007; Singh et al., 2012). In turn, high AKT levels inhibit MAPK pathway via inhibition of ERK, keeping the ERK activity in the appropriate range for self-renewal, since elevated MAPK signaling promotes differentiation (Singh et al., 2012). Additionally, high FGF2 concentration supports hPSC self-renewal via BMP signaling inhibition (Levenstein et al., 2006).

There are conflicting results on the role of the TGFβ pathway in the hPSC self-renewal. While some report that TGFβ/Activin/Nodal signaling is required for the maintenance of hPSC pluripotency (Beattie et al., 2005; James et al., 2005; Xiao et al., 2006), others show that Activin A treatment promotes formation of mesendoderm, a common progenitor of definitive endoderm and definitive mesoderm lineages (K. A. D'Amour et al., 2005; McLean et al., 2007). Consistently with the former, the downstream effectors of TGFβ pathway, SMAD2/3, cooperate with NANOG, SOX2 and OCT3/4 in the regulation of their target genes (Brown et al., 2011; Chng et al., 2010; James et al., 2005; Vallier, Mendjan, et al., 2009; R. H. Xu et al., 2008). However, SMAD2/3 were also shown to target definitive endoderm genes (Brown et al., 2011).

The role of WNT in hPSC pluripotency maintenance is not fully understood. Sato et al. showed that activation of the WNT pathway by pharmacological inhibition of GSK3 support hPSC pluripotency without inducing differentiation (Sato et al., 2004). In contrast, Cai et al. reported that WNT activation by the treatment of hPSCs with WNT3A (Wingless-Type MMTV Integration Site 3A) promotes differentiation (Cai et al., 2007). The WNT pathway activity is minimal in undifferentiated hPSCs and increases upon differentiation (Davidson et al., 2012; Dravid et al., 2005). The effect of GSK3 inhibition or WNT activation on hPSC pluripotency appears to be dose-dependent, since minimal canonical WNT activation and basal β-CAT levels does not hinder hPSC self-renewal, while elevated levels induce differentiation. Additionally, the differences might also be attributed to the duration of treatment, since another study found that WNT3A treatment and GSK3 inhibitor treatment required 1 week and 3 weeks, respectively, to significantly impair

hPSC self-renewal (Davidson et al., 2012). Further, short-term activation of the canonical WNT pathway supports hPSC self-renewal by activation of PI3K/AKT in CDH1 (Cadherin 1) - mediated mechanism. Conversely, long-term activation induces differentiation due to the increased levels of β-CAT (T. S. Huang et al., 2015).

PI3K/AKT, MAPK/ERK, TGFβ and WNT pathways cooperate to maintain hPSC self-renewal and neither FGF2 nor TGFβ signaling alone can maintain the hPSC self-renewal (R. H. Xu et al., 2008). While TGFβ signaling is essential for hPSC self-renewal in presence of active PI3K/AKT pathway, it drives the specification of definitive endoderm when PI3K/AKT signaling is absent (McLean et al., 2007; Singh et al., 2012; Vallier et al., 2005). In hPSCs PI3K/AKT pathway is activated which (1) regulates SMAD2/3, thereby activating NANOG expression, and (2) inhibits ERK, preventing GSK3 suppression. Active GSK3 forms degradation complexes with β-CAT and decreases its levels to sustain the level compatible with the pluripotency maintenance. Upon PI3K/AKT inhibition, SMAD2/3 levels increase and ERK is activated. ERK activation blocks GSK3-mediated β-CAT degradation. Stabilized β-CAT forms complex with SMAD2/3 shifting their target genes from pluripotency-related to differentiation-related (Singh et al., 2012). Further, suppression of TGFβ pathway in the presence of FGF2 promotes neuroectodermal differentiation of hPSCs (Vallier, Touboul, Chng, et al., 2009).

The BMP signaling is inhibited in hPSCs (James et al., 2005). Activation of the BMP signaling in hPSCs leads to the decrease of OCT3/4, SOX2 and NANOG expression and drives differentiation towards trophectoderm and primitive endoderm cells (Greber et al., 2008; Vallier, Touboul, Brown, et al., 2009; R. H. Xu et al., 2008).

Hippo pathway inhibition is essential for the pluripotency maintenance in hPSCs. LATS2 knockdown (KD), synonymous with Hippo inhibition, significantly enhances the human iPSC generation from human fibroblasts (Qin et al., 2012). Further, knockdown of TAZ, mimicking Hippo activation, leads to the loss of pluripotency factor expression in hPSCs (Varelas et al., 2008). The expression of NANOG and OCT3/4 is regulated by the Hippo pathway (Beyer et al., 2013). Hippo pathway is involved in the crosstalk with TGFβ signaling. TAZ supports hPSC pluripotency by binding SMAD2/3 and regulating their translocation into the nucleus (Varelas et al., 2008) and YAP/TAZ KD reduces SMAD2/3 nuclear accumulation (Beyer et al., 2013). Loss of nuclear accumulation of SMAD2/3 results in neuroectoderm differentiation (Varelas et al., 2008). Downstream effectors of Hippo pathway, including YAP, TAZ, and TEAD proteins form a complex with SMAD2/3 and OCT3/4 to modulate the expression of the pluripotency factors while repressing mesendoderm-related genes (Beyer et al., 2013). Without YAP/TAZ and TEAD in the complex, the SMAD2/3 activity promotes mesendoderm differentiation (Beyer et al., 2013). YAP also prevents Activin A-mediated WNT3 expression which otherwise promotes mesendodermal commitment (Estarás et al., 2017).

1.1.2.3. The core pluripotency factors

The core pluripotency factors, OCT3/4, SOX2 and NANOG are crucial for hPSC self-renewal (**Fig. 1**). OCT3/4 inhibits differentiation into extraembryonic (Babaie et al., 2007; Hay et al., 2004; Matin et al., 2004; Z. Wang et al., 2012) or mesodermal tissues (Hay et al., 2004; Rodriguez et al., 2007; Z. Wang et al., 2012). Wang et al. suggested that this effect might be cell line-specific and connected with BMP pathway activation status (Z. Wang et al., 2012). NANOG expression in hPSCs blocks differentiation into ectoderm (Fong et al., 2008; Vallier, Mendjan, et al., 2009; Z. Wang et al., 2012) and extraembryonic tissues (Fong et al., 2008; Hyslop et al., 2005; Zaehres et al., 2005). Several studies showed that SOX2 KD results in the promotion of trophectodermal and endodermal fates (Adachi et al., 2010; Fong et al., 2008). Interestingly, Wang et al. (Z. Wang et al., 2012) reported that SOX2 expression is not essential for pluripotency maintenance due to partial compensation by SOX3. SOX3 is expressed at low levels in hPSCs, yet it is upregulated upon SOX2 KD. In consequence, cells remain pluripotent, however they show a bias towards mesendodermal lineages upon spontaneous differentiation. KD of both SOX2 and SOX3 induces mesendoderm differentiation. How the overexpression of pluripotency factors affects hPSCs is not clear. Wang et al. (Z. Wang et al., 2012) overexpressed all three core pluripotency factors and did not observe induction of differentiation, and therefore concluded that in hPSCs core pluripotency factors act predominantly as differentiation repressors and their overexpression does not jeopardize pluripotency. However, they noted that cells with increased expression of each pluripotency factor carry a bias towards specific lineages. The overexpression of OCT3/4 improved definitive endoderm formation and inhibited ectodermal commitment (Z. Wang et al., 2012). This is consistent with another report showing that OCT3/4 overexpression induces endodermal fate (Rodriguez et al., 2007). The overexpression of NANOG entirely blocked ectoderm differentiation in the study by Wang et al. (Z. Wang et al., 2012).

The core pluripotency factors bind the promoters of multiple genes and act as activators for the pluripotency-related genes and repressors for differentiation-related genes (Boyer et al., 2005). They also regulate the components of the pluripotency-related signaling pathways (Boyer et al., 2005; Davidson et al., 2012), for instance, OCT3/4 inhibits β-CAT in hPSCs (Davidson et al., 2012).

OCT3/4, SOX2, and NANOG are involved in auto- and cross-regulatory feedback loops. All three pluripotency factors were shown to bind to their own promoters and modulate their own expression (Boyer et al., 2005; Das et al., 2012). Additionally, NANOG is regulated by both SOX2 and OCT3/4 in hPSCs (Boyer et al., 2005; Rodda et al., 2005; Z. Wang et al., 2012) and OCT3/4 also regulates SOX2 (Chavez et al., 2009). In contrast, Wang et al. state that while OCT3/4 and NANOG co-regulate each other, SOX2 is not involved in this loop, since SOX2 KD does not affect OCT3/4 and NANOG expression (Z. Wang et al., 2012).

1.2. Early cell fate decisions in developing embryo

1.2.1. Trophectoderm vs inner cell mass segregation

The first cell specification event during mammalian development takes place in the preimplantation embryo. After fertilization, the cells undergo a series of symmetrical divisions, sequentially forming the structures containing 2, 4, 8, 16, and 32 cells. At the 32-cell stage, the cells begin differentiating into trophectoderm (TE) and ICM, ultimately forming blastocyst. In the blastocyst, TE cells form a single-layered sheet that surrounds a fluid-filled cavity, where the ICM cells reside in a tightly packed group. The TE and ICM cells differ in terms of morphology and gene expression. While the TE cells are polarized and express Cdx2 (Caudal Type Homeobox 2) and Gata3 (GATA Binding Protein 3) (Home et al., 2009; Ralston et al., 2010; Ralston & Rossant, 2008; Strumpf et al., 2005), the ICM cells remain non-polar and retain Oct3/4 and Nanog expression (Dietrich & Hiiragi, 2007; Ralston et al., 2010). Later in the development, TE cells will contribute to the extraembryonic tissue formation, including trophoblast and placenta, which are essential for the implantation. The ICM provides the pool of the pluripotent stem cells that will further differentiate into epiblast and give rise to all three germ layers, namely endoderm, mesoderm, and ectoderm, which will ultimately form the whole embryo (**Fig. 2**) (Fujimori, 2010; Marikawa & Alarcon, 2014; Stephenson et al., 2012; Zernicka-Goetz et al., 2009). The mechanism of TE vs ICM segregation in mouse blastocyst is relatively well studied and appears to be dependent on the Hippo pathway and Yap. Due to the ethical concerns, this kind of research was not performed in human (Zernicka-Goetz et al., 2009).

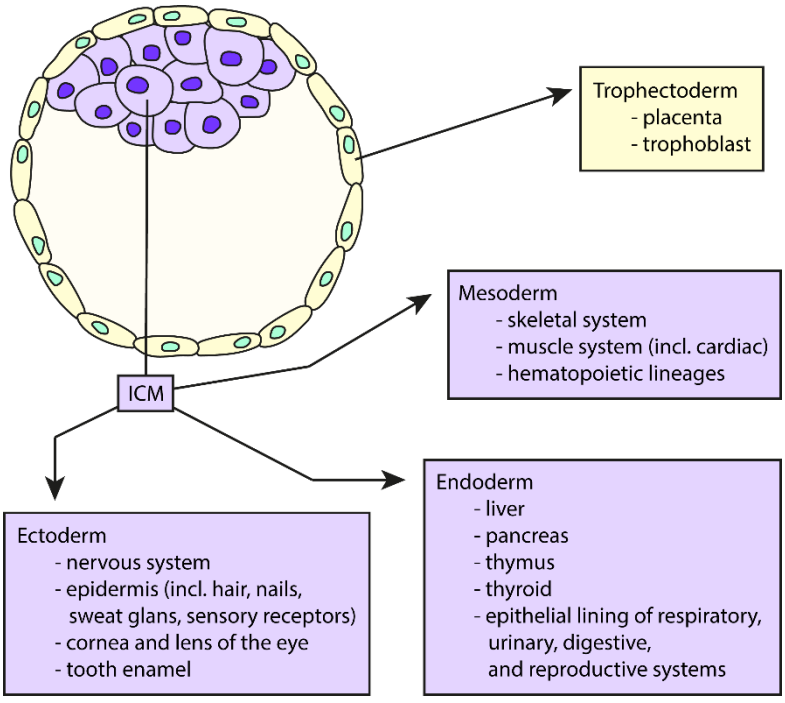

Fig. 2: Early cell fate decisions in the developing embryo. During early embryo development PSCs segregate, forming trophectoderm, which will give rise to placenta and trophoblast, and ICM cells, which will differentiate into cells of three germ layers, namely ectoderm, endoderm, and mesoderm. ICM – inner cell mass.

1.2.2. The germ layer specification

The fate decisions of ICM cells are crucial for the proper embryo formation. The ectoderm is specified by inhibition of canonical WNT, BMP, and TGFβ signaling and upregulation of FGF signaling (Kumar et al., 2021). The ectoderm will give rise to the nervous system, neural crest, tooth enamel, cornea and lens of the eye, and epidermis, together with its derivatives such as hair, nails, sweat glands, and sensory receptors. Further, mesendodermal determination relies on canonical WNT pathway inhibition and TGFβ activation. The endodermal derivatives include liver, pancreas, thymus, thyroid, and epithelial lining of respiratory, urinary, digestive, and reproductive systems. Mesodermal lineages differentiate into skeletal and muscle system, including cardiac muscles, and hematopoietic lineages (**Fig. 2**).

1.3. The hPCS *in vitro* differentiation as a model for studies on cell fate decisions

In vivo PSCs within ICM differentiate into all cells within the body in a highly regulated process that relies on the intricate balance of signaling pathways. The mechanisms behind this intrinsic regulation are not entirely understood. *In vitro* hPSCs retain their ability to self-organize and upregulate the signals needed for differentiation into cells of all three lineages, when deprived of the pluripotency-maintaining signals. This process is named spontaneous differentiation and results in the highly heterogeneous cell population. There are several systems for *in vitro* spontaneous differentiation, including micropatterned colonies, embryoid bodies, gastruloids and blastoids (Morales et al., 2021). Embryoid bodies (EBs) are three-dimensional (3D) aggregates of hPSCs which recapitulate some aspects of early development, such as tight cell packing and differentiation into all three germ layers, however, lack axial elongation typical for early developing embryos.

As opposed to spontaneous differentiation, directed differentiation relies on mimicking the natural developmental processes and guiding cells through the consecutive developmental stages by the administration of a cocktail of growth factors and small molecules. Directed differentiation protocols are frequently used to derive a specific cell type of choice, e.g. pancreatic β-cells, liver cells, neurons.

1.4. Pancreas

1.4.1. Pancreas structure and function

The pancreas is a glandular organ composed of the exocrine and endocrine compartments. The exocrine part, which accounts for ~95% of the pancreatic tissue, includes acinar and ductal cells. The acinar cells produce and secrete the digestive enzymes responsible for the breakdown of carbohydrates, proteins and fatty acids. The duct cells collect the enzymes and transport them into

the duodenum for digestion. The endocrine part comprises five types of hormone-producing cells: α, β, δ, ε and PP-cells, that secrete glucagon, insulin, somatostatin, ghrelin, and pancreatic polypeptide, respectively. The role of the endocrine cells is to collectively regulate blood glucose levels. Insulin decreases and glucagon increases the glucose concentration in blood, while somatostatin, ghrelin, and pancreatic polypeptide regulate the α- and β-cell function. The endocrine cells are organized in the clusters called the Langerhans islets. There are certain differences in the composition and architecture of human and murine Langerhans islets. Mouse pancreatic islets exhibit a characteristic core-mantle architecture with β-cells located within the core and other cell types surrounding them. Instead, in humans the endocrine cells are not highly organized, rather randomly distributed within islets. In mice pancreatic islets are composed of 60-80% β-cells, 15-20% α-cells, up to 10% δ-cell and rare ε and PP cells. In human, β-cells account for up to 50% of all endocrine cells, α-cells up to 40% and remaining cell types together up to 10% (Brissova et al., 2005; Steiner et al., 2010). **Fig. 3** illustrates the pancreatic structure.

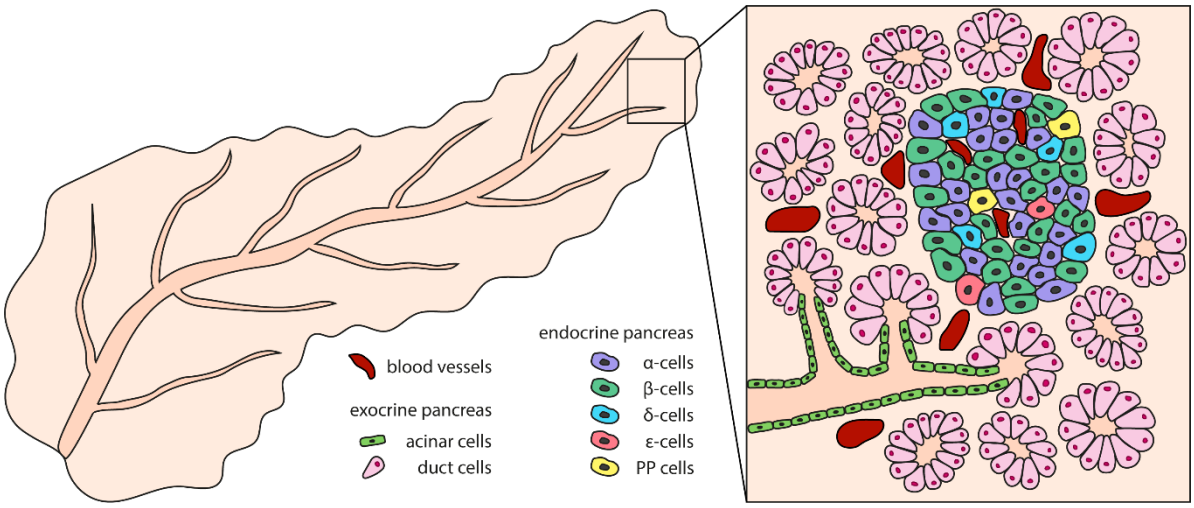

Fig. 3: Schematic structure of human pancreas. The pancreas is composed of the endocrine (α, β, δ, ε and PP) cells which collectively regulate blood glucose level by the production of the appropriate hormones, and exocrine (acinar and duct) cells which are responsible for the secretion and transport of the digestive enzymes.

1.4.2. Pancreatic development *in vivo*

Pancreatic differentiation in human starts around 29-33 dpc (days post conception) with the endoderm thickening and forming two distinct buds, called dorsal and ventral pancreatic buds, which will subsequently fuse into a single organ around 37-40 dpc. The cells within the buds are multipotent pancreatic progenitors (MPPs), capable of differentiating into all pancreatic cell types. The MPPs are marked by the expression of PDX1, SOX9, GATA4, and NKX6.1 (Pancreatic and Duodenal Homeobox 1, SRY-Box Transcription Factor 9, GATA Binding Protein 4, and NK6 Homeobox 1). Between 5 and 7 wpc (weeks post conception) MPPs proliferate, and buds undergo

morphogenesis to form microlumens, which then assemble into tubular structures called epithelial cords. Around 7 wpc epithelial cells within cords further specify into “tip” and “trunk” domains and form branching structures that will later become the ducts of the pancreas. Tip and trunk domains are distinguishable by the expression of GATA4, which is sustained in the tip cells and diminishes in the trunk cells. Together with the specification into tip and trunk domains, the MPPs potency becomes restricted. The tip cells, which lose NKX6.1 expression by 10 wpc and SOX9 expression between 10 and 14 wpc, will differentiate into acinar cells later in development. In turn, pancreatic progenitors within trunk domains are bipotent, capable of differentiating into both duct and endocrine cells. A transient expression of NGN3 (Neurogenin 3) marks EPs which will give rise to all endocrine cell types within the pancreas, while trunk cells without the NGN3 expression will eventually become duct cells (Jennings et al., 2013, Jennings et al.,2015; Nair & Hebrok, 2015). The NGN3 expression in humans starts around 8 wpc and continues until around 20 wpc, with new EPs being constantly born (Jennings et al., 2013; Salisbury et al., 2014). Unlike mice, which have biphasic Ngn3 expression, humans exhibit only a single wave of NGN3 expression (Jennings et al., 2013; Salisbury et al., 2014). NGN3(+) EPs differentiate into endocrine cells, with β-cells being the first detectable hormone-producing cell type in human pancreatic development (Jeon et al., 2009; Piper et al., 2004). A unique feature of human pancreatic development is the presence of up to 30% of multihormonal INS(+) / GCG(+) cells within endocrine lineage (Anderson et al., 2013; Jeon et al., 2009; Riedel et al., 2012).

The requirement of NGN3 for endocrine cell formation in humans has been unclear. Reported individuals carrying mutations in NGN3 gene, still showed a low but detectable secretion of the c-peptide (C-PEP), an insulin maturation by-product, indicating the presence and at least partial functionality of β-cells. All of the patients presented with diabetes, however the age of onset differed significantly, from 13 days-old to 23 years-old (Hancili et al., 2017; Rubio-Cabezas et al., 2011, 2014; J. Wang et al., 2006; Zhang et al., 2019). The NGN3 knockout in hPSCs revealed that complete NGN3 deficiency prevents hormone-producing cell formation. In contrast, NGN3 KD, up to 90% only minimally affected the endocrine cells, which is in line with the idea that NGN3 mutations in the patients were rather hypomorphic than truly null mutations (Mcgrath et al., 2015). In turn, Rosen et al. consistently detected a small number (~0.5%) of INS(+) cells in differentiated NGN3 knockout hPSCs, however the majority of them were not functional in terms of glucose-stimulated insulin secretion. The authors suggest that while NGN3 is important for endocrine lineages, the requirement is not absolute and there might be a yet unidentified compensatory mechanism involved. Nevertheless, NGN3 is crucial for the efficient endocrine lineage differentiation (Rosen & Gonza, 2016).

1.4.3. *In vitro* directed differentiation of hPSCs towards pancreatic lineages

Most pancreatic differentiation protocols involve up to 7 consecutive stages that mimic natural development: definitive endoderm (DE), primitive gut tube (PGT), posterior foregut (also called pancreatic endoderm), pancreatic progenitors (PPs), EPs, immature β-cells and maturing β-cells (Pagliuca et al., 2014; Rezania et al., 2014; Velazco-Cruz et al., 2019). The first step is differentiating hPSCs into DE cells, characterized by the expression of SOX17, FOXA2, and CXCR4 (SRY-Box Transcription Factor 17, Forkhead Box A2, and C-X-C Motif Chemokine Receptor 4). This is obtained by activating the canonical WNT and TGFβ pathways (K. D'Amour et al., 2005; K. a D'Amour et al., 2006; Velazco-Cruz et al., 2019; Pagliuca et al., 2014)). Next, cells differentiate into primitive gut tube, marked by SOX17, FOXA2, and HNF1B (HNF1 Homeobox B) (K. D'Amour et al., 2006; Kroon et al., 2008; Russ et al., 2015; Velazco-Cruz et al., 2019). Further, PPs are characterized by the expression of: PDX1, NKX6.1, and SOX9. Next, cells differentiate into EPs, marked by PDX1, NKX6.1, NGN3, NEUROD1 (Neuronal Differentiation 1), and CHGA (Chromogranin A). The last step of the differentiation are β-cells, which should show the expression of PDX1, NKX6.1, and CHGA, INS (Insulin), and C-PEP (C-peptide). Mature β-cells do not express any other pancreatic hormones, e.g. GCG (Glucagon) or SST (Somatostatin). The overview on the *in vitro* pancreatic differentiation can be found at **Fig. 4**. For the proper differentiation, not only induction of the pancreatic fate is necessary, but also inhibition of the alternative cell fates.

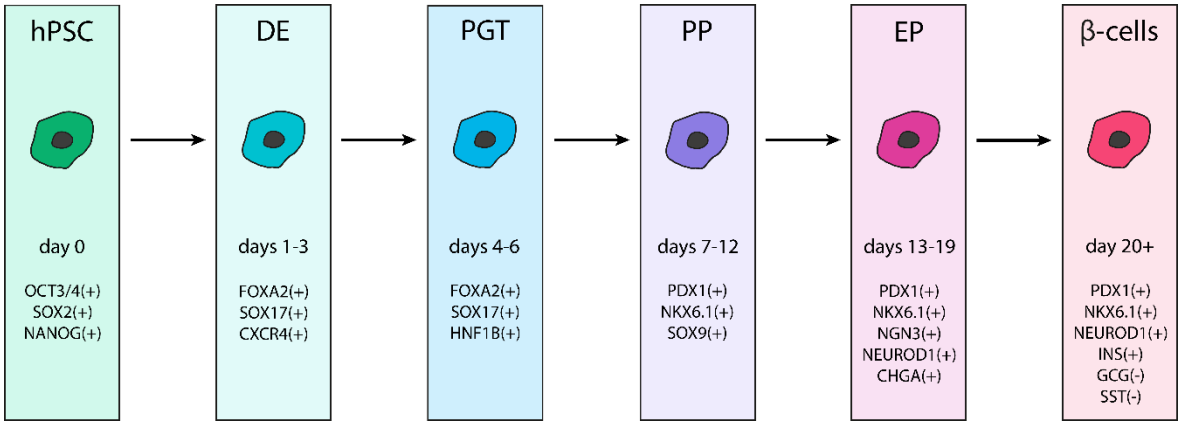

Fig. 4: An overview on the stages of *in vitro* pancreatic differentiation. hPSC – human pluripotent stem cell, DE – definitive endoderm, PGT – primitive gut tube, PP – pancreatic progenitor, EP – endocrine progenitor.

While we generally know how to guide cells into the pancreatic β-cells, there is still room for improvement. Firstly, the efficiency of the pancreatic differentiation decreases with each successive step - while current protocols yield high numbers of differentiated cells at early stages, for instance with 95% efficiency in DE generation, only 20-50% of cells ultimately differentiate into β-cells. Secondly, many differentiation protocols generate multihormonal cells, which fail to terminally differentiate into functional β-cells and do not respond to changing glucose levels in a proper manner. It was shown that premature expression of NGN3 drives the formation of multihormonal cells

(Hogrebe et al., 2020; Johansson et al., 2007). Next, β-cells obtained by *in vitro* differentiation often exhibit decreased insulin content and secretion, and blunted response to glucose compared to the primary human islets (Hanley, 2014; Kushner et al., 2014; Pagliuca et al., 2014; Rezania et al., 2014).

Although the transcriptional regulation of the developmental processes was extensively studied over the last years, there is a considerable gap of knowledge concerning the mechanistic cues and underlying morphological events that accompany differentiation. In search of such signals, we identified AMOTL2 as a potential regulator of hPSC cell fate.

1.5. AMOTL2

1.5.1. Angiomotin family proteins

Human angiomotin (AMOT) was initially identified in the yeast two-hybrid system through its ability to bind angiostatin, a potent inhibitor of angiogenesis and metastases. Angiomotin promotes endothelial cell migration, while angiostatin antagonizes its function, likely by blocking complex formation with other proteins (O'Reilly et al., 1994; Troyanovsky et al., 2001). Two additional proteins with high sequence similarity were identified as members of the angiomotin family and named AMOTL1 (Angiomotin Like 1) and AMOTL2 (Angiomotin Like 2). The protein sequences of all three family members are highly conserved across species. AMOTL1 and AMOTL2 lack the angiostatin-binding domain of AMOT and therefore are unlikely to bind angiostatin (Bratt et al., 2002). All angiomotin family members share five highly conserved regions within their amino acid (aa) sequence (the aa positions provided are for AMOTL2):

1) YAP-binding regions, which in AMOTL2 include LPTY and PPQY motifs located at 104-107aa and 210-213aa, respectively. AMOT and AMOTL1 have one more YAP-binding site;
2) LATS phosphorylation site at S159, within the HVRSLS motif (154-159aa);
3) actin-binding region, 142-175aa;
4) putative coil-coiled domain, also called angiomotin domain: 308-737aa;
5) PDZ-binding motif EILI (777-780aa)

Despite the high sequence and domain similarity among angiomotins, AMOTL2 is a unique member of the family. First, phylogenetic analysis showed that while all three proteins share the evolutionary origin, AMOTL2 seems to be an evolutionary outlier compared to AMOT and AMOTL1 (Bratt et al., 2002). Second, AMOTL2 but not AMOT or AMOTL1 is a downstream target of both YAP and TAZ (Lee et al., 2018). Next, AMOTL2 is uniquely regulated and phosphorylated by mTORC2-RICTOR (Mechanistic Target Of Rapamycin Kinase Complex 2 - RPTOR Independent Companion Of MTOR Complex 2) complex, while other angiomotins are not associated with the complex and lack the S760 phosphorylation site (Artinian et al., 2015). Further, the NEDD4 (NEDD4 E3

Ubiquitin Protein Ligase) ubiquitin ligase promotes degradation of AMOT and AMOTL1 but not AMOTL2 (Chenji Wang et al., 2012). AMOTL2 directly binds AKT and decreases its phosphorylation but AMOTL1 does not show a functional redundancy in AKT signaling (Han et al., 2017). At the pluripotency stage, Amotl2 but not Amotl1 is expressed in mouse preimplantation embryos (Hirate et al., 2013), and similarly, in human, AMOTL2 is the most abundant family member in ICM and naive PSCs (Subramani et al., 2023).

1.5.2. Identification of Amotl2 as delaminating EP marker in e16.5 murine pancreas

We first identified the *Amotl2* gene in the single-cell RNA-sequencing (scRNA-seq) data of the developing murine pancreata performed by a former PhD student of Prof. Borowiak, Marissa Scavuzzo (Scavuzzo et al., 2018). The scRNA-seq revealed that *Ngn3*(+) EPs from embryonic day (e)14.5 and e16.5 group into four transcriptionally distinct clusters, aligning with a developmental trajectory that reflects EP maturation (**Fig. 5A-D**). This suggests that new *Ngn3*(+) EPs are constantly born at both timepoints, and they undergo similar maturation. Interestingly, despite conserved canonical markers, e14.5 and e16.5 EPs cluster separately on the principal component analysis (PCA) plots (**Fig. 5E**), suggesting that corresponding subtypes change over time. As assessed by single-cell Assay for Transposase-Accessible Chromatin (ATAC)-sequencing, gene expression and chromatin accessibility, the key α- and β-cell motifs become enriched at e14.5 and e16.5, respectively (**Fig. 5F**). Additionally, more Gcg(+) endocrine cells are born at e14.5, while Ins(+) cells are dominant at e16.5 (**Fig. 5G**), indicating that EPs are temporally biased, with e16.5 EPs being more prone to form β-cells, and e14.5 EPs preferentially forming α-cells. As my Master thesis, I further analyzed the *Ngn3*(+) EP scRNA-seq data, to identify candidate genes involved in EP regulation. My task was to analyze e16.5 dataset, as the one biased towards β-cell fate and in cluster 2 (subtype 2), which exhibited high expression of EMT (epithelial-mesenchymal transition) and mesenchymal genes, together with epithelial genes, potentially reflecting EP delamination from the pancreatic epithelium, a poorly understood process that might influence endocrine cell fate. I hypothesized that cell fate and delamination are interconnected, namely morphological changes and mechanistic signals during EP exit from epithelial cords influence endocrine cell fate determination. Therefore, I selected a group of genes uniquely enriched in subtype 2 (EP2) of e16.5 EPs, one of which was *Amotl2* (**Fig. 5H**, first panel), on which I focus in this thesis.

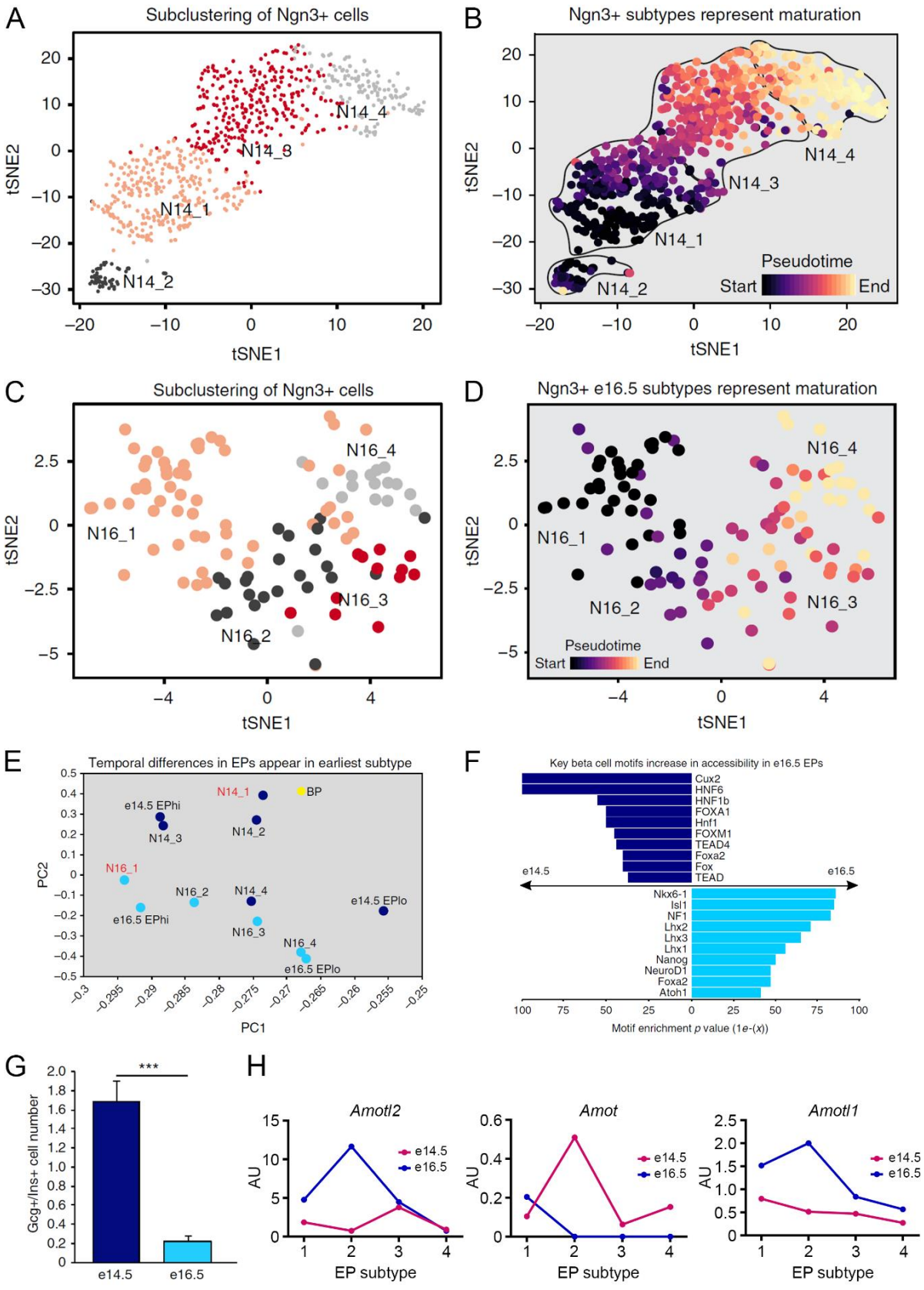

Fig. 5: Amotl2 expression in murine pancreatic development by scRNA-seq. A-G from (Scavuzzo et al., 2018); **A, C.** Subclustering of e14.5 (**A**) and e16.5 (**C**) *Ngn3*(+) cells visualized using tSNE. Colors indicate cluster identity. Clusters were numbered by developmental trajectory. **B, D.** Pseudotemporal ordering of single cells from e14.5 (**B**) and e16.5 (**D**) revealing the developmental trajectory. **E.** PCA of e14.5 and e16.5 *Ngn3*(+) cell subtypes and original *Ngn3*(+) cell clusters. As a control, e14.5 BPs are shown in yellow. **F.** Top differentially enriched motifs in accessible chromatin regions of e14.5 (in navy) and e16.5 EPs (in light blue). **G.** Quantification of Gcg(+) cell number over Ins(+) cell number from e14.5 and e16.5 pancreata. N=4

for e14.5 and N=6 for e16.5. $p < 0.005$ by two-sided Student's t-test. **H.** *Amotl2*, *Amot*, and *Amotl1* mRNA expression in EP subtypes at e14.5 and e16.5. tSNE – t-distributed stochastic neighbor embedding, PCA – principal component analysis, BPs – bipotent progenitors, AU – arbitrary units

Amotl2 expression was 2.5-fold higher in e16.5 EP2 than in EP1 and EP3 from the same timepoint and 16-fold higher than in e14.5 EP2 (**Fig. 5H**). I also examined the expression of other angiomotin family members. *Amot* was generally expressed at very low levels in EPs from both timepoints and undetectable in e16.5 EP2, EP3, and EP4 (**Fig. 5H**, middle panel). While the *Amotl1* expression (**Fig. 5H**, right panel) followed a somewhat similar pattern to *Amotl2*, with an increase in e16.5 EP2, it was expressed at the markedly lower levels. To conclude, *Amotl2* is a dominant family member in murine *Ngn3*(+) EPs and is highly upregulated in 16.5 EP2.

If AMOTL2 is expressed in human *in vivo* pancreatic differentiation and if the population of AMOTL2(+) EPs exists in human, remains unknown.

1.5.3. AMOTL2

AMOTL2 is a cytoplasmic protein that localizes either in cytosol or at the cellular junctions, facilitating signal transduction, cytoskeleton organization, and modulation of signaling pathways. Angiomotins, including AMOTL2, are known regulators of Hippo pathway. By the interactions with YAP/TAZ and LATS1/2, AMOTL2 regulates Hippo pathway regulation on multiple levels. First, AMOTL2 directly binds YAP/TAZ (**Fig. 6**, **Fig. 7**) and sequestrates them in the cytoplasm , therefore inhibiting their activity (Lucci et al., 2013; Paramasivam et al., 2011; W. Wang et al., 2011; Zhao et al., 2011). Second, AMOTL2 binds to LATS1/2 and promotes its autophosphorylation and activation (**Fig. 6**, **Fig. 7**). LATS1/2 phosphorylation is further passed onto YAP, which marks it for ubiquitination and degradation (Chan et al., 2013; Mana-Capelli & McCollum, 2018; Paramasivam et al., 2011). Third, AMOTL2 is one of the YAP/TAZ downstream regulated genes,

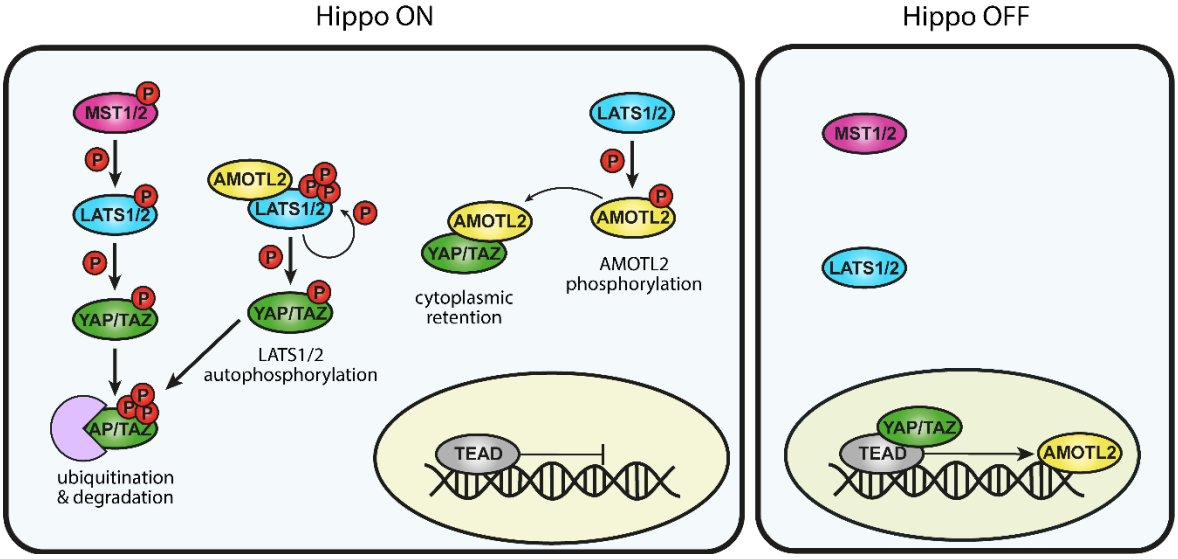

Fig. 6: AMOTL2 cooperates with Hippo pathway to regulate YAP/TAZ activity. P - phosphorylation

which forms a negative feedback loop (**Fig. 6**) (Han et al., 2017). Additionally, AMOTL2 can be phosphorylated by LATS1/2 at S159, which inhibits its ability to bind F-actin, simultaneously promoting YAP binding (Chan et al., 2013). Due to the close proximity of YAP-binding sites, LATS1/2 phosphorylation site and actin-binding region, actin competes with YAP (Hildebrand et al., 2017; S. Mana-Capelli et al., 2014) and LATS1/2 (S. Mana-Capelli et al., 2014) for binding to AMOTL2 (**Fig. 7**). Binding of a scaffold junctional protein MAGI1, which associates with actin, is also dependent on AMOTL2 LPTY YAP-binding sites (**Fig. 7**) (Hildebrand et al., 2017; Hultin et al., 2014; Kantar et al., 2021). Interaction with PAR is essential for AMOTL2-actin association, which is involved in establishing cell polarity (**Fig. 7**) (Hultin et al., 2017; Mojallal et al., 2014). AMOTL2 can also associate with CDH1 (**Fig. 7**) (Hildebrand et al., 2017).

Apart from the Hippo pathway, AMOTL2 is involved in FGF and canonical WNT signaling. AMOTL2 was reported to negatively regulate AKT phosphorylation and activation by direct association (**Fig. 7**) (Han et al., 2017; W. Wang et al., 2011). Wang W. et al. also described AMOTL2 inhibiting effect on ERK activity (W. Wang et al., 2011). In contrast, in the study by Wang Y. et al. AMOTL2 positively regulated MAPK/ERK signaling in PDZ-independent mechanism (Y. Wang et al., 2011). AMOTL2 was phosphorylated at Y107 by FGF receptor kinase activity which allowed it to bind c-SRC and retain it in the cytoplasm (**Fig. 7**), where it phosphorylated and activated the MAPK/ERK signaling cascade (Y. Wang et al., 2011). As for canonical WNT signaling, AMOTL2 regulated WNT pathway trapping β-CAT in recycling endosomes (**Fig. 7**), which blocks its translocation into nucleus and subsequent activation of gene expression in both zebrafish and human (Agarwala et al., 2015; X. Chen et al., 2021; Hultin et al., 2014; Z. Li et al., 2012).

AMOTL2 was reported to regulate cell size, tissue architecture, and cytoskeleton, predominantly in Hippo-dependent manner, in various endothelial and epithelial, immortalized and transformed, mouse, canine, and human cell lines. However, AMOTL2 role in primed hPSCs was not previously studied. Dattani et al. knocked out AMOTL2 in naive hPSCs, which resulted in destabilization of the naive pluripotency and differentiation towards trophectoderm (Dattani et al., 2022). Naïve, primed, and formative pluripotency are different pluripotency stages. Under standard culture conditions, hPSCs cell lines are a mixture of primed and formative pluripotency, with the proportions depending on the cell line (Arthur et al., 2024). With specific culture conditions applied, hPSCs can be maintained in the naive stage. The pluripotency stages differ significantly in terms of colony morphology, gene regulatory networks and pathway dependency, epigenetic state, energy metabolism, self-renewal and ability to form all three germ layer derivatives *in vitro* (Arthur et al., 2024; Pera & Rossant, 2021), and therefore it is reasonable that AMOTL2 deficiency might have a different influence on primed and naive hPSCs. The *AMOTL2* mRNA expression was observed in human iPSCs (Pagliari et al., 2021) and the presence of AMOTL2 protein was identified in hPSC line H9 (Zaltsman et al., 2019), but its role was not followed up by authors. AMOTL2 mRNA

and protein expression were also identified in human blastocyst (Hildebrand et al., 2017), yet the functional experiments in this paper were performed with mouse blastocysts.

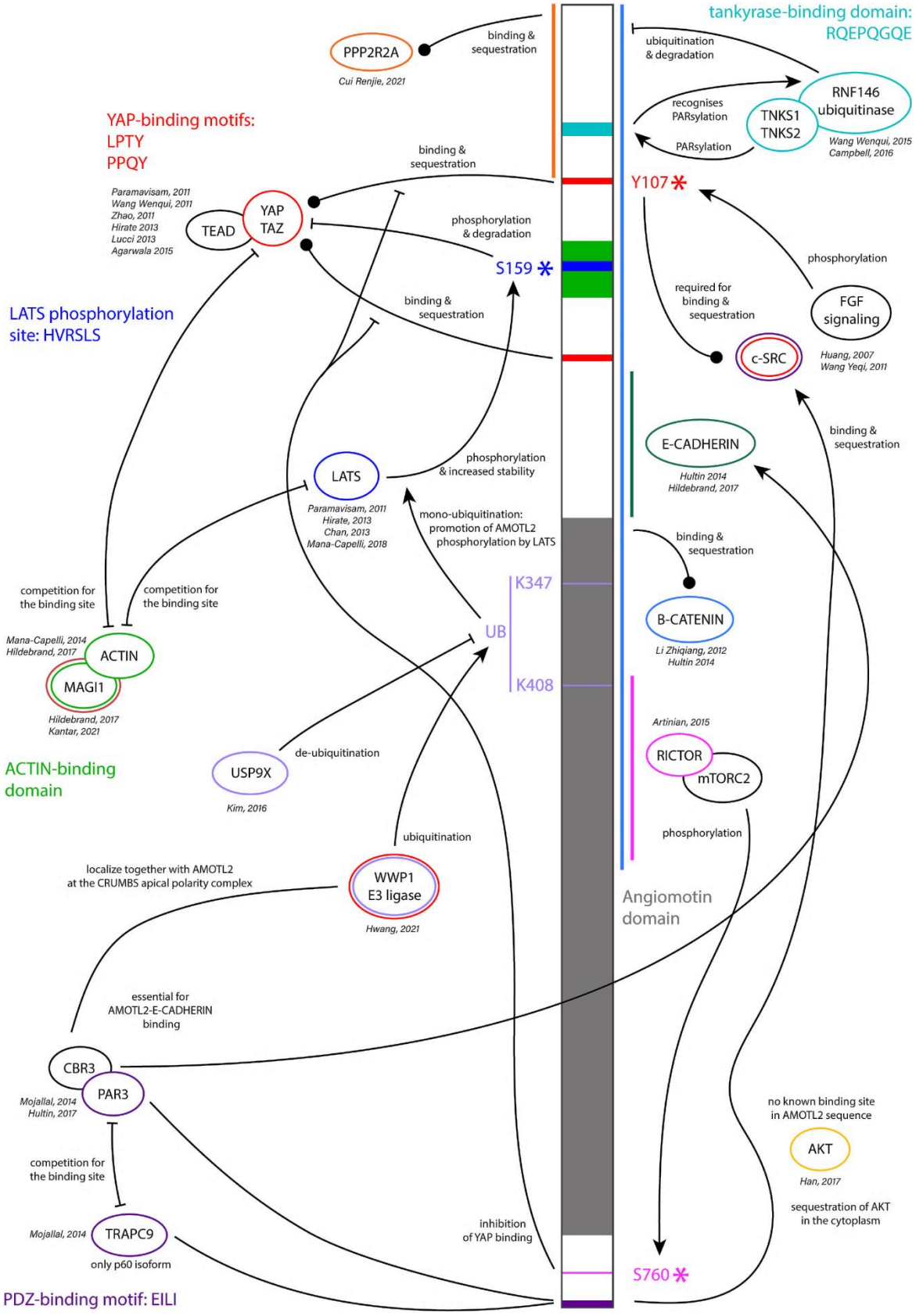

Fig. 7: An overview on AMOTL2 functional domains and interacting partners; * - phosphorylation, UB - ubiquitination, K – lysine, S – serine, ● - binding & sequestration; ➞ - activation; ⊣ - inhibition; colors of the proteins correspond with the binding places within AMOTL2 sequence

2. Aims of the thesis

1. To establish AMOTL2 expression patterns in developing human pancreas *in vivo* and confirm the existence of the NGN3(+) / AMOTL2(+) EPs.
2. To establish AMOTL2 expression patterns in hPSCs *in vitro* and confirm the existence of the NGN3(+) / AMOTL2(+) EPs.
3. To assess the transcriptional differences between AMOTL2(+) and AMOTL2(-) populations in human EPs.
4. To design and generate hPSC lines with AMOTL2 KO.
5. To identify AMOTL2 KO phenotype in hPSCs.
6. To identify AMOTL2 influence on pluripotency and cell fate.

3. Results

3.1. AMOTL2 is expressed in hPSCs and during *in vivo* pancreatic development

In this dissertation I investigated the expression and role of AMOTL2 in human context. For that, I performed a broad meta-analysis of the publicly available scRNA-seq datasets to explore the AMOTL2 expression patterns in hPSCs and pancreatic differentiation.

3.1.1. AMOTL2 is expressed in *NGN3*(+) EPs and other cell types in human fetal pancreas *in vivo* and human pancreatic differentiation *in vitro*

Olaniru et al. (Olaniru et al., 2023) provided a comprehensive work including scRNA-seq data from human fetal pancreas samples from 10 developmental stages, from 8 wpc to 20 wpc, as a publicly available gene browser. I analyzed the *AMOTL2* mRNA expression, to reveal that it could be observed in mesenchyme, endothelial, duct, acinar, and Schwann cells, but importantly, also in the fraction of *NGN3*(+) EPs and early endocrine cells (**Fig. 8A, B**). I extracted the specific

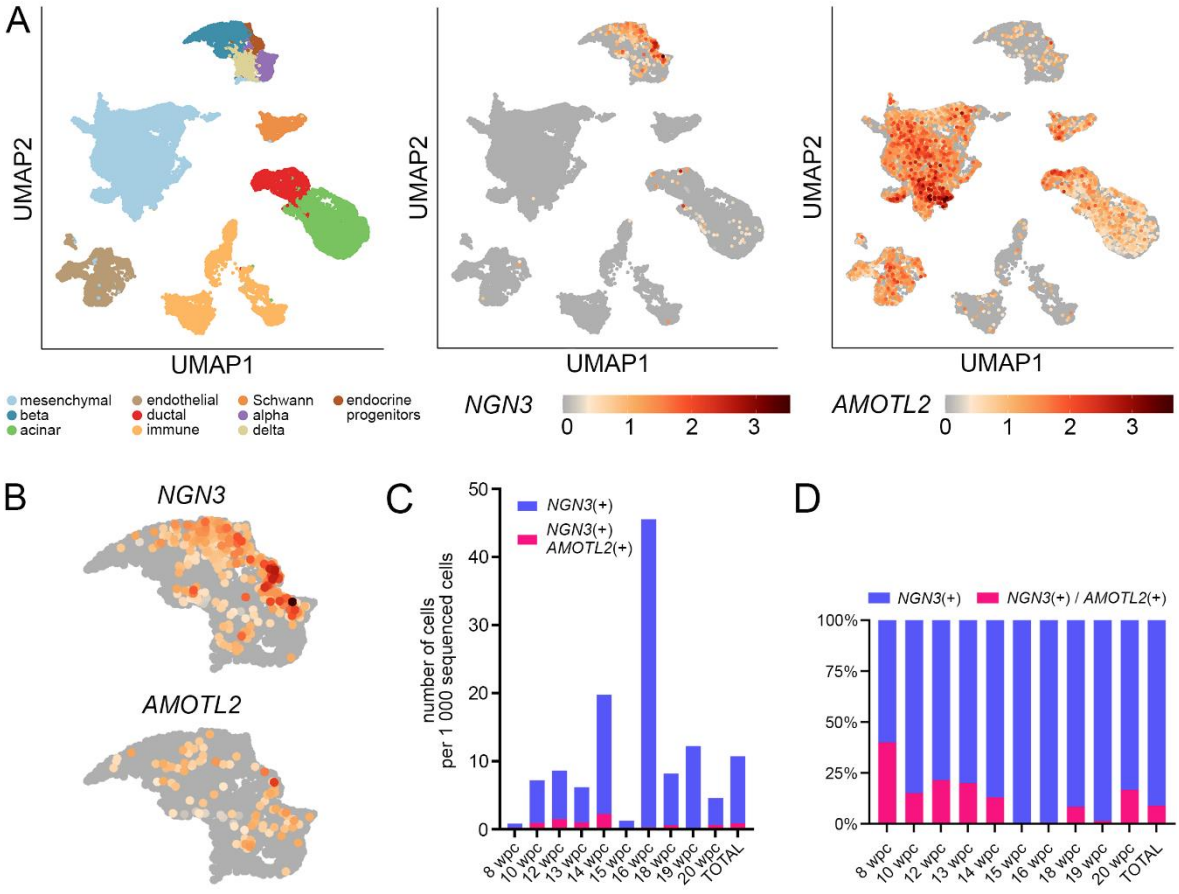

Fig. 8: AMOTL2 expression in NGN3(+) EPs in scRNA-seq of the human developing pancreas from (Olaniru et al., 2023). A. Expression of *NGN3* and *AMOTL2* in the different fetal pancreatic cell types. **B.** The close-up on the EP/endocrine cell cluster with *NGN3* and *AMOTL2* expression. **C.** The number of **NGN3**(+) cells and *NGN3*(+) / *AMOTL2*(+) cells identified at the consecutive developmental stages normalized to 1 000 sequenced cells. **D.** Fraction of *AMOTL2*(+) cells among *NGN3*(+) EPs. EPs – endocrine progenitors; UMAP - Uniform Manifold Approximation and Projection

cell numbers (**Table 1**) showing 524 *NGN3*(+) cells within 53 204 sequenced cells among 10 developmental stages.

This accounts for less than 1% of all cells, showing how small and transient the *NGN3*(+) EP population is. I also identified the *NGN3*(+) / *AMOTL2*(+) population, which was previously only identified in mice (Scavuzzo et al., 2018). Among *NGN3*(+) EPs, 47 cells also co-expressed *AMOTL2*, which is 9% of *NGN3*(+) cells, and 0.09% of all sequenced cells. For this reason, scRNA-seq is an extremely valuable tool to study *NGN3*(+) / *AMOTL2*(+) progenitors, since conventional methods lack the resolution needed to detect populations this small. The *NGN3*(+) EPs were present at all stages, from 8 wpc to 20 wpc, which is consistent with a previous knowledge about human pancreatic development (Jennings et al., 2013; Nair & Hebrok, 2015; Salisbury et al., 2014). The peak in *NGN3* expression occurred between 14 wpc and 16 wpc. There was a dramatic drop in *NGN3*(+) EP number at 15 wpc, yet this might be a technical artifact, since the number of sequenced cells was significantly lower than at other timepoints (**Table 1**). Further, I showed that the highest number of *NGN3*(+) EPs, calculated per 1 000 sequenced cells, was present at 16 wpc, while the greatest number of *NGN3*(+) / *AMOTL2*(+) cells could be found at 14 wpc (**Fig. 8C**, **Table 1**). Within the stages with higher numbers of *NGN3*(+) EPs (10 - 19 wpc), the fraction of *AMOTL2*(+) cells among *NGN3*(+) EPs reached the highest values of 20% at 12 and 13 wpc (**Fig. 8D, Table 1**).

Table 1: *AMOTL2* mRNA expression in *NGN3*(+) EPs in scRNA-seq of the human developing pancreas. Based on (Olaniru et al., 2023).

	NGN3(+)	*NGN3*(+) / *AMOTL2*(+)	% of *AMOTL2*(+) in *NGN3*(+)	Total number of sequenced cells
8 wpc	5	2	40%	8 267
10 wpc	33	5	15%	5 284
12 wpc	56	12	21%	7 874
13 wpc	35	7	20%	6795
14 wpc	108	14	13%	6 168
15 wpc	2	0	0%	1 579
16 wpc	161	1	1%	3 557
18 wpc	48	4	8%	6 347
19 wpc	70	1	1%	5 814
20 wpc	6	1	17%	1 519
TOTAL	524	47	9%	53 204

Further, I performed the immunofluorescent staining at 10 wpc and 13 wpc human fetal pancreas and confirmed AMOTL2 protein expression at both timepoints. I quantified the numbers of AMOTL2(+) cells and the level of its co-expression with other pancreatic markers. I found more AMOTL2(+) cells at 13 wpc than at 10 wpc, which is in line with scRNA-seq data (Olaniru et al., 2023). At 10 wpc all AMOTL2(+) cells co-expressed the pan-endocrine marker CHGA and 90%

of AMOTL2(+) cells co-expressed β-cell marker, C-PEP (**Fig. 9A, B**). At 13 wpc, the vast majority of AMOTL2(+) cells (~95%) co-expressed CHGA and α-cell marker GCG (Fig. 9E, F), and ~50% co-expressed also β-cell marker C-PEP (**Fig. 9C, D, F**). This is consistent with the presence of multihormonal C-PEP(+) / GCG(+) cells during early pancreatic development (Riopel et al., 2014). There were almost no AMOTL2(+) / SST(+) cells at 13 wpc (**Fig. 9D, F**).

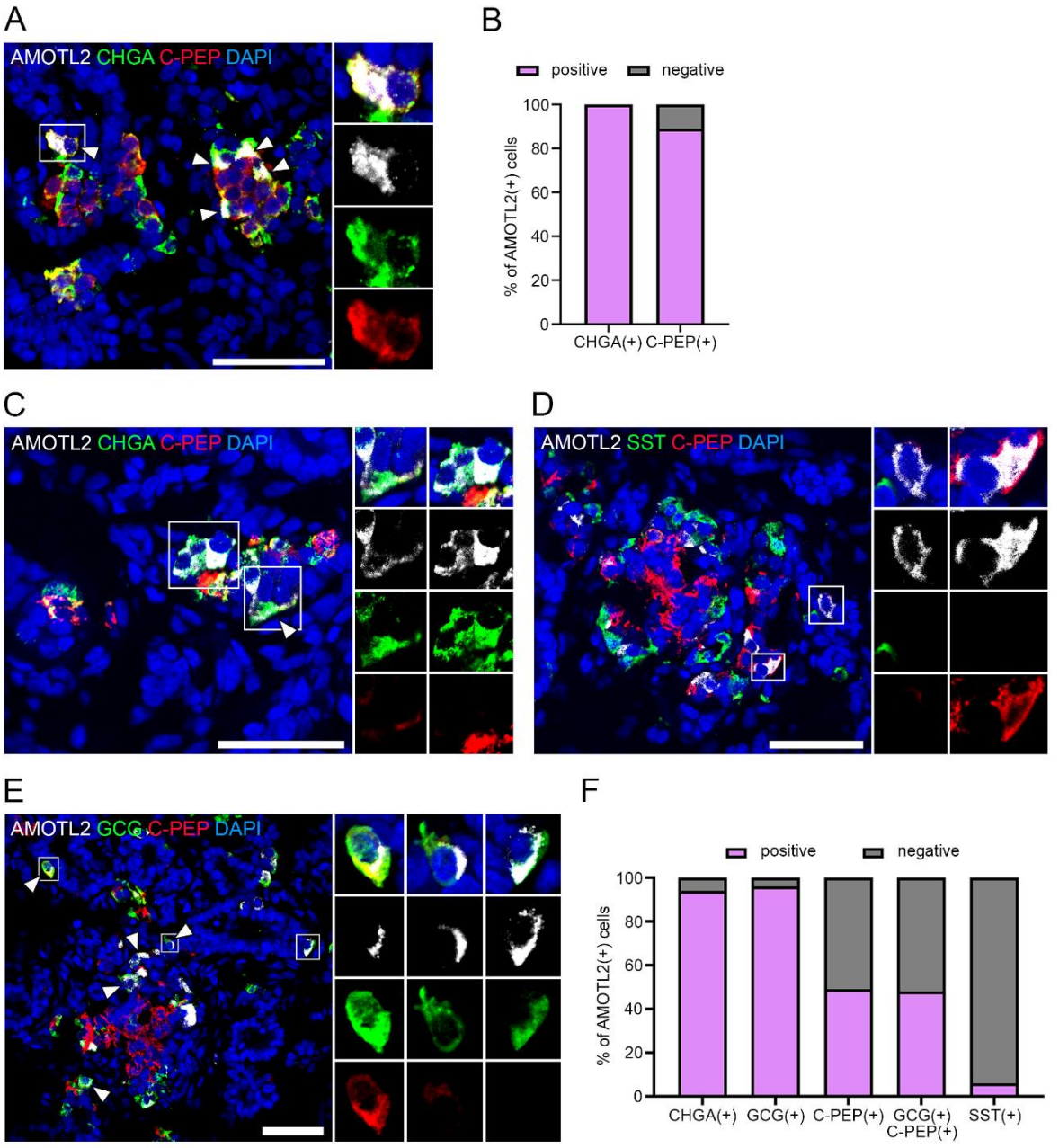

Fig. 9: AMOTL2 protein expression in the samples of human developing pancreas from 10 and 13 wpc. **A.** Representative images of immunofluorescent staining at 10 wpc against AMOTL2 (white), CHGA (green), and C-PEP (red). Nuclei are stained in blue with DAPI. The arrows and close-up show cells co-expressing all three proteins. Scale bar = 50 μm. **B.** Quantification of protein co-expression at 10 wpc, showing the fraction of AMOTL2(+) / CHGA(+) or AMOTL2(+) / C-PEP(+) cells. **C-E.** Representative images of immunofluorescent staining at 13 wpc: **C.** against AMOTL2 (white), CHGA (green), and C-PEP (red). **D.** against AMOTL2 (white), SST (green), and C-PEP (red). **E.** against AMOTL2 (white), GCG (green), and C-PEP (red). Nuclei are stained in blue with DAPI. The arrows and close-ups show cells co-expressing different combinations of markers. Scale bar = 50 μm. **F.** Quantification of protein co-expression at 13 wpc, showing the fraction of AMOTL2(+) / CHGA(+), AMOTL2(+) / GCG(+), AMOTL2(+) / C-PEP(+), AMOTL2(+) / SST(+) or triple-positive AMOTL2(+) / GCG(+) / C-PEP(+) cells.

I also performed the meta-analysis of scRNA-seq data from hPSC pancreatic differentiation, which serves as an in vitro model of human pancreatic development. In both analyzed datasets, *AMOTL2* was expressed at the very low levels from the beginning of the differentiation,

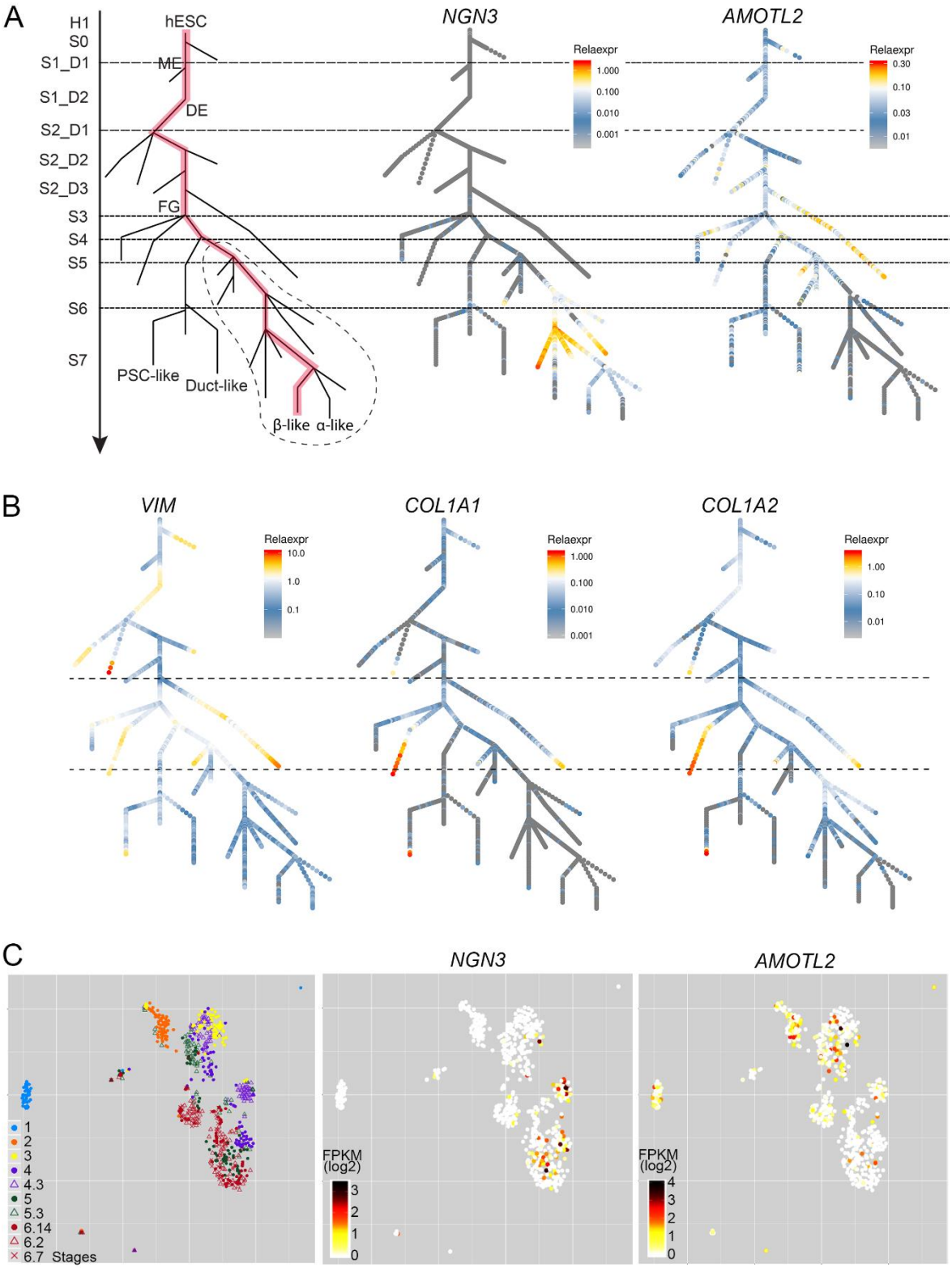

Fig. 10: *AMOTL2* expression in scRNA-seq datasets of hPSC pancreatic differentiation from (Weng et al., 2020) (A-B) and (Sharon, Vanderhooft, et al., 2019) (C). hESC – human embryonic stem cells, ME – mesendoderm, DE – definitive endoderm, FG – foregut, PSC – pancreatic stellate cells, H1 – H1 cell line, S – stage, D – day, FPKM – fragments per kilobase million

with the peak at the PP stage (stage 4) and in early EPs (stage 5), and its expression did not persist into endocrine β-cells (**Fig. 10A, C**)(Sharon, Vanderhooft, et al., 2019; Weng et al., 2020). Additionally, in the first dataset, the low expression of *AMOTL2* could be found in duct-like cells (**Fig. 10A**) (Weng et al., 2020). The highest expression of *AMOTL2* occurred in the branch unidentified by authors yet based on the expression of *VIM* (Vimentin), *COL1A1* (Collagen Type I Alpha 1 Chain), and *COL1A2* (Collagen Type I Alpha 2 Chain), I hypothesized that it could be a mesenchymal lineage (**Fig. 10A, B**).

Further, I analyzed the scRNA-seq data of *in vitro* pancreatic differentiation from our laboratory. The original experiment was carried out by Dr. Natalia Ziojła as a part of her PhD thesis, to compare wild type (WT) and ETV1 KO cells at day 12 (d12) of pancreatic differentiation. Day 12 in our protocol is stage 4 when both PP and EP cells are present. Using Loupe Browser, I analyzed the scRNA-seq data using only WT dataset and identified the clusters based on the known marker gene expression (**Fig. 11A**). I assigned the *VIM*(+) / *COL1A1*(+) cluster as mesenchyme (**Fig. 11A-C**), *NKX6.1*(+) / *PDX1*(+) cluster as PPs (**Fig. 11A, D, E**), *NGN3*(+) cluster as early EPs (**Fig. 11A, G**), and *NGN3*(-) / *NEUROD1*(+) cells as late EPs which adopt endocrine fate (**Fig. 11A, G, H**). I further subclustered PP and *NGN3*(+) EP populations to extract *AMOTL2*(+) cells in both groups. Among total of 5 943 sequenced cells, 393 *NGN3*(+) cells (6.6% of total population) and 70 *NGN3*(+) / *AMOTL2*(+) cells (1.2% of total population and 17.8% of *NGN3*(+) EPs were identified. Among 4 696 PP cells, 1 281 co-expressed *AMOTL2* (27.3% of PPs and 21.6% of all sequenced cells). *AMOTL2* expression was also identified in 47% of the mesenchymal cells.

Next, I plotted the expression of known EP/early endocrine markers. During development, *NGN3* appears first, marking the start of the EP population, and activating the expression of its downstream target *NEUROD1* (H.-P. Huang et al., 2000). *CHGA* is activated in EPs that adopt endocrine cell fate and start to express pancreatic hormones (Portela-Gomes et al., 2008). *FEV* (FEV Transcription Factor, ETS Family Member) was identified in mice as a late EP/early endocrine marker and its expression was also confirmed in human development (Byrnes et al., 2018). Finally, *INS* is expressed in late EP and committed β-cells. In our scRNA-seq data from d12 pancreatic differentiation these markers followed similar pattern, increasing from *NGN3*(+) / *AMOTL2*(+) cells, through *NGN3*(+) / *AMOTL2*(-) cells, up to late EPs (**Fig. 11G-K**), which suggests that *NGN3*(+) / *AMOTL2*(+) cells are the developmentally younger EP population than *NGN3*(+) / *AMOTL2*(-) cells.

Further, I extracted a group of differentially expressed genes (DEGs) between *NGN3*(+) / *AMOTL2*(+) and *NGN3*(+) / *AMOTL2*(-) EPs. Within genes upregulated in *NGN3*(+) / *AMOTL2*(-) EPs there were *CHGA* and *INS* (**Fig. 12A**), which further confirms that this cluster is developmentally older than *NGN3*(+) / *AMOTL2*(+) EPs. Interestingly, several genes connected with cell adhesion and migration were identified among the genes upregulated in the *NGN3*(+) / *AMOTL2*(+) cluster (**Fig. 12A**). For instance, FN1 (Fibronectin 1) gene was identified, which is known to regulate cell adhesion, migration processes including those during embryogenesis, wound healing, and metastasis

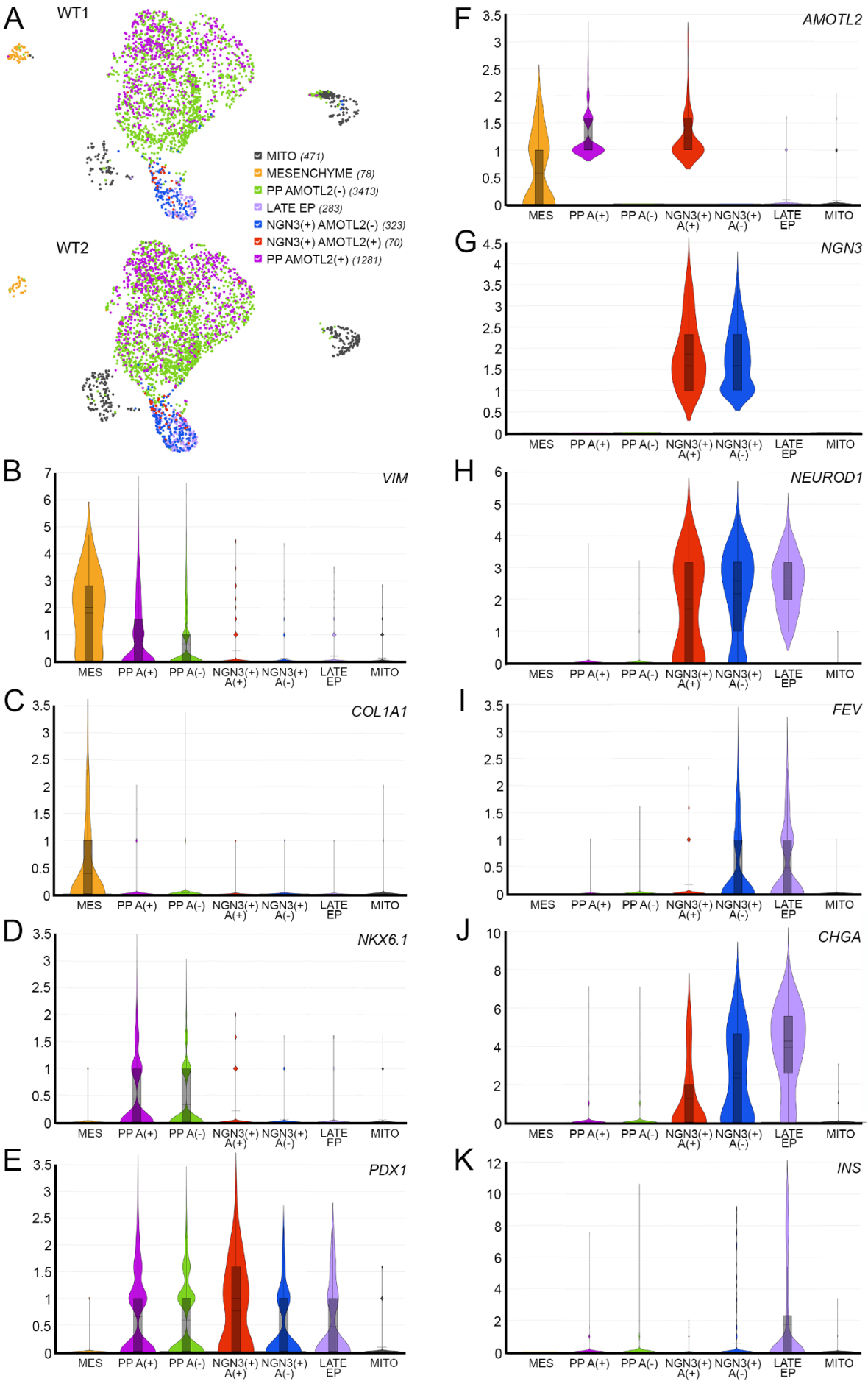
A
WT1
WT2
MITO (471)
MESENCHYME (78)
PP AMOTL2(-) (3413)
LATE EP (283)
NGN3(+) AMOTL2(-) (323)
NGN3(+) AMOTL2(+) (70)
PP AMOTL2(+) (1281)
B
VIM
C
COL1A1
D
NKX6.1
E
PDX1
F
AMOTL2
G
NGN3
H
NEUROD1
I
FEV
J
CHGA
K
INS
MES
PP A(+)
PP A(-)
NGN3(+) A(+)
NGN3(+) A(-)
LATE EP
MITO

Fig. 11: The analysis of the scRNA-seq of day 12 hPSC pancreatic differentiation (performed in our laboratory by Dr. Natalia Ziojła). A. The UMAP plots for two biological replicates with marked clusters. Numbers in the brackets indicate the number of cells in respective clusters. **B-K.** Expression of the selected genes in clusters. **B-C.** marker genes for the mesenchyme cluster: *VIM* (**B**) and *COL1A1* (**C**); **D-E.** marker genes for the PP cluster: *NKX6.1* (**D**) and *PDX1* (**E**); **F.** *AMOTL2* expression; **G-K.** expression of EP/early endocrine markers: *NGN3* (**G**), *NEUROD1* (**H**), *FEV* (**I**), *CHGA* (**J**), *INS* (**K**). WT - wild type, MITO - mitochondrial, PP - pancreatic progenitors, EP - endocrine progenitors, MES - mesenchyme, A - AMOTL2

(Patten & Wang, 2021; Zollinger & Smith, 2017). Further, SLIT3 (Slit Guidance Ligand 3), which interacts with Roundabout signaling pathway to affect cell migration by actin polymerization and is required for β-cell survival (Geutskens et al., 2012; Yang et al., 2013). SEMA3C (Semaphorin 3C) is a neuronal guidance cue and correlates with changes in cell invasion and adhesion in cancer (Bica et al., 2023; Toledano et al., 2019). FRAS1 (Fraser Extracellular Matrix Complex Subunit 1) is predicted to regulate epidermal-basement membrane adhesion and organogenesis an to be involved in ECM organization (Pavlakis et al., 2011; Short et al., 2007). Finally, NRG3 (Neuregulin 3) affects neuroblast proliferation, migration, and differentiation by signaling through ERBB4 (Erb-B2 Receptor Tyrosine Kinase 4) (Anton et al., 2004; Howard, 2008).

Next, I performed the functional term enrichment analysis to compare *NGN3*(+) / *AMOTL2*(+) with *NGN3*(+) / *AMOTL2*(-) population (**Fig. 12B**). The biological processes upregulated in *NGN3*(+) / *AMOTL2*(+) cluster included terms associated with development (nervous system development, neural tube development, heart development, muscle organ development, and body morphogenesis), cell adhesion and migration (chemorepulsion involved in cell migration, cardiac endothelial to mesenchymal transition, response to wounding, cell attachment to the substrate, cell-matrix adhesion, and cell-substrate junction assembly), and regulation of proliferation and apoptosis. Additionally, three signaling pathways were identified: non-canonical WNT pathway, TGFβ pathway, and Roundabout pathway. Within biological processes downregulated in *NGN3*(+) / *AMOTL2*(+) cluster, there were terms connected with regulation of cardiac muscle contraction and relaxation, nervous system and neurotransmitter production (serotonin biosynthetic process, dopamine biosynthetic process, catecholamine biosynthetic and metabolic process, neurotransmitter loading into synaptic vesicle, neuron projection maintenance), and regulation of G-protein-coupled receptor signaling pathway. Moreover, there was a group of downregulated terms including positive regulation of dense core granules, protein localization to secretory granules, positive regulation of peptide hormone secretion, negative regulation of glycogen catabolic process, which are all terms connected with insulin production by β-cells.

Summarizing, *NGN3*(+) / *AMOTL2*(+) cluster was enriched in terms associated with development, adhesion, and migration, while in *NGN3*(+) / *AMOTL2*(-) cluster dominate terms connected with hormone and neurotransmitter biosynthesis and secretion, suggesting the endocrine commitment. This further supports the hypothesis that *NGN3*(+) / *AMOTL2*(+) EPs developmentally

precede *NGN3*(+) / *AMOTL2*(-) EPs and that *NGN3*(+) / *AMOTL2*(+) cells might be a delaminating EP population.

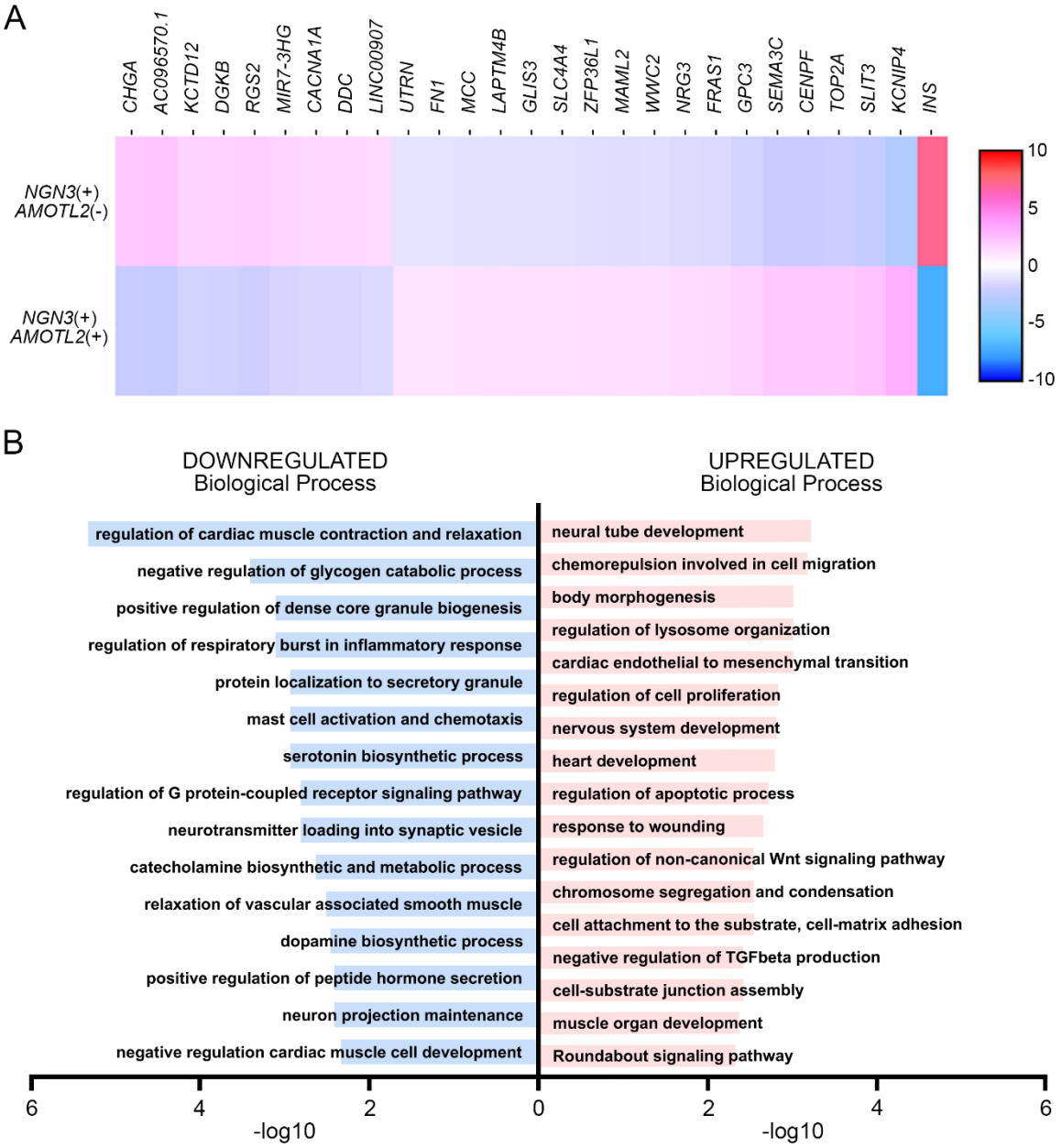

Fig. 12: Comparison of *NGN3*+ / *AMOTL2*(+) and *NGN3*+ / *AMOTL2*(-) cluster expression profiles. A. Heatmap showing the significant differentially expressed genes (DEGs) in the *NGN3*(+) / *AMOTL2*(+) population, compared to the *NGN3*(+) / *AMOTL2*(-) population (p-value<0.01). Heatmap generated with the Loupe Browser software. **B.** Selected biological processes significantly changed in the *NGN3*(+) / *AMOTL2*(+) population, compared to the *NGN3*(+) / *AMOTL2*(-) population.

3.1.2. AMOTL2 is not expressed in endocrine cells in adult human pancreas

Data from scRNA-seq datasets from human developing pancreas and *in vitro* pancreatic differentiation, suggested that *AMOTL2* expression could be found in a fraction of the earliest hormone-producing cells, yet its expression did not seem to persist in mature endocrine cells. To confirm this, I examined several scRNA-seq data (Baron et al., 2016; Enge et al., 2017; Fang et al., 2019) from adult human pancreata to reveal *AMOTL2* absence in endocrine cells but presence in a fraction of ductal and pancreatic stellate cells (**Fig. 13A-C**). Additionally, in two datasets (**Fig. 13B, C**) (Baron et al., 2016; Enge et al., 2017), *AMOTL2* was expressed in a portion of acinar and endothelial cells.

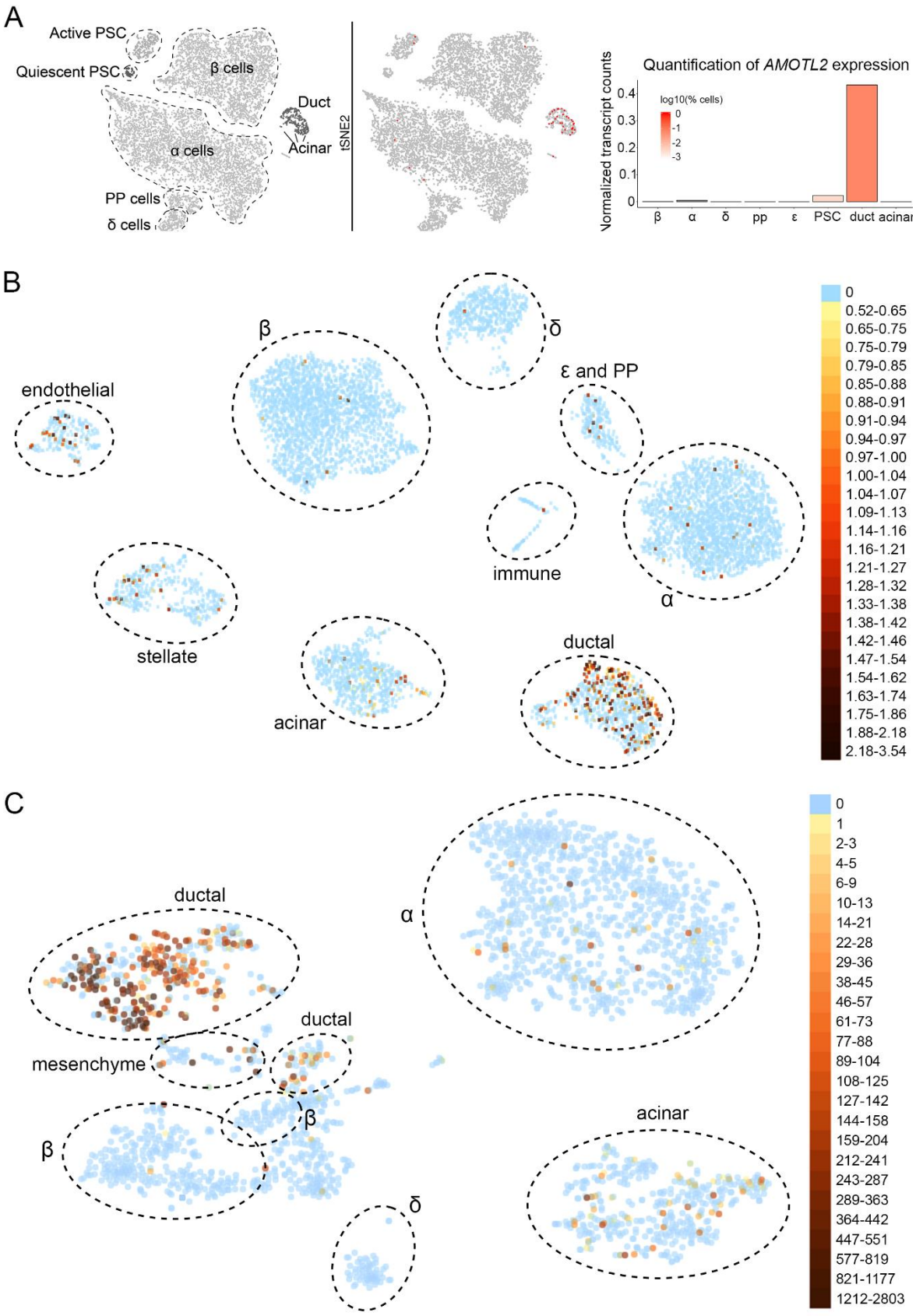

Fig. 13: *AMOTL2* in adult pancreas. A. based on (Z. Fang et al., 2019) **B.** based on (Baron et al., 2016) **C.** based on (Enge et al., 2017); PSC - pancreatic stellate cells, PP – pancreatic polypeptide cells

3.1.3. AMOTL2 is expressed in hPSCs and definitive endoderm

The hPSC pancreatic differentiation atlases showed *AMOTL2* expression also at the pluripotent and DE stage of pancreatic differentiation (**Fig. 10A, C**). Therefore, I also included the analysis of scRNA-seq datasets from *in vivo* preimplantation embryos and different hPSC lines.

AMOTL2 mRNA was detected in hPSCs, and its expression increased as they differentiated into DE (Yiangou et al., 2019) (**Fig. 14A**). *AMOTL2* could also be found in human preimplantation embryos (**Fig. 14B-D**). In the data from Petropoulos et al. (Petropoulos et al., 2016), *AMOTL2* was expressed from late e4 (morula) stage till e7 (late blastocyst) stage (**Fig. 14B**). Similarly, at GRAPPA atlas (Boroviak et al., 2018), *AMOTL2* expression started at the morula stage and persisted in both early and late ICM (**Fig. 14C**). Additionally, in Yan dataset (Yan et al., 2013), *AMOTL2* was expressed at blastocyst stage, and in hESCs isolated from ICM (**Fig. 14D**).

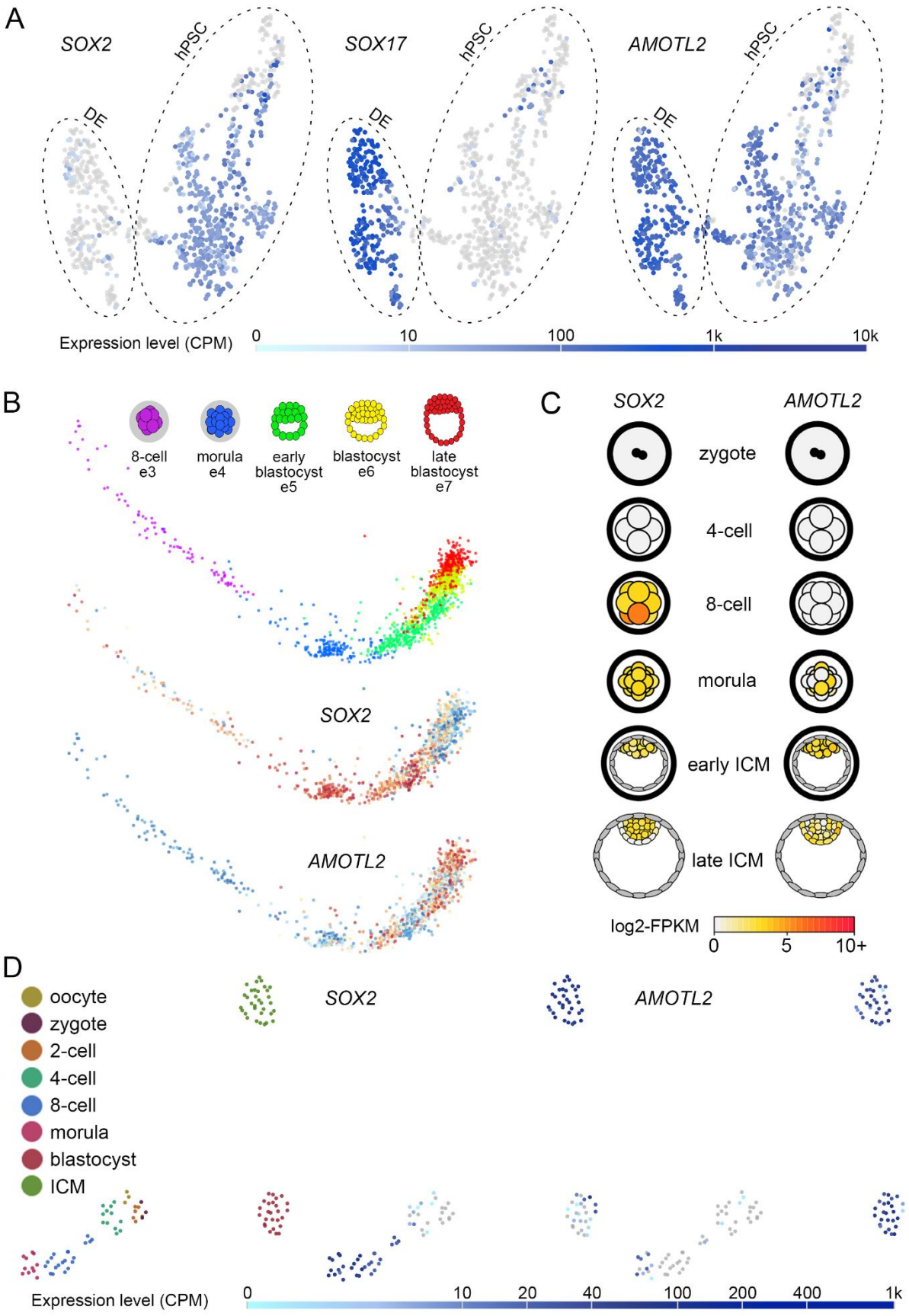

Fig. 14: *AMOTL2* in human embryo, hPSCs and definitive endoderm. SOX2 - hPSC marker, SOX17 - definitive endoderm marker **A.** based on (Yiangou et al., 2019) **B.** based on (Petropoulos et al., 2016) **C.** based on GRAPPA expression atlas (Boroviak et al., 2018) **D.** based on (Yan et al., 2013); hPSC - human pluripotent stem cells, DE - definitive endoderm, ICM - inner cell mass, CPM - counts per million (mapped reads), FPKM - fragments per kilobase million

Further, I examined the gene expression of angiomotin family members in the Hues8-iCas9 hPSC line by bulk RNA-sequencing (RNA-seq), confirming *AMOTL2* expression at mRNA level. The expression level of *AMOTL1* was comparable to *AMOTL2*, while *AMOT* expression was 20-fold lower (**Fig. 15A**). I also performed the immunostaining to confirm that at the protein level, the vast majority of SOX2(+) hPSCs co-express AMOTL2 (**Fig. 15B**).

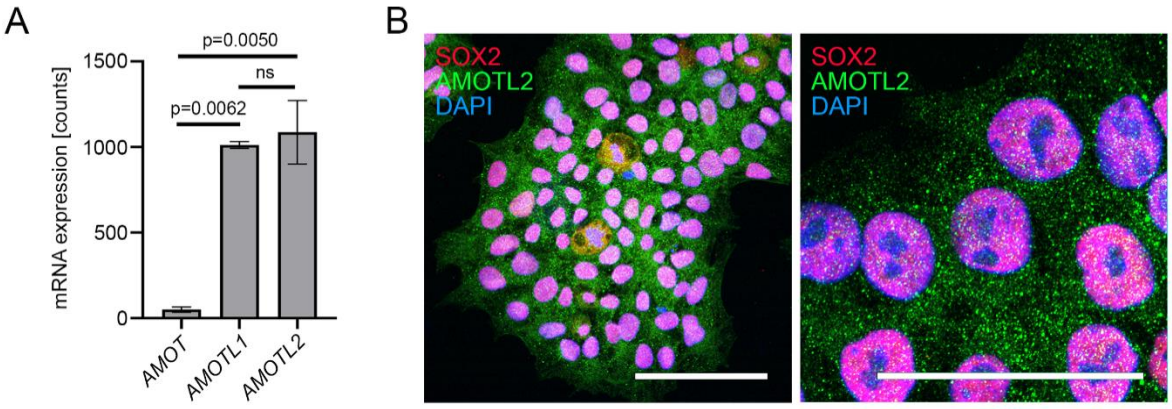

Fig. 15: AMOTL2 in hPSCs. A. AMOT family mRNA expression assessed by bulk RNA-seq. Statistics: t-Student test N=2 **B.** Representative images of immunostaining against SOX2 (red) and AMOTL2 (green). Nuclei stained in blue with DAPI. N=3 Left panel: scale bar = 100 µm. Right panel: scale bar = 50 µm.

3.2. AMOTL2 knockout in hPSCs with CRISPR-Cas9 method

To experimentally explore the role of AMOTL2 in pluripotency and *in vitro* pancreatic differentiation, I generated hPSC line with AMOTL2 gene KO using the clustered regularly interspaced short palindromic repeats (CRISPR)-Cas9 system. I designed the single guide RNAs (sgRNAs) according to the following criteria:

- I chose three sgRNAs, with 75 nt and 50 nt intervals (**Fig. 16B, C**). First, such an approach increases the specificity of the targeting in comparison to only one sgRNA. Second, it improves the chance of creating either one long or many smaller deletions, which is harder to be repaired by the cell compared to the single short deletion, and therefore increases the frameshifting rate and KO efficiency.
- To generate a deletion and induce frameshifting resulting in the premature STOP codon early in the aa sequence, in a way that would change amino acid sequence before any identified domain (**Fig. 16A, C**).
- To cover as many isoforms as possible. There are ten known isoforms of AMOTL2, ranging from 33 aa to 837 aa (**Fig. 16B**), with a canonical isoform of 779 aa. I compared the isoform amino acid sequences and selected a fragment common for all but one isoform (33aa). Targeting such sites in the KO experiment minimizes the potential functional compensation by remaining isoforms. Importantly, 33 aa isoform does not contain any identified domains.

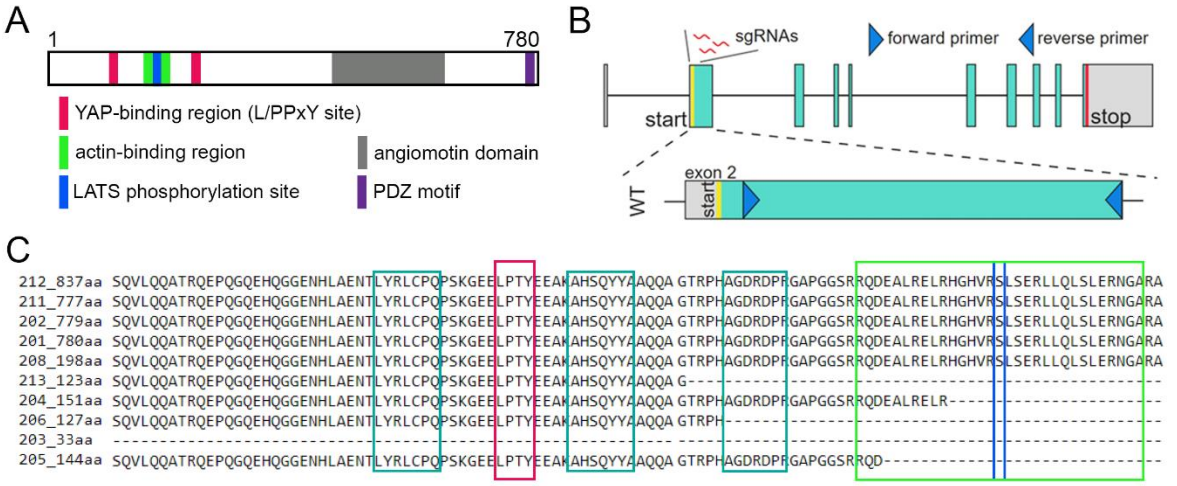

Fig. 16: AMOTL2 knockout in hPSCs using CRISPR/Cas9 method. A. Functional domains within AMOTL2 protein sequence (based on Mana-Capelli, 2014) **B.** AMOTL2 KO design strategy with primers used for the initial readout of the deletion presence and its approximate length. **C.** Detailed positions of selected sgRNAs (dark green) in relation to protein domains: YAP-binding region (red), actin-binding region (light green), and LATS phosphorylation site (blue).

I generated AMOTL2 KO in Hues8-iCas9 cells, a hPSC line with doxycycline-inducible Cas9 protein expression (Zhu et al., 2014). This cell line was developed using TALEN technique to insert the Cas9 protein-coding inducible cassette into AAVS1 locus. This system significantly increases the KO efficiency since it requires transfection with only sgRNAs instead of the additional plasmid

encoding Cas9 protein. I introduced the sgRNAs into Hues8-iCas9 cells in various combinations and performed bulk DNA isolation and sequencing to find the sgRNA set with the highest KO efficiency. I analyzed the results using ICE (Interference of CRISPR Edits) analysis software by Synthego (Conant et al., 2022) (**Fig. 17**, **Fig. 18**), which conducts deconvolution of bulk sequencing data and displays the types of indel (insertion-deletion) events within the sample. ICE analysis showed generally low KO efficiency, up to 31% of indel (insertion-deletion) events, and 27% of STOP codon-inducing indels. The most commonly occurring mutation was 1nt insertion at sgRNA_B cut site. Longer deletions accounted for up to 8%.

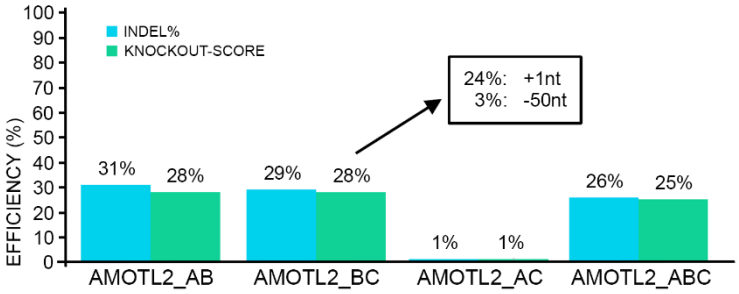

Fig. 17: AMOTL2 KO efficiency depending on the combination of sgRNA used. A, B, C - sgRNAs, INDEL - insertion-deletion

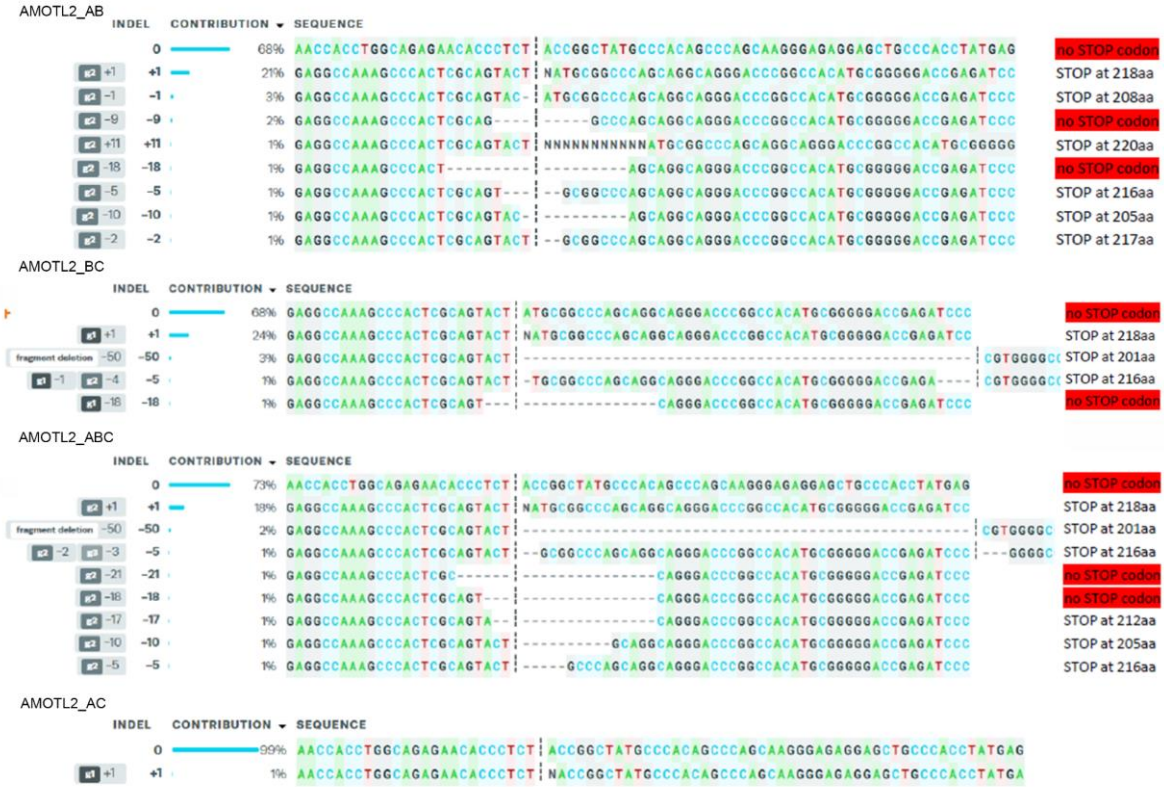

Fig. 18: ICE analysis of AMOTL2 KO including the exact mutation and the frequency of their occurrence

Next, I selected the transfections with the highest frequency of longer deletions (BC and ABC) (**Fig. 17**), passaged them into single cells and cultured into colonies to ensure the clonal AMOTL2 KO cell lines. After 10 days, I isolated the DNA from each clonal line, performed PCR (polymerase chain reaction) with primers encompassing the deletion (**Fig. 19A**), and sequenced selected PCR products to determine the exact mutations (**Table 2**).

For further analyses I selected the AD3 clone, with nonsense mutations on both alleles and presence of multiple STOP codons close to the deletion site (**Fig. 19B, C**). At the first allele there was 83nt deletion resulting in a frameshift and STOP codon at 132aa. At the second allele there was 50nt deletion resulting in frameshift and STOP codon at 143aa. Both mutations removed the actin binding site, and the second YAP-binding motif. Additionally, at allele one the first YAP-binding motif was also lost due to frameshift. The AD3 clone will be further referred to as AMOTL2 KO. Some experiments were also conducted on AD6 (-1nt/-1nt homozygous knockout) and AA3 (a heterozygote with monoallelic mutation of -10nt), in which cases it will be clearly stated.

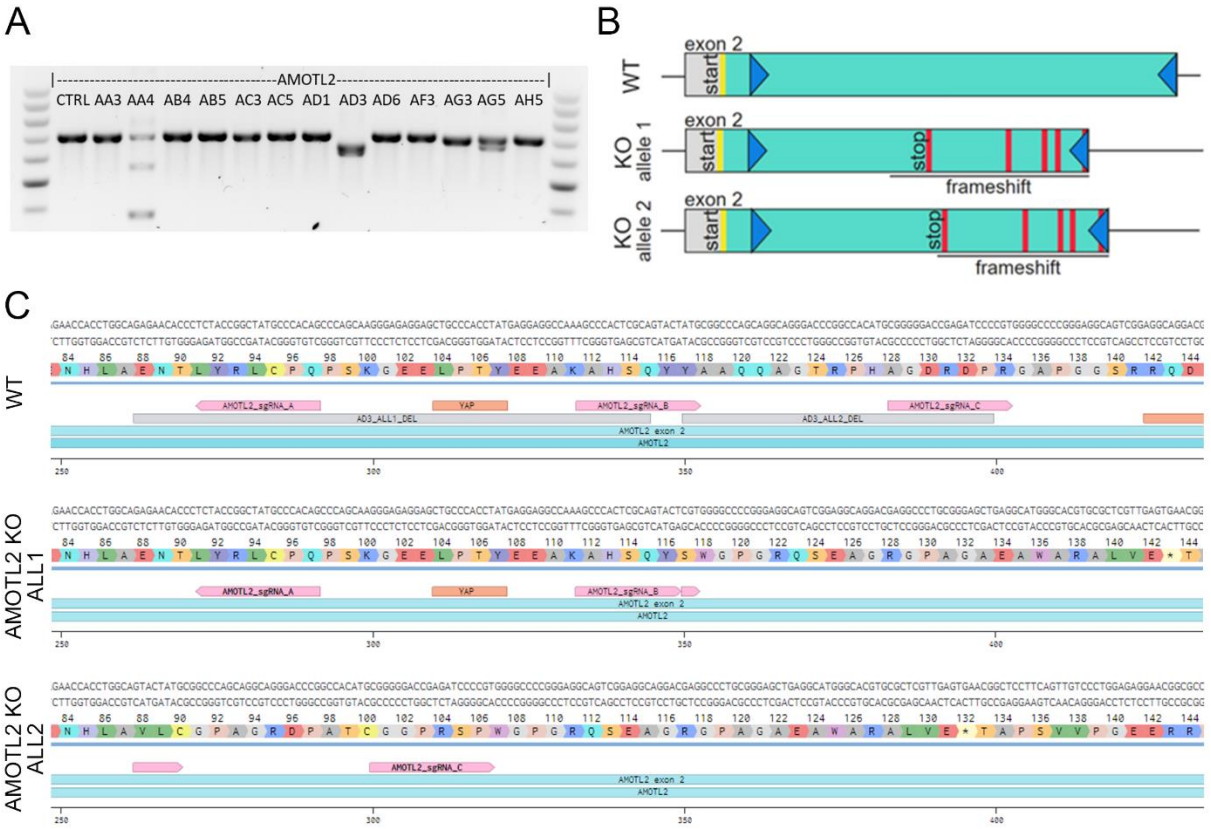

Fig. 19: AMOTL2 KO in hPSCs. A. Agarose gel electrophoresis of PCR products from single-cell clones. **B.** Schematic outline of the WT and AD3 clone mutations caused by deletion of the parts of DNA. **C.** A detailed view of WT and AD3 clone, showing exact deletions, frameshifting, loss of functional domains and STOP codons. CTRL - control, WT - wild type, KO - knockout, ALL - allele, * - STOP codon, YAP - YAP binding site

Table 2: AMOTL2-deficient single-cell clonal cell lines. The length of the deletions at both alleles is shown and a phenotype is designated. +/- monoallelic mutation, -/- biallelic mutation

	AA3	AB4	AB5	AC3	AF3	AG5	AH5	AC5	AD1	AD3	AD6	AG3
ALLELE_1	-	-	-	-	-	-	-	+1nt	+1nt	-83nt	+1nt	-11nt
ALLELE_2	-10nt	-7nt	+1nt	-5nt	+1nt	-44nt	+1nt	+1nt	+1nt	-50nt	+1nt	-20nt
PHENOTYPE	+/-	+/-	+/-	+/-	+/-	+/-	+/-	-/-	-/-	-/-	-/-	-/-

Additionally, I generated the KO specifically targeting the longest, 837 aa, isoform, which as the only one of AMOTL2 isoforms has an alternative starting site and additional exon at the beginning of the sequence. I used three sgRNAs, targeting a region of the coding sequence in exon 1, which is unique for 837aa isoform (**Fig. 20A**). As previously, I introduced sgRNAs hPSCs, passaged transfected cells into single cells and cultured into colonies to ensure the clonal AMOTL2 knockout cell lines. After 10 days, I isolated the DNA from each clonal line, performed PCR with primers encompassing the deletion (**Fig. 20B**) and sequenced selected PCR products to determine the exact mutations (**Table 3**). I selected three clones - H1, B1, and B8. The H1 one clone had a deletion of 22nt and STOP codon at 52aa at allele one and deletion of 38nt with STOP codon at 22aa at the second allele (**Fig. 20C**). The B1 clone was a heterozygote with a monoallelic deletion of 37nt, and B8 clone was a homozygote with a deletion of 86nt at both alleles. All clones with the deletion in isoform 837aa will be further called AMOTL2(837)-/- in contrast to the clones with deletion in exon 2 of all isoforms, called AMOTL2-/-.

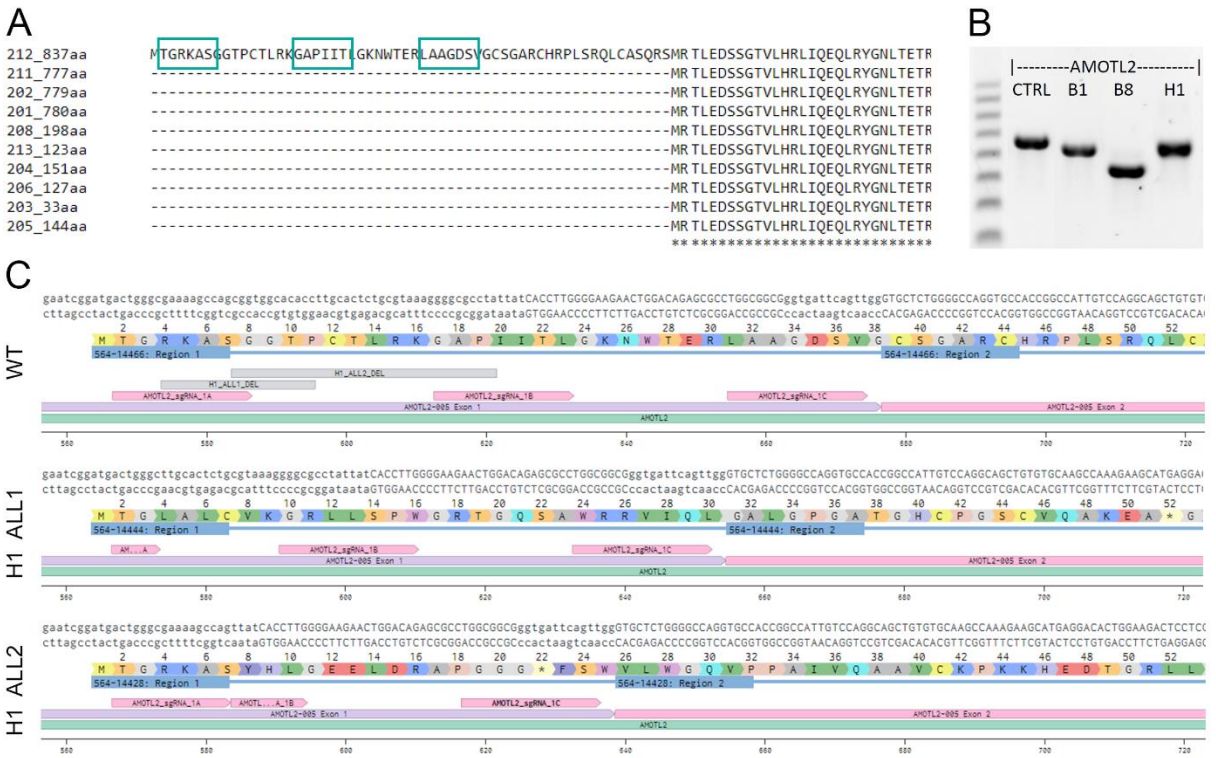

Fig. 20: AMOTL2 KO in hPSCs, isoform 837 aa. A. Detailed positions of the selected sgRNAs targeting specifically isoform 837 aa. **B.** Agarose gel electrophoresis of PCR products from single-cell clones. **C.** A detailed view of WT and H1 clone, showing the exact deletions, frameshifting, and STOP codons. CTRL - control, WT - wild type, ALL - allele, * - STOP codon

Table 3: AMOTL2-deficient single-cell clonal cell lines, isoform 837 aa. The length of the deletions at both alleles is shown and a phenotype is designated. +/- monoallelic mutation, -/- biallelic mutation.

	B1	B8	H1
ALLELE_1	-	-86nt	-22nt
ALLELE_2	-37nt	-86nt	-38nt
PHENOTYPE	+/-	-/-	-/-

3.3. RNA-sequencing of WT and AMOTL2 KO hPSCs

To explore the transcriptional changes in AMOTL2 KO hPSCs compared to WT, bulk RNA-seq was performed. I analyzed the data using iDEP software (Ge et al., 2018). The size of the individual libraries, assessed by total reads count, was similar, oscillating around 6 million read counts per sample (**Fig. 21A**). The distribution (**Fig. 21B**) and density (**Fig. 21C**) of the transformed data (transformation algorithm: EdgeR: log2(CMP+4)) were highly similar between the samples, which made them suitable for the further comparisons.

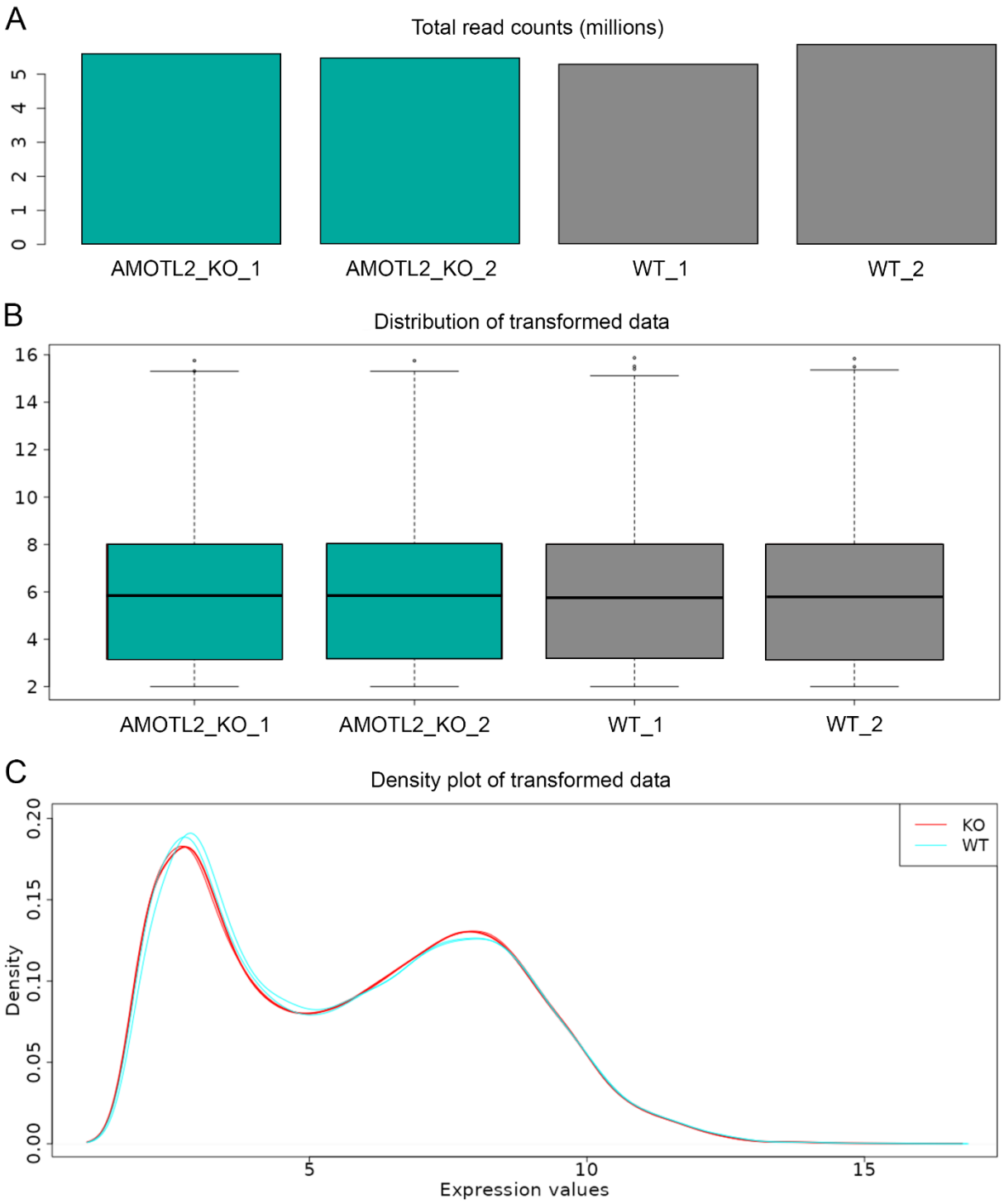

Fig. 21: Preprocessing of the RNA-seq data. A. The size of the libraries as total read counts. **B.** Distribution of the transformed data. **C.** Density plot of the transformed data; WT - wild type, KO - knockout.

I performed the hierarchical clustering based on the 1 000 most variable genes which showed that AMOTL2 KO repeats cluster together and WT repeats cluster together (**Fig. 22**). The WT and AMOTL2 KO samples differed significantly, indicating that AMOTL2 deficiency results in the major changes in the transcriptome.

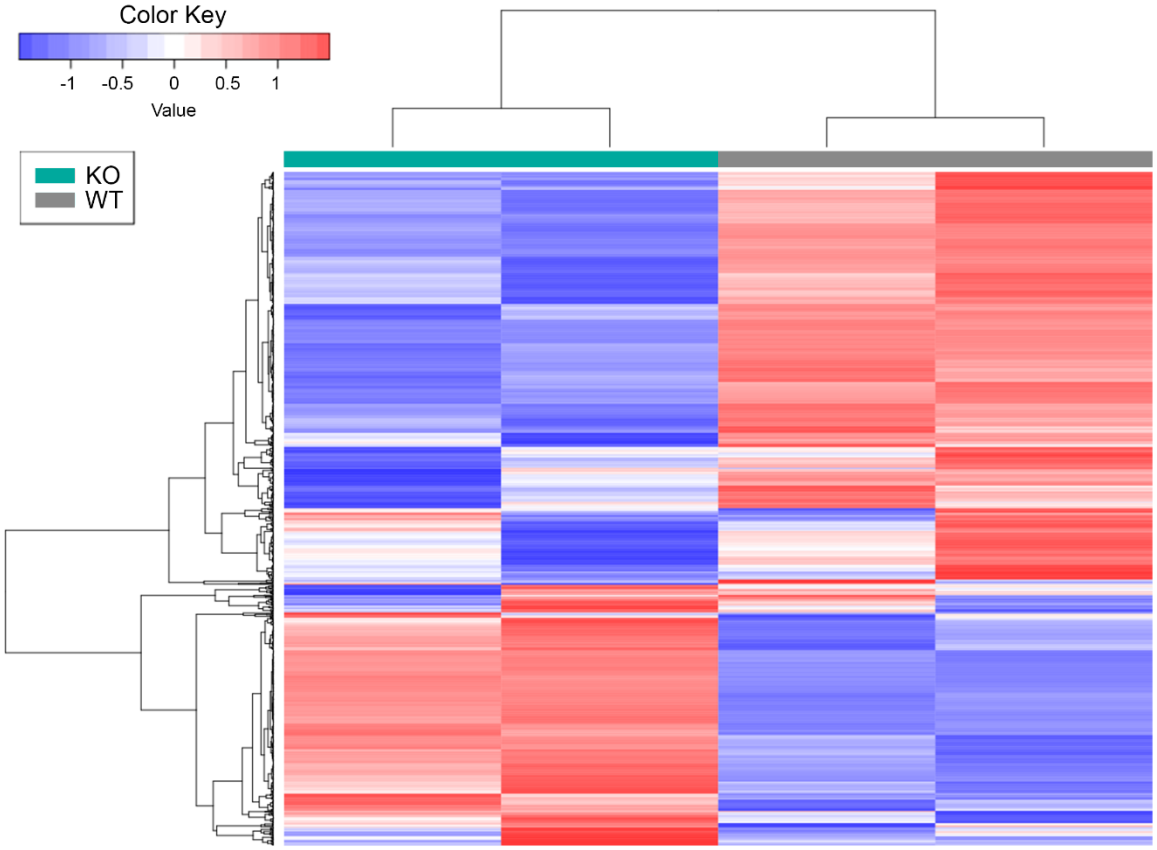

Fig. 22: Hierarchical clustering of 1 000 most variable genes between WT and AMOTL2 KO hPSC samples.
WT - wild type, KO - knockout

Next, I identified DEGs using DESeq2 software (Love et al., 2014) (**Fig. 23**). For FDR (False Discovery Rate) < 0.05 and Fold Change ≥ 2, 238 downregulated and 491 upregulated transcripts were identified in AMOTL2 KO hPSCs compared to WT. For further analysis I used only protein-coding genes, which gives 220 and 460 downregulated and upregulated genes, respectively.

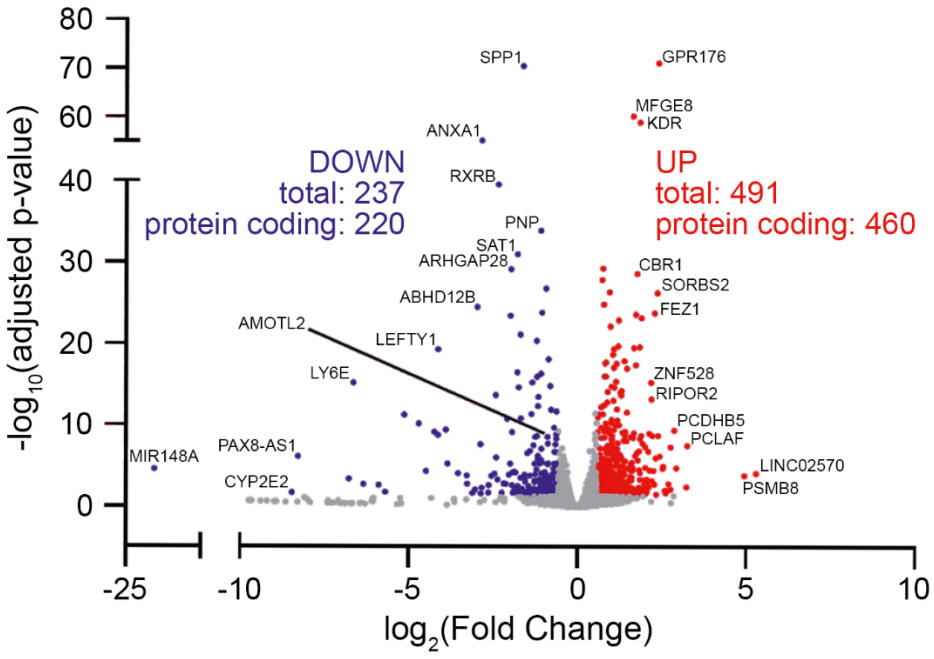

Fig. 23: Volcano plot of statistically significant DEGs between WT and AMOTL2 KO hPSCs.

Using GeneCodis software (Garcia-Moreno et al., 2022), I identified enriched pathways and biological processes (**Fig. 24**). Further, I grouped the statistically significant ($p<0.01$) enriched pathways into four main categories: 1) cell adhesion, extracellular matrix (ECM), and migration (**Fig. 24A**); 2) cell fate and development (**Fig. 24B**); 3) metabolism (**Fig. 24C**); and 4) signaling pathways (**Fig. 24D**).

The downregulated terms associated with cell adhesion (**Fig. 24A**) were ECM, actin filaments and regulation of actin cytoskeleton organization, negative regulation of cell adhesion mediated by integrins, and regulation of cell migration. The upregulated terms connected to cell adhesion included plasma membrane, cell adhesion, cell junction, ECM organization, negative regulation of microtubule polymerization, cortical cytoskeleton organization, regulation of cell shape, cell projection, and positive regulation of cell adhesion. This suggests that AMOTL2 KO results in major changes in ECM and cytoskeleton, further resulting in the cell adhesion and migration changes.

The next group of downregulated functional terms, connected with cell fate and development (**Fig. 24B**), covered the terms such as signaling pathways regulating the pluripotency of stem cells, cell fate commitment, cell differentiation, embryonic pattern specification, anatomical structure morphogenesis, and primitive streak formation. Additionally, terms connected with all three germ layers were downregulated, specifically: nervous system development, endodermal cell differentiation and lung

A

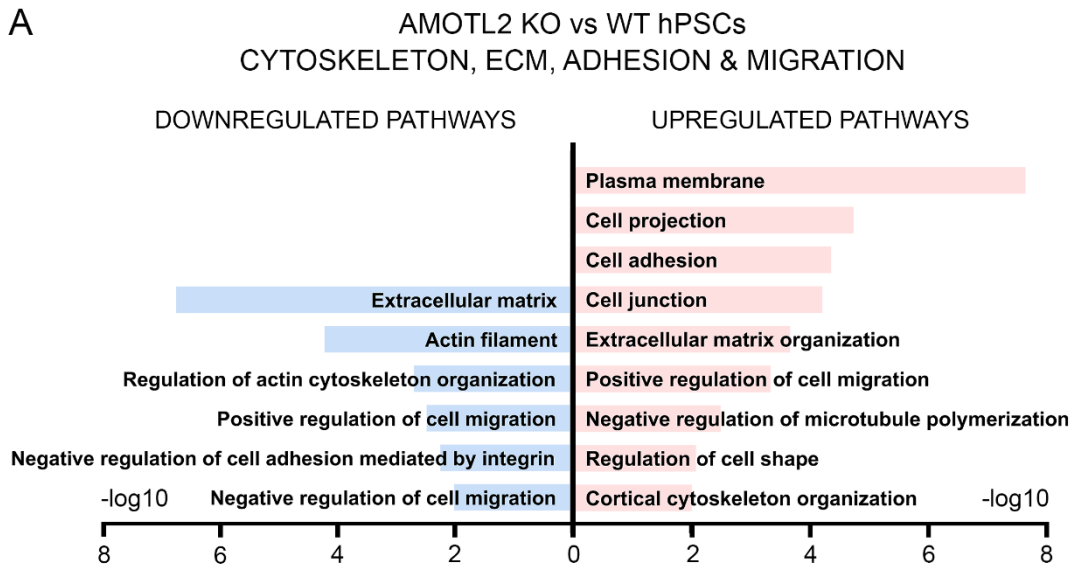
AMOTL2 KO vs WT hPSCs
CYTOSKELETON, ECM, ADHESION & MIGRATION
DOWNREGULATED PATHWAYS
UPREGULATED PATHWAYS
Plasma membrane
Cell projection
Cell adhesion
Extracellular matrix
Cell junction
Actin filament
Extracellular matrix organization
Regulation of actin cytoskeleton organization
Positive regulation of cell migration
Positive regulation of cell migration
Negative regulation of microtubule polymerization
Negative regulation of cell adhesion mediated by integrin
Regulation of cell shape
-log10
Negative regulation of cell migration
Cortical cytoskeleton organization
-log10
8 6 4 2 0 2 4 6 8

B

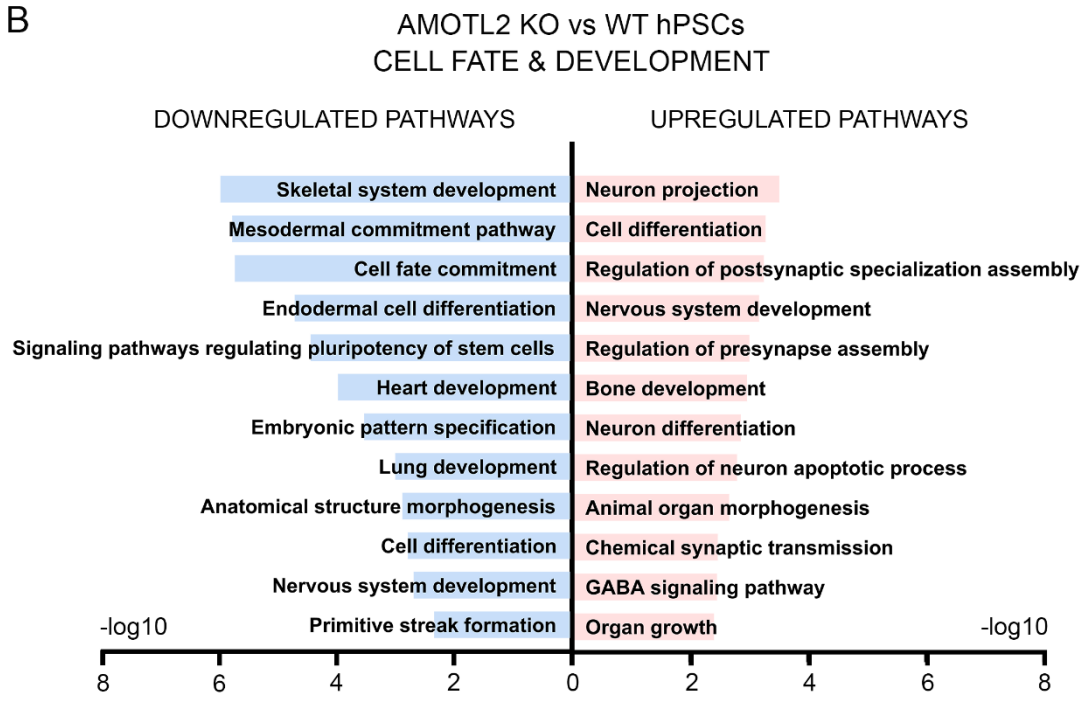
AMOTL2 KO vs WT hPSCs
CELL FATE & DEVELOPMENT
DOWNREGULATED PATHWAYS
UPREGULATED PATHWAYS
Skeletal system development
Neuron projection
Mesodermal commitment pathway
Cell differentiation
Cell fate commitment
Regulation of postsynaptic specialization assembly
Endodermal cell differentiation
Nervous system development
Signaling pathways regulating pluripotency of stem cells
Regulation of presynapse assembly
Heart development
Bone development
Embryonic pattern specification
Neuron differentiation
Lung development
Regulation of neuron apoptotic process
Anatomical structure morphogenesis
Animal organ morphogenesis
Cell differentiation
Chemical synaptic transmission
Nervous system development
GABA signaling pathway
-log10
Primitive streak formation
Organ growth
-log10
8 6 4 2 0 2 4 6 8

C

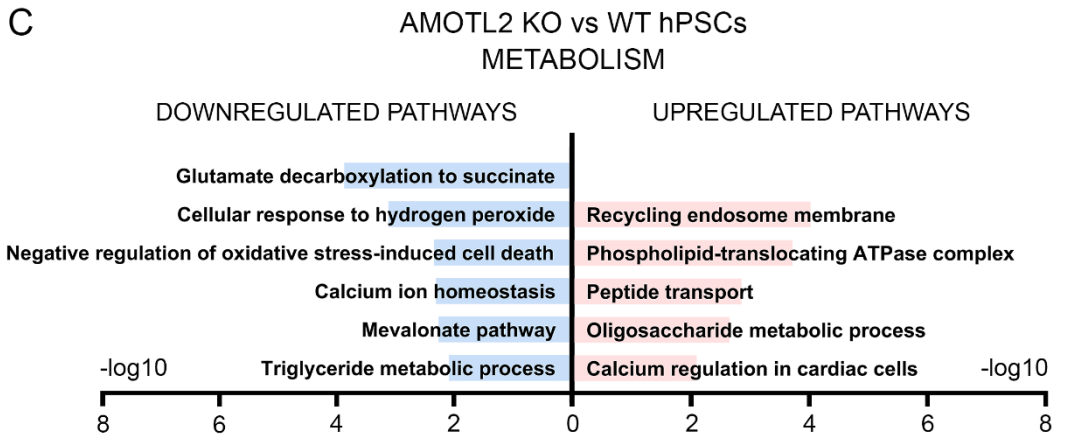
AMOTL2 KO vs WT hPSCs
METABOLISM
DOWNREGULATED PATHWAYS
UPREGULATED PATHWAYS
Glutamate decarboxylation to succinate
Cellular response to hydrogen peroxide
Recycling endosome membrane
Negative regulation of oxidative stress-induced cell death
Phospholipid-translocating ATPase complex
Calcium ion homeostasis
Peptide transport
Mevalonate pathway
Oligosaccharide metabolic process
-log10
Triglyceride metabolic process
Calcium regulation in cardiac cells
-log10
8 6 4 2 0 2 4 6 8

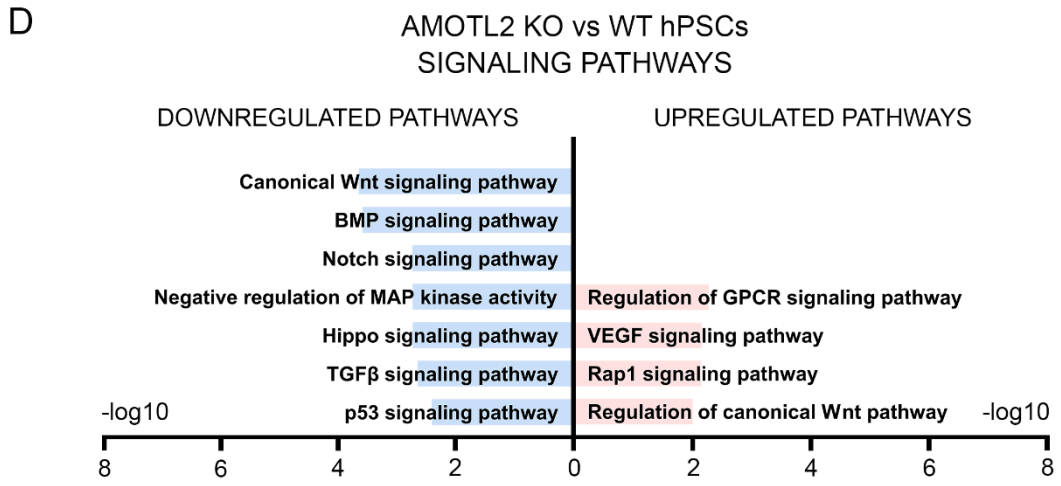

Fig. 24: Selected statistically significant (p<0.01) pathways and biological processes in AMOTL2 KO vs WT hPSCs. A. Terms connected to cytoskeleton, ECM, adhesion, and migration. **B.** Terms connected to cell fate and development. **C.** Terms connected to metabolism. **D.** Signaling pathways. WT - wild type, KO - knockout, ECM - extracellular matrix.

development, and mesodermal commitment pathway, with two derivatives – skeletal system development and heart development. The upregulated terms from this category included cell differentiation, animal organ morphogenesis, and organ growth. Additionally, there were multiple terms connected with ectoderm, such as nervous system development, neuron projection, regulation of presynapse assembly, regulation of postsynaptic specialization assembly, chemical synaptic transmission, GABA signaling pathways, neuron differentiation, regulation of neuron apoptotic process, and mesoderm-related term – bone development. This suggests a possible developmental bias of AMOTL2 KO hPSCs towards ectoderm, at the expense of endoderm and mesoderm.

Further, the terms connected with metabolism (**Fig. 24C**) were also changed between AMOTL2 KO and WT hPSCs. Among the downregulated terms there were glutamate decarboxylation to succinate, mevalonate pathway, and triglyceride metabolic process, cellular response to hydrogen peroxide and negative regulation of oxidative stress-induced cell death, and calcium ion homeostasis. The upregulated terms encompassed recycling endosome membrane, phospholipid-translocating ATPase complex and peptide transport, oligosaccharide metabolic process, and calcium regulation in cardiac cells. This implies the changes in the energy production, ROS, and intracellular calcium.

Among the downregulated signaling pathways (**Fig. 24D**) there were canonical WNT signaling pathway, BMP signaling pathway, TGFβ signaling pathway, Notch signaling pathway, negative regulation of MAP kinase activity, Hippo signaling pathway, and p53 signaling pathway. The signaling pathways upregulated in AMOTL2 KO were: regulation of GPCR signaling pathway, VEGF (vascular endothelial growth factor) signaling pathway, Rap1 (RAP1 GTPase Activating Protein) signaling pathway, and regulation of canonical WNT signaling pathway. Additionally, negative regulation of cell population proliferation and positive regulation of apoptotic process were both downregulated.

Further, I examined how the expression of angiomotin family proteins changed upon AMOTL2 KO. The bulk RNA-seq also revealed *AMOTL2* mRNA downregulation without compensation from neither *AMOTL1* nor *AMOT* (**Fig. 25**).

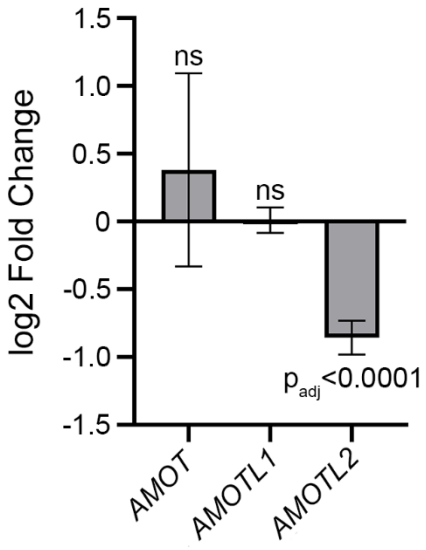

Fig. 25: AMOT family mRNA expression in AMOTL2 KO hPSCs compared to WT. N=2; Statistical significance calculated with DESeq2

3.4. AMOTL2 controls colony morphology in hPSCs

During standard culture I observed changes in the colony morphology between the AMOTL2-/- and WT hPSCs (**Fig. 26A, B**). The colony architecture was dissimilar, with WT cells growing in compact, round colonies with sharp edges (as typical for hPSCs). In contrast, AMOTL2-/- colonies were sparsely arranged, with holes and protruding cells. Similar phenotype was observed in two independent AMOTL2-/- clones (AD3 and AD6). Additionally, AMOTL2+/- heterozygote (AA3 clone) exhibited a phenotype more similar to WT hPSCs.

For quantification purposes, I stained AMOTL2 KO and WT hPSCs against β-CAT to visualize cell body (**Fig. 26D, E**). I analyzed the images of single AMOTL2 KO and WT hPSC colonies with a custom Cell Profiler pipeline, to outline the colonies and calculate the shape descriptors (**Fig. 26C**). I chose the Form Factor for the quantification of the colony shape. Form Factor is commonly used to measure nuclear shape but can also be adapted for colony or organoid shape. It assumes values from 0 to 1, with 1 being a perfect circle and lower values indicating the more irregular shape, caused by the presence of blebs or invaginations (Janssen et al., 2022). Further, I chose Euler Number as a descriptor of the number of holes in a given object (**Fig. 26C**). With the increasing number of holes, Euler Number assumes negative values and therefore lower (more negative) values indicate more holes in the object.

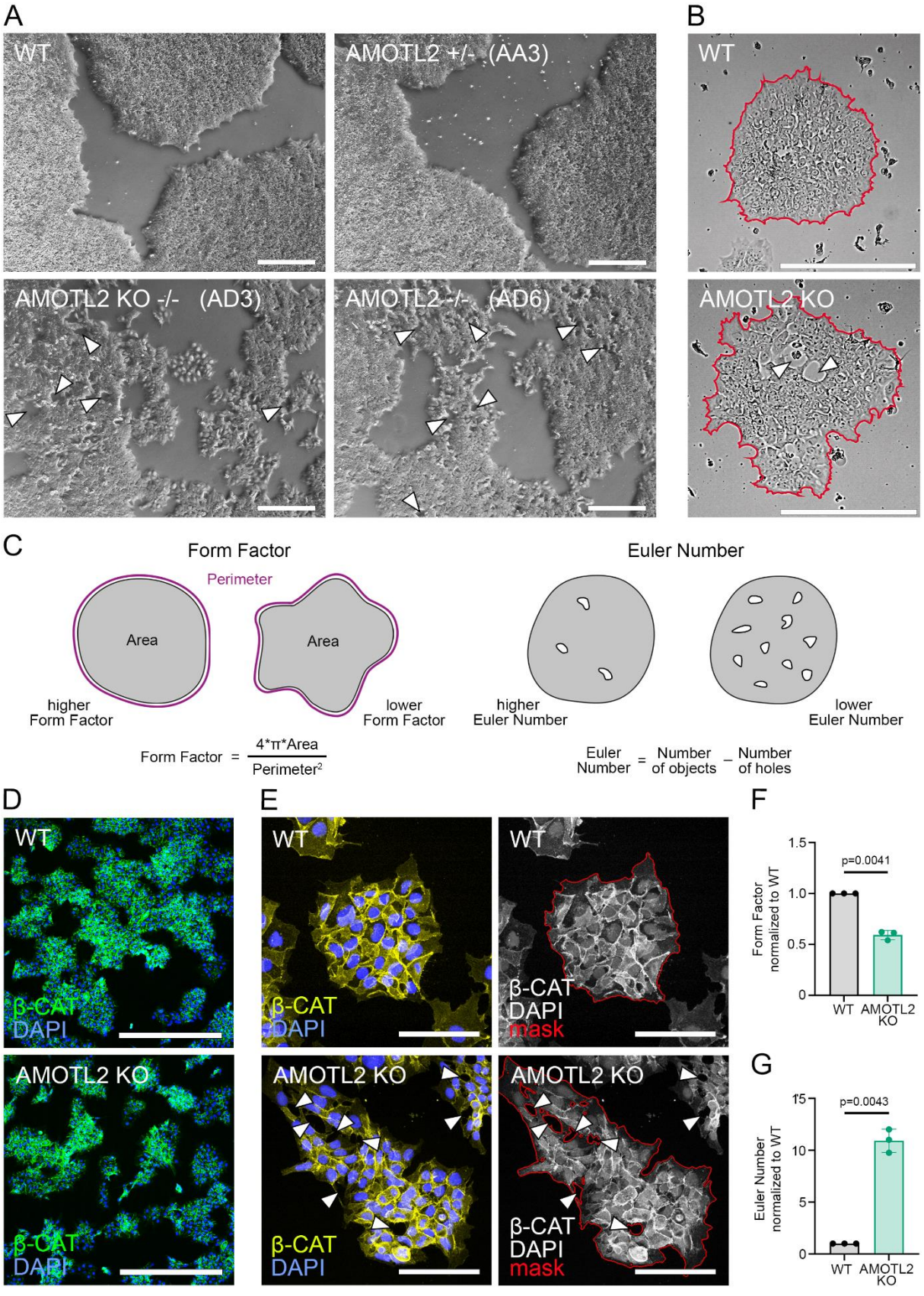

Fig. 26: Colony morphology of AMOTL2-deficient hPSCs compared to WT. A. Representative brightfield photographs of AMOTL2-/-, AMOTL2+/- and WT hPSCs. Arrows indicate holes in the colonies. Scale bar = 500 µm. N=3 **B.** Representative brightfield photographs of single colonies of AMOTL2 KO and WT hPSCs. Arrows indicate holes in the colonies. Scale bar = 500 µm. N=3. **C.** Visual representation and mathematical definition of the Form Factor and Euler Number parameters used as shape descriptors. **D.** Representative images of immunostaining against β-CAT (green) and DAPI (blue) showing the differences is colony morphology between

AMOTL2 KO and WT hPSCs. Scale bar = 500 μm. N=3. **E.** Representative images of immunostaining against β-CAT (yellow) and DAPI (blue) showing single AMOTL2 KO and WT colonies (left panel) and colony outline overlay (red) from Cell Profiler (right panel). Arrows indicate holes in the colonies. Scale bar = 100 μm. N=3. **F.** Quantification of AMOTL2 KO and WT hPSCs colony shape as Form Factor. Statistics: t-Student test with Welch's correction. N=3 **G.** Quantification of the number of holes in the AMOTL2 KO and WT hPSC colonies using Euler Number. Statistics: t-Student test with Welch's correction. N=3.

AMOTL2 KO colonies had on average 1.7-fold lower Form Factor compared to WT colonies, indicating that they were less regular (**Fig. 26E, F**). The number of holes in the AMOTL2 KO colonies was dramatically, on average 11-fold, higher than in WT cells, as indicated by Euler Number. Of note, while Euler Number itself decreases with the number of holes, the normalization to the WT results in a positive value, increasing with the number of holes (**Fig. 26E, G**).

3.5. AMOTL2 deficiency increases confluency in hPSCs

During standard culture I repeatedly observed an increase in the confluency of AMOTL2-/- hPSCs compared to WT. To confirm this phenotype, I passaged AMOTL2 KO and WT hPSCs as single cells, counted them and seeded at the same densities. Further, I cultured them for 24h in the growth medium with ROCKi (ROCK inhibitor, Y-27632), and then for the additional 48h without ROCKi, up to the total of 72h. The photographs based on which confluency was examined were taken every 2h by Incucyte S3 System. I assessed the confluency and the rate of the cell growth over time. The confluency was calculated as the percentage of the area of the field of view occupied by cells. Additionally, for several experiments, I cultured the hPSCs in the presence of a SiR-DNA fluorescent dye that allows labeling live cells and provides an opportunity to observe the cell numbers from the first moments of the culture. I first examined the starting confluency and cell number, defined here as the cells that were attached at the first scan, 2h after the passage. I observed no significant differences in the initial confluency (**Fig. 27A-C**) or initial cell number (**Fig. 27D-F**) between WT and AMOTL2 KO hPSCs. This suggests that the initial adhesion of AMOTL2 KO hPSCs was not changed. In contrast, I detected a highly significant increase in confluency of AMOTL2 KO vs WT hPSCs during the next days of culture, with 19% increase after 24h and 26% increase after 48h and 29% increase after 72h (**Fig. 27A-C**). The increase in confluency also corresponded with increased cell numbers. There were on average 17%, 22%, and 29% more AMOTL2 KO hPSCs compared to WT at 24h, 48h, and 72h, respectively (**Fig. 27D-F**).

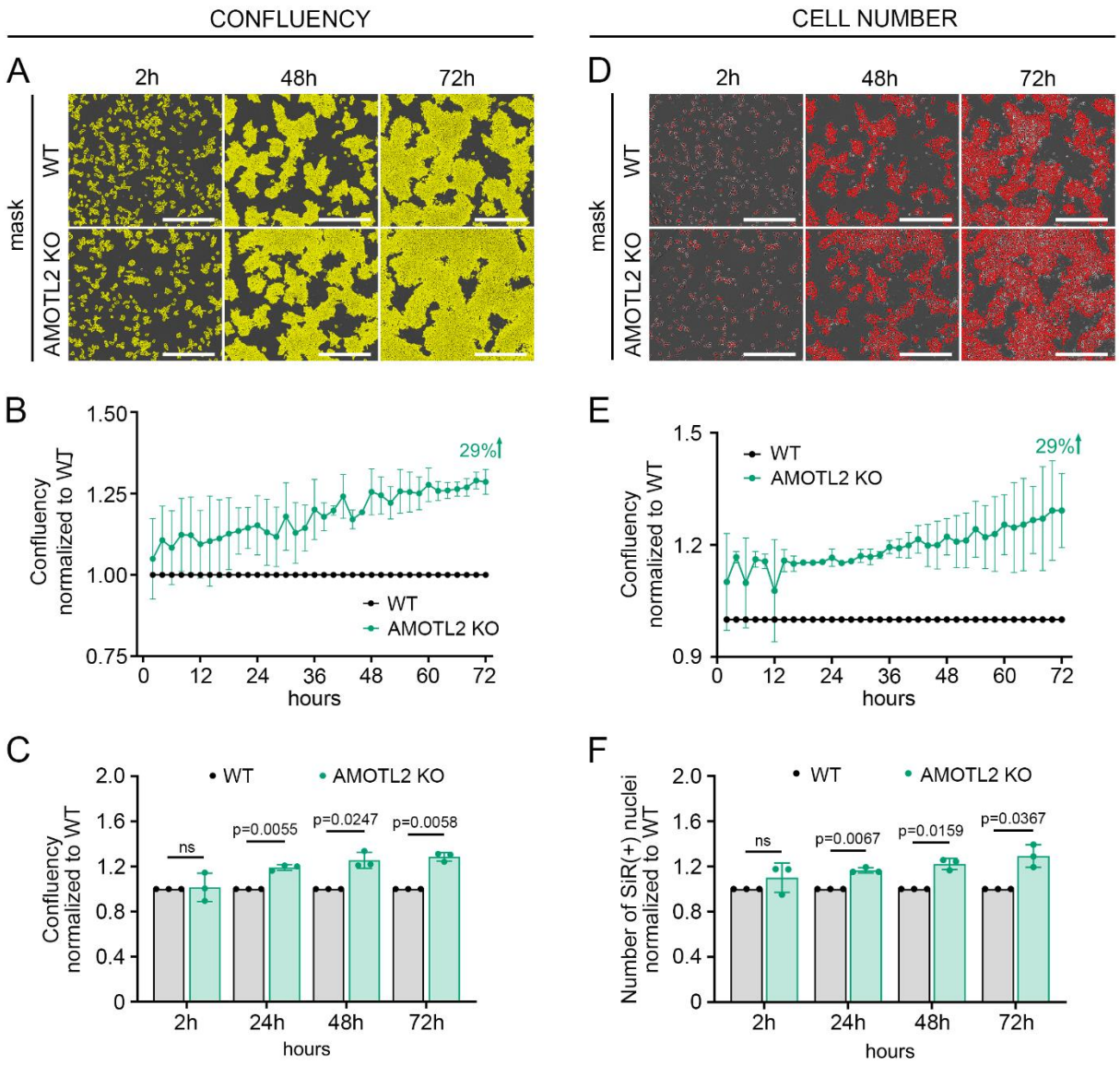

Fig. 27: Changes in AMOTL2 KO confluency and cell number compared to WT. A. Representative images of WT and AMOTL2 KO confluency over 2h, 48h and 72h culture. Scale bar = 500 µm. N=4 **B.** Growth curve of WT and AMOTL2 KO hPSCs as confluency normalized to WT. N=4. **C.** Confluency normalized to WT at 2h, 24h, 48h, and 72h. N=4 Statistics: t-Student test with Welch's correction **D.** Representative images of WT and AMOTL2 KO cell number over 2h, 48h and 72h culture. Scale bar = 500 µm. **E.** Growth curve of WT and AMOTL2 KO cells as cell number normalized to WT. N=3 **F.** Cell number normalized to WT at 2h, 24h, 48h, and 72h. N=3 Statistics: t-Student test with Welch's correction.

The increase in confluency was even more pronounced in AMOTL2(837)-/- hPSCs. After 48h of culture, I observed a statistically significant, 77%, 67% and 67% increase in the confluency in three independent AMOTL2(837)-deficient clones (B1, B8, and H1, respectively) compared to WT cells (**Fig. 28**). Of note, there was no difference in the confluency increase between clones with biallelic deletion (H1 and B8) and B1 clone with monoallelic mutation after 48h. The initial confluency was also unchanged in AMOTL2(837)-deficient clones.

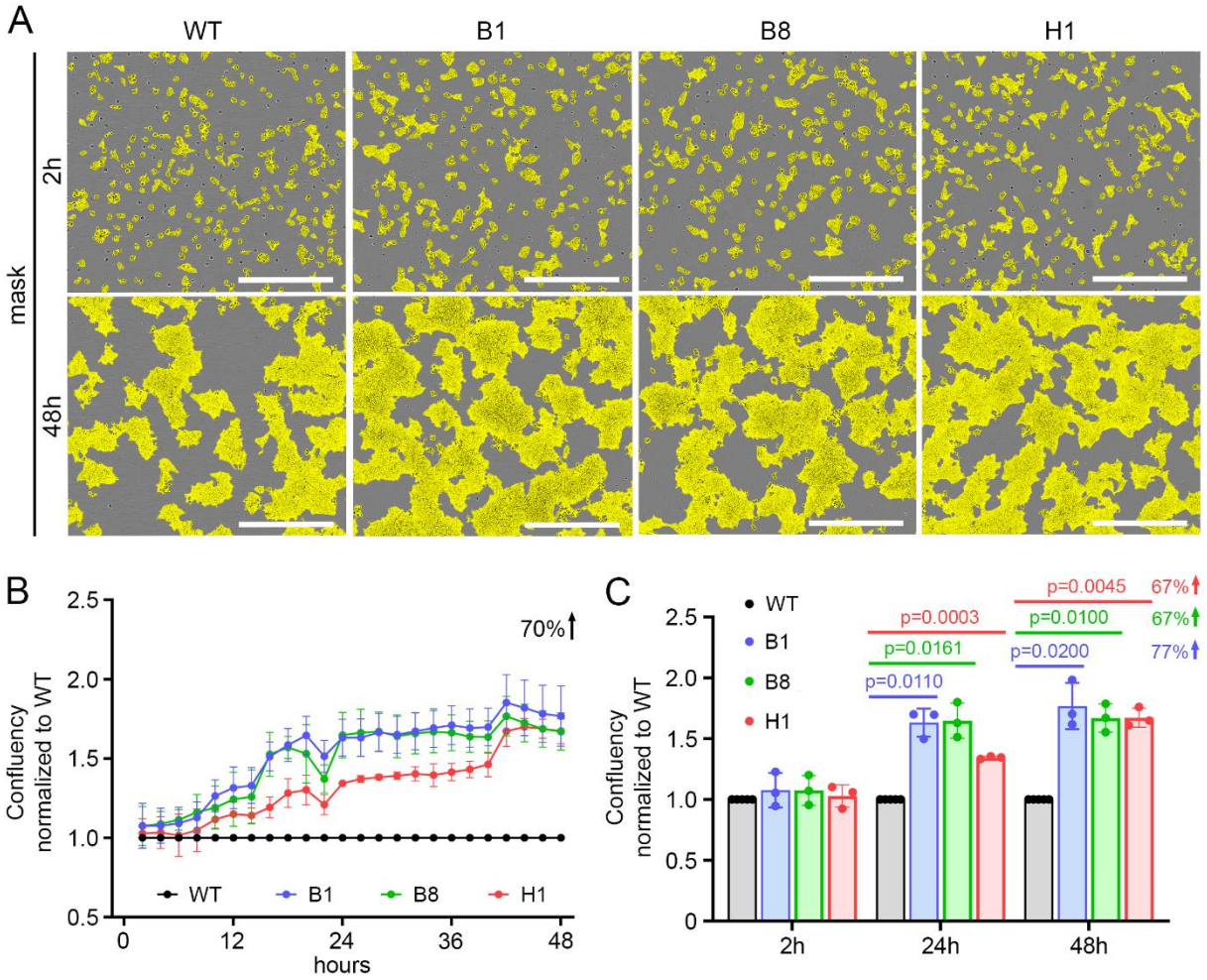

Fig. 28: Changes in AMOTL2 KO confluency, isoform 837 aa. A. Representative images of WT and AMOTL2(837)-deficient confluency over 2h and 48h culture. Scale bar = 500 µm. **B.** Growth curve of WT and AMOTL2(837)-deficient cells as confluency normalized to WT. N=3 **C.** Confluency normalized to WT at 2h, 24h, and 48h. N=3 Statistics: t-Student test with Welch's correction; p-values compared to WT, only statistically significant $p<0.05$ are shown.

3.6. AMOTL2 deficiency promotes hPSC proliferation and decreases apoptosis

The increased confluency and cell numbers of AMOTL2-deficient hPSCs might stem from increased proliferation or decreased apoptosis, or the combination of the two. The bulk RNA-seq of AMOTL2 KO and WT hPSCs revealed a significant downregulation of the genes negatively regulating proliferation and positively regulating apoptosis in AMOTL2 KO compared to WT (**Fig. 29A, E**), suggesting that both increased proliferation and decreased apoptosis might be responsible for higher cell numbers in AMOTL2 KO.

To assess the proliferation rate, I performed an immunofluorescent staining for the proliferation marker phosphorylated histone H3 (pHH3) in AMOTL2 KO and WT cells (**Fig. 29B**). Histone H3 is phosphorylated from late G2 phase and through the M phase of the cell cycle, and dephosphorylated upon the exit from mitosis, making it a highly specific marker of mitotically active cells. Additionally, in the imaging, pHH3 exhibits two distinct staining patterns: speckled for G2 phase, and more clumpy,

solid for M phase (Khieu et al., 2019). I performed the quantitative analysis based on the images using a custom CellProfiler pipeline. I trained the software to count both solid, strong signals and speckles, which are all positive signals. The nuclei with less than three speckles were assigned as pHH3(-) and filtered out from the analysis as it is technically very challenging to assess if the nuclei with low speckle count are just starting to be phosphorylated or if it is a technical artifact from immunostaining. I normalized the pHH3(+) cells to the total cell number, based on the DAPI staining (also counted by CellProfiler). The results showed a statistically significant increase in the proliferation rate of AMOTL2 KO hPSCs compared to WT. When I counted all positive signals (both G2 and M phase), the increase varied from 5% to 30%, with the mean of 17% (**Fig. 29C**). When I considered only M phase cells, a very consistent increase of 14% was observed in hPSC proliferation (**Fig. 29D**).

Next, I measured the apoptosis rate using immunofluorescent staining against Cleaved Caspase 3 (**Fig. 29F**). The nuclei were counted using CellProfiler, while Cleaved Caspase 3(+) cells were counted manually. The apoptotic rate was on average 18% lower in AMOTL2 KO compared to WT (**Fig. 29G**).

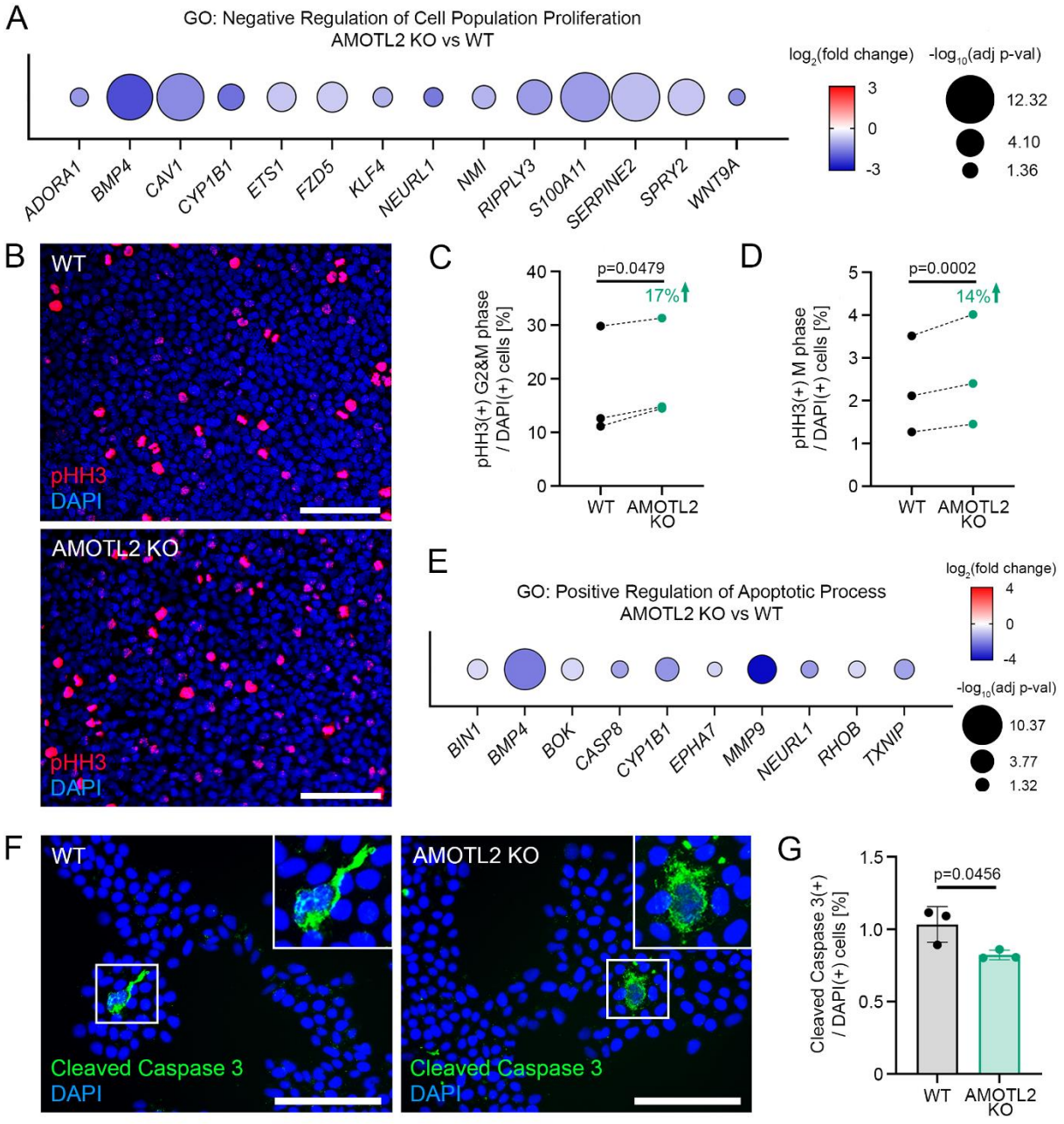

Fig. 29: Proliferation and apoptosis rates in AMOTL2 KO versus WT hPSCs. A. Selected DEGs involved in the negative regulation of proliferation from bulk RNA-seq. N=2. Statistical significance calculated with DESeq2. **B.** Representative images of AMOTL2 KO and WT hPSCs stained against pHH3 (red). Nuclei stained in blue with DAPI. Scale bar = 300 µm. **B-C.** Quantification of pHH3(+) cells normalized to the total cell number (DAPI). Statistics: paired t-Student test. N=3. **C.** G2 and M phase, **D.** M phase only. **E.** Selected DEGs involved in the positive regulation of apoptotic process from bulk RNA-seq. N=2. Statistical significance calculated with DESeq2. **F.** Representative images of AMOTL2 KO and WT hPSCs stained against Cleaved Caspase 3 (green). Insets show close-ups on the positively stained cells. Nuclei stained in blue with DAPI. Scale bar = 200 µm. N=3. **G.** Quantification of Cleaved Caspase 3(+) cells normalized to the total cell number (DAPI). N=3. Statistics: paired t-Student test. N=3

3.7. AMOTL2 deficiency alters pluripotency

3.7.1. AMOTL2 deficiency does not impair the canonical pluripotency factor expression

The expression of the classical pluripotency markers, OCT3/4, SOX2, and NANOG was not changed in the bulk RNA-seq, yet the pathways involved in stem cell pluripotency, such as canonical WNT signaling, BMP signaling or TGFβ signaling were (**Fig. 24D**). Therefore, to further assess the changes in the pluripotency of AMOTL2 KO hPSCs at the protein level, I performed the immunofluorescent staining against SOX2, NANOG, and OCT3/4 (**Fig. 30A-C**). I measured the mean fluorescence intensity and normalized it to DAPI. There were no significant differences in the mean intensity of SOX2 and NANOG between the WT and AMOTL2 KO (**Fig. 30A, B**), while OCT3/4 was increased in AMOTL2 KO (**Fig. 30C**).

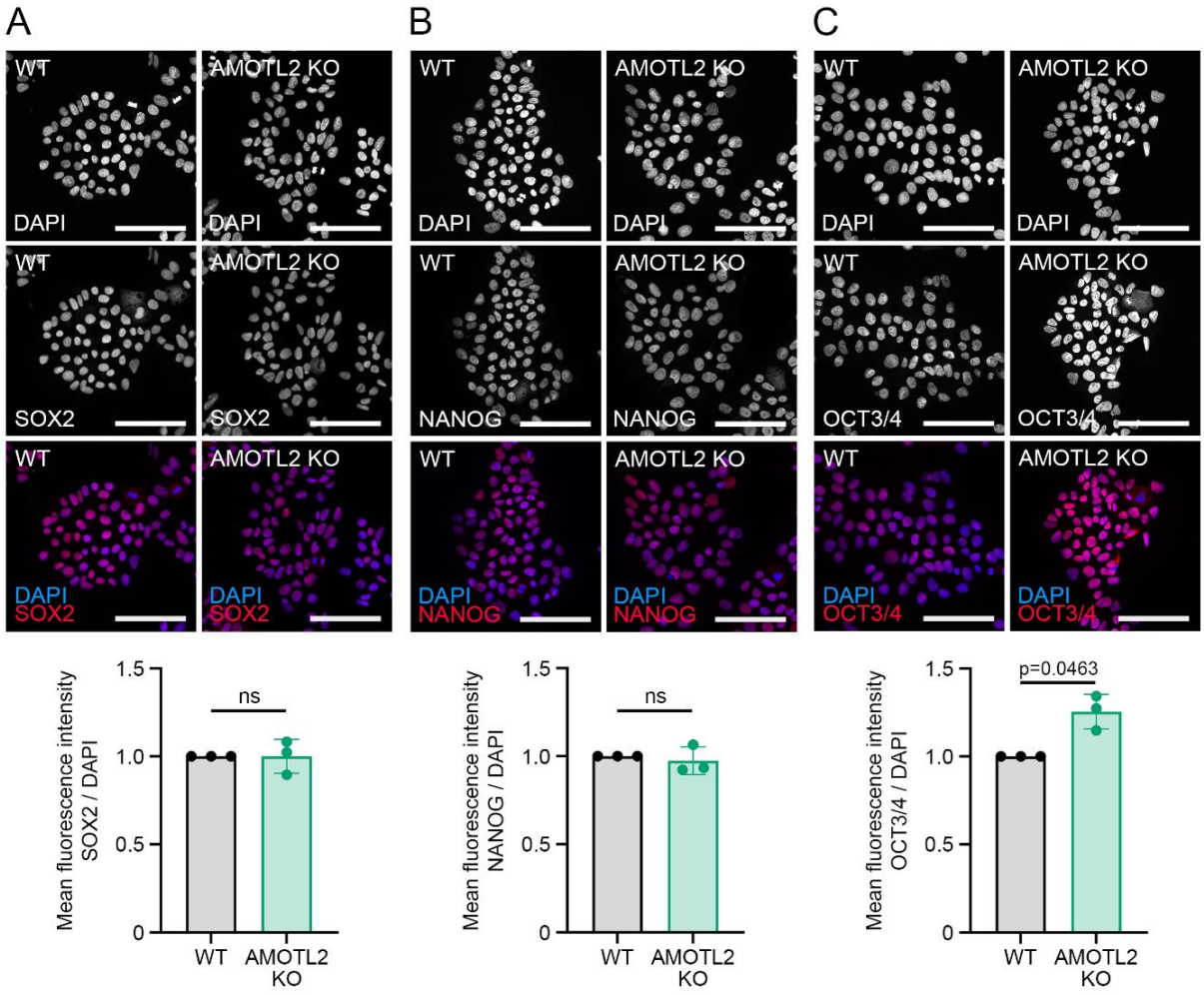

Fig. 30: Pluripotency factors in AMOTL2 KO and WT hPSCs. Representative images of immunofluorescent staining against SOX2 (**A**), NANOG (**B**), and OCT3/4 (**C**) Nuclei stained in blue with DAPI. Scale bar = 100 µm. N=3 Below, quantification of the mean fluorescence intensity of the pluripotency marker expression normalized to DAPI. Statistics: t-Student test with Welch's correction. N=3

3.7.2. AMOTL2 deficiency results in the differentiation bias towards ectoderm at the expense of endoderm

The bulk RNA-seq pointed at cell fate bias in AMOTL2 KO, revealing the dysregulation of the terms connected with nervous system development, and downregulation of endoderm and mesoderm development (**Fig. 24B**). Selected genes from these GO terms are shown in **Fig. 31A**. Additionally, the crucial signaling pathways which are inhibited with small molecules in the ectoderm differentiation protocols, namely BMP signaling pathway and TGFβ signaling pathway were downregulated, and canonical WNT signaling pathway was dysregulated in AMOTL2 KO (**Fig.D**;). Moreover, in the scRNA-seq atlas of hPSCs and DE (Yiangou et al., 2019) (**Fig. 14A**) *AMOTL2* expression was present in both hPSCs and DE, and the expression level was higher in DE. Together, this suggests that AMOTL2 might be crucial to endoderm formation.

To study this effect further, I spontaneously differentiated AMOTL2 KO and WT hPSCs in the form of 3D cell aggregates called embryoid bodies (EBs), over the course of 9 days (**Fig. 31B**). On day 2 and day 9, I collected the RNA from WT and AMOTL2 KO cells (**Fig. 31B**) to examine the expression of the genes specific for each of the three germ layers: *FOXA2*, *GATA4*, *SOX*7, and *SOX17* for endoderm, *MEIS2*, *MIXL1*, *PDGFRA*, and *TNNT2* for mesoderm, and *OTX2*, *PAX6*, *SOX1*, and *SOX2* for ectoderm (**Fig. 31C**). On both day 2 and day 9 the expression of endoderm-related genes was decreased in AMOTL2 KO compared to WT cells, instead, the expression of ectoderm-related genes was increased in AMOTL2 KO. The statistically significant ($-\log_{10}$ (adj p-val)$>$1.30) decrease was observed for *FOXA2*, *GATA4*, and *SOX17* on day 2 and *GATA4*, *SOX7*, and *SOX17* on day 9. The statistically significant increase was detected for all ectoderm-related genes on both day 2 and day 9, except for *SOX2* at day 9. As for the expression of mesoderm-related genes, on day 2 *PDGFRA* and *TNNT2* were minimally, yet significantly downregulated, and this downregulation became more pronounced on day 9, while *MEIS2* and *MIXL1* remained unchanged on both day 2 and day 9 (**Fig. 31C**). This indicates that AMOTL2 KO EBs preferentially differentiate towards ectoderm lineages, greatly at the expense of endoderm and at a minor expense of mesoderm.

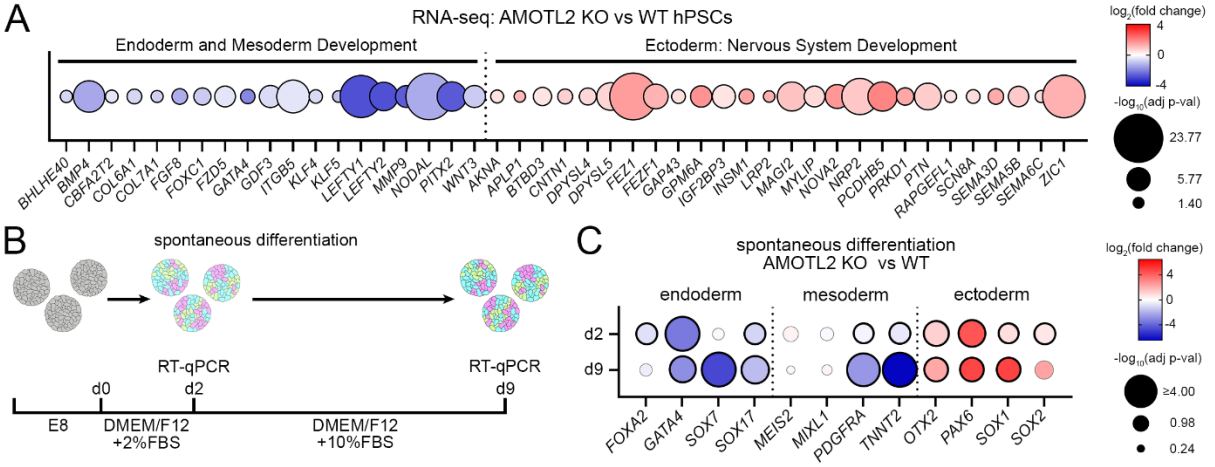

Fig. 31: AMOTL2 deficiency results in the differentiation bias towards ectoderm at the expense of endoderm. A. Selected DEGs involved in endoderm and nervous system development from RNA-seq. N=2. Statistical significance calculated with DESeq2. **B.** Schematic outline of EB spontaneous differentiation. **C.** Gene expression analysis of the germ line-specific genes after 2 and 9 days in AMOTL2 KO compared to WT cells. N=3. Statistics: t-Student test with Welch's correction. Statistically significant genes are marked with thicker border. RT-qPCR – real time-quantitative polymerase chain reaction, d2 – day2

To further confirm the cell fate bias of AMOTL2 KO hPSCs, the 2D directed differentiation towards ectodermal progenitors was performed for 8 days, with the addition of LDN193189 (LDN), SB431542 (SB), and CHIR99021 (CHIR) for days 1-4, and LDN with CHIR for days 5-8 (**Fig. 32A**). On day 8, I fixed the cells for immunofluorescent staining and flow cytometry. The differentiating cells form the specific structures, the spots of densely packed cells that express the ectoderm markers. In WT cells, the spots were small and not abundant, while in AMOTL2 KO the dense spots were widespread, taking almost all available space (**Fig. 32B**). I stained the WT and AMOTL2 KO cells against ectoderm markers, CDH2 and SOX2. Compared to WT, AMOTL2 KO cells exhibited on average 2-fold and 2.5-fold higher expression of CDH2 and SOX2, respectively (**Fig. 32B, C**). Next, I used flow cytometry to assess another ectoderm marker, SOX1 and OCT3/4 as a control. The median fluorescence intensity was 1.5-fold increased in AMOTL2 KO (**Fig. 32D**: left panel; **Fig. 32E**). The expression of OCT3/4 was still present in ectodermal progenitors, with 92% of WT but only 51% of AMOTL2 KO cells being OCT3/4(+). OCT3/4 median fluorescence intensity was almost 4.4-fold decreased in AMOTL2 KO (**Fig. 32D**: right panel; **Fig. 32E**). To investigate this deeper, I co-stained WT and AMOTL2 KO cells against SOX1 with OCT3/4, and OTX2 with OCT3/4. In AMOTL2 KO, SOX1(+) / OCT3/4(-) cells accounted for 60% of all cells, while the same population in WT was only 8% (**Fig. 32F, G**). Similarly, for the OTX2(+) / OCT3/4(-) population accounted for 69% in AMOTL2 KO but only 6% in WT (**Fig. 32H, I**). The co-expression of pluripotent and ectoderm markers in early neural progenitors was reported previously (Noisa et al., 2012), with the pluripotency markers diminishing and ectoderm markers increasing over time. This suggests that AMOTL2 KO ectoderm progenitors are more mature compared to WT and the ectoderm differentiation is accelerated in AMOTL2 KO.

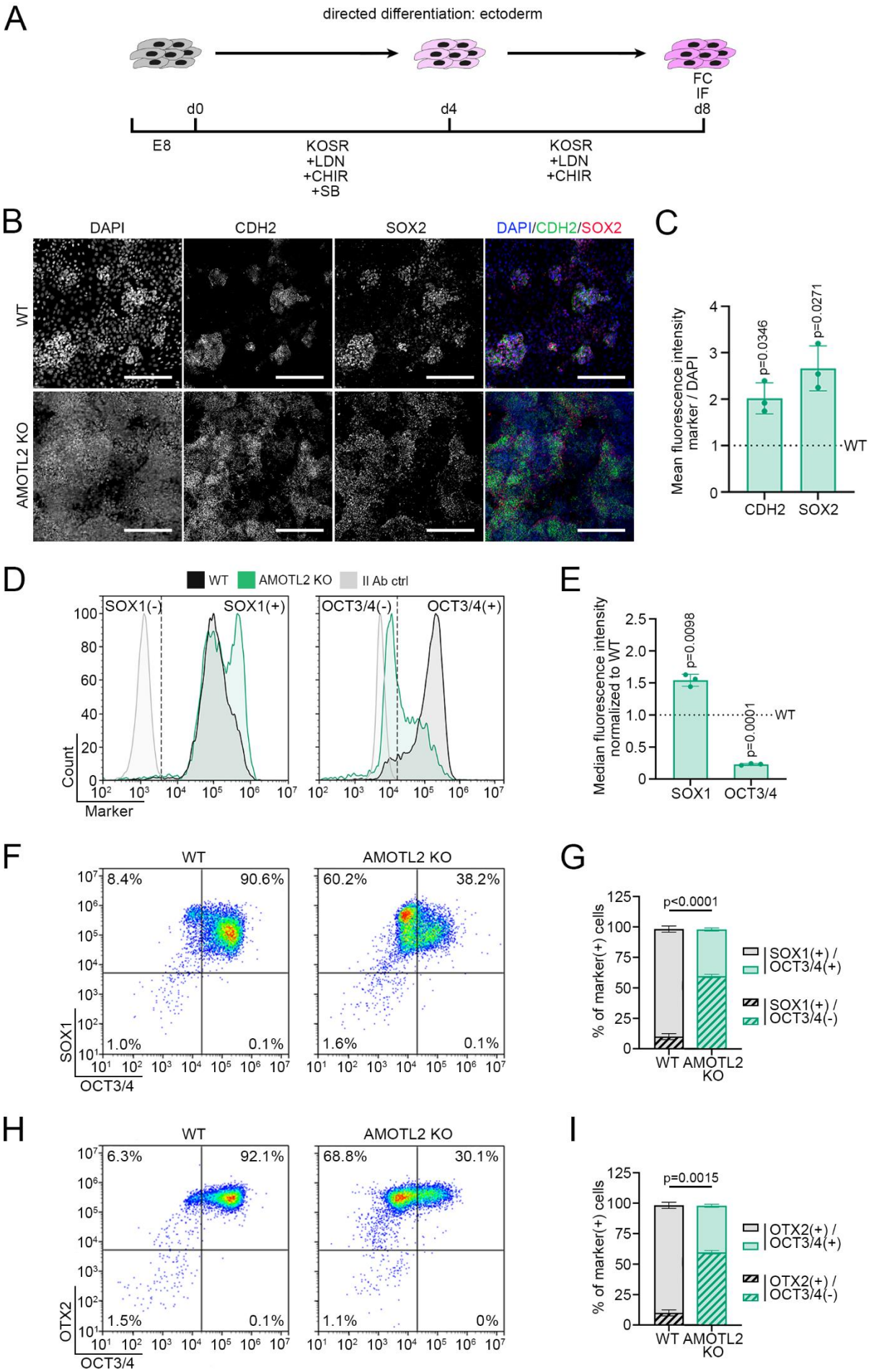
A
directed differentiation: ectoderm
FC
IF
d8
d0
d4
E8
KOSR
+LDN
+CHIR
+SB
KOSR
+LDN
+CHIR
B
DAPI
CDH2
SOX2
DAPI/CDH2/SOX2
WT
AMOTL2 KO
C
Mean fluorescence intensity
marker / DAPI
p=0.0346
p=0.0271
WT
CDH2
SOX2
D
WT
AMOTL2 KO
II Ab ctrl
SOX1(-)
SOX1(+)
OCT3/4(-)
OCT3/4(+)
Count
Marker
E
Median fluorescence intensity
normalized to WT
p=0.0098
p=0.0001
WT
SOX1
OCT3/4
F
WT
AMOTL2 KO
8.4%
90.6%
1.0%
0.1%
60.2%
38.2%
1.6%
0.1%
SOX1
OCT3/4
G
p<0.0001
% of marker(+) cells
SOX1(+) /
OCT3/4(+)
SOX1(+) /
OCT3/4(-)
WT
AMOTL2
KO
H
WT
AMOTL2 KO
6.3%
92.1%
1.5%
0.1%
68.8%
30.1%
1.1%
0%
OTX2
OCT3/4
I
p=0.0015
% of marker(+) cells
OTX2(+) /
OCT3/4(+)
OTX2(+) /
OCT3/4(-)
WT
AMOTL2
KO

Fig. 32: AMOTL2 deficiency accelerates ectoderm formation. A. Schematic outline of the directed differentiation towards ectoderm. **B.** Representative images of immunofluorescent staining against CDH2 (green) and SOX2 (red). Nuclei stained in blue with DAPI. Scale bar = 200 μm. N=3. **C.** Quantification of the mean fluorescent intensity of CDH2 and SOX2 normalized to DAPI, calculated from the immunofluorescent staining photographs. The values for AMOTL2 KO were normalized to WT. N=3. Statistics: t-Student test with Welch's correction. **D.** Representative histograms for flow cytometry analysis of SOX1 and OCT3/4. N=3. **E.** Flow cytometry analysis of the SOX1 and OCT3/4 median fluorescence intensity. N=3. Statistics: t-Student test with Welch's correction. **F.** Representative density plots for flow cytometry analysis co-stained SOX1 and OCT3/4. N=3. **G.** Quantification of the percentage of two subpopulations: SOX1(+) / OCT3/4(+) and SOX1(+) / OCT3/4(-). N=3. Statistics: t-Student test with Welch's correction. **H.** Representative density plots for flow cytometry analysis co-stained OTX2 and OCT3/4. N=3. **I.** Quantification of the percentage of two subpopulations: OTX2(+) / OCT3/4(+) and OTX2(+) / OCT3/4(-). N=3. Statistics: t-Student test with Welch's correction. WT - wild type, KO - knockout, EB - embryoid body, AA - Activin A, CHIR - Chiron99021, LDN - LDN193189, SB - SB431542, FC – flow cytometry, IF – immunofluorescence, d4 – day4

3.8. AMOTL2 deficiency induces changes in cytoskeleton yet F-actin depolymerization is not responsible for the cell fate bias in AMOTL2 KO

AMOTL2 KO in hPSCs resulted in the major dysregulation of the terms connected with cytoskeleton, adhesion, and ECM in the bulk RNA-seq (**Fig. 24A**), in particular, the dysregulation in adhesion-related proteins (**Fig.33A**) and downregulation of the genes connected to the actin cytoskeleton organization (**Fig. 33B**) was observed in AMOTL2 KO. Out of the adhesion proteins, *CDH1*, *β-CAT*, *ITGA5* (Integrin Subunit Alpha 5), and *VCL* (Vinculin) were not significantly changed in RNA-seq (**Fig. 33A**). The *CDH2* (Cadherin 2), *CDH7* (Cadherin 7), and *VIM* were upregulated, while *δ-CAT* (Catenin Delta 1) was downregulated in AMOTL2 KO hPSCs. Within actin-related genes (**Fig. 33B**), *ACTA1* (Actin Alpha 1), encoding one of the actin isoforms was downregulated. Further, *ANXA1* (Annexin A1), which can be involved in Ca^{2+}-dependent F-actin cytoskeleton stabilization (Hayes et al., 2004) was dramatically decreased in AMOTL2 KO hPSCs. Another downregulated gene was *RHOB* (Rat Sarcoma Virus, GTPase), a small GTPase that promotes F-actin assembly (Fernandez-Borja et al., 2005). The F-actin fiber organization was disrupted, and fiber thickness was decreased in AMOTL2 KO hPSCs (data not shown).

The F-actin organization was previously reported to be involved in cell fate decisions in other contexts, for instance in osteogenic commitment of mesenchymal stem cells (L. Chen et al., 2015; Müller et al., 2013), the ICM vs trophectoderm determination (Skory et al., 2023), or induction of the endocrine progenitors during pancreatic differentiation (Hogrebe et al., 2020). Therefore, the disruption of F-actin cytoskeleton in AMOTL2 KO hPSCs prompted us to examine if this might be a reason for the ectodermal lineage bias in differentiating AMOTL2 KO cells. I repeated the spontaneous differentiation of AMOTL2 KO and WT hPSCs with 10μM Y-27632 (referred as ROCK inhibitor, ROCKi) which inhibits ROCK1/2 by inducing actin depolymerization (Hirose et al., 1998; Narumiya et al., 2000). If actin depolymerization was indeed responsible for the lineage bias, one would expect more ectodermal phenotype in ROCKi-treated WT EBs. On day 2 and day 9 of the spontaneous differentiation, I collected the RNA from WT and AMOTL2 KO cells (**Fig. 33C**). Comparing WT

ROCKi(+) with AMOTL2 KO ROCKi(-) showed that F-actin depolymerization in WT did not change the lineage bias, since WT ROCKi(+) hPSCs still preferentially differentiated into endoderm and mesoderm at both d2 and d9 (**Fig. 33D, E**). Further, comparison of WT ROCKi(+) with WT ROCKi(-) EBs and AMOTL2 KO ROCKi(+) with AMOTL2 KO ROCKi(-) EBs shown a trend suggesting that treatment with ROCKi promotes differentiation in general but not necessarily towards a particular germ layer at the early stages of differentiation (d2), and deepens the phenotype at the later stages (d9), in both cases irrespective of the genetic background (**Fig. 33D, E**).

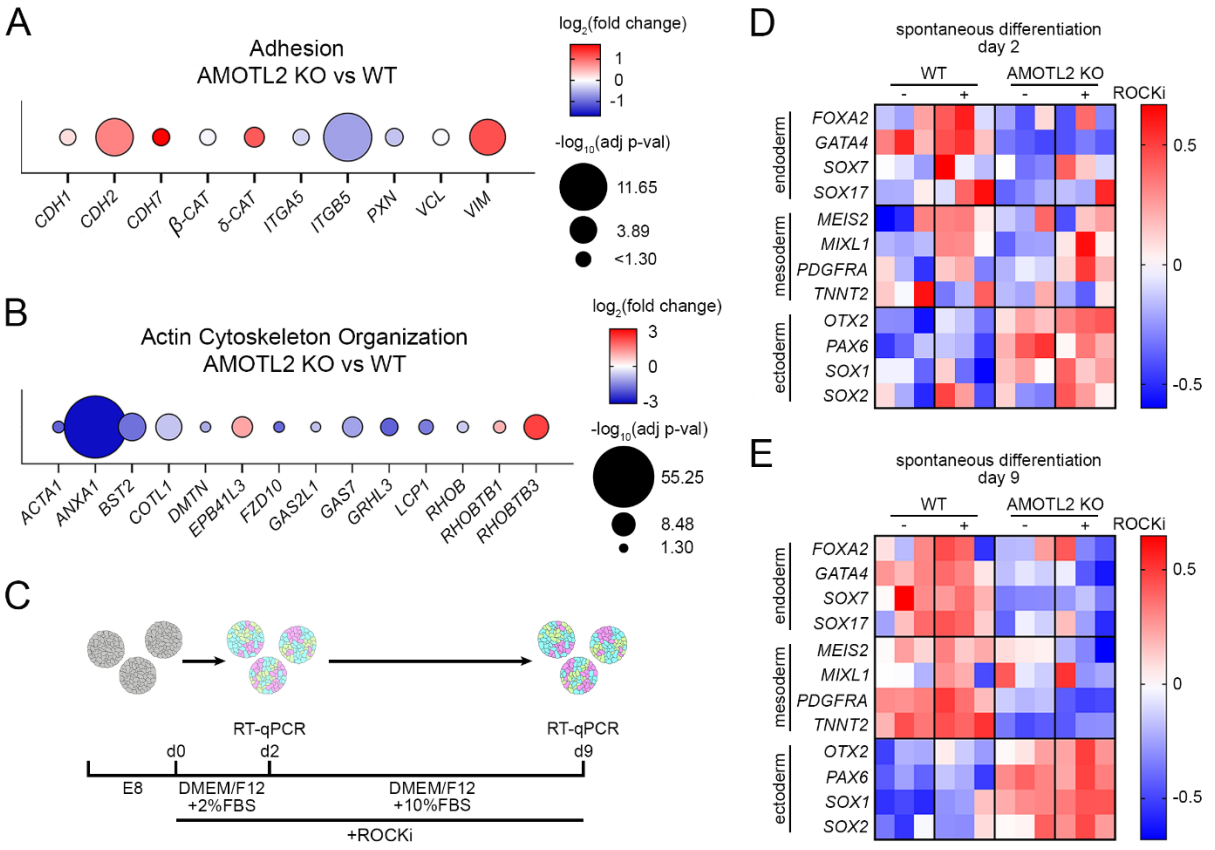

Fig. 33: AMOTL2 deficiency induces changes in hPSCs cytoskeleton. A. Selected genes connected with adhesion from RNA-seq. N=2. Note that genes with -$\log_{10}$ (adj p-val)＜1.3 are not significantly changed. Statistical significance calculated with DESeq2. **B.** Selected DEGs involved in actin cytoskeleton organization from RNA-seq. N=2. Statistical significance calculated with DESeq2. **C**. Schematic illustration of the protocol used for spontaneous EB differentiation with ROCKi. **D-E.** Gene expression analysis of day 2 (**D**) and day 9 (**E**) spontaneously differentiating EBs with ROCKi. N=3

3.9. AMOTL2 influences size and shape of spontaneously differentiating EBs

During the AMOTL2 KO and WT hPSCs spontaneous differentiation, I took photographs of EBs daily to assess the morphological differences in their size and shape (**Fig. 34**). I calculated the size as the area of single organoids from 2D images. For the shape, I used the Form Factor parameter (**Fig. 26C**). I calculated both parameters using a custom Cell Profiler pipeline.

At day 0, before pluripotency-maintaining factors were removed, there were no statistically significant differences in size of the WT and AMOTL2 KO EBs (**Fig. 34A, B**). After removal of the pluripotency-

maintaining factors, the WT ROCKi(-) EBs were gradually increasing in size during the first six days of the spontaneous differentiation but did not grow further after day 6, which might be connected to the fact that the more differentiated the cells are, the lower their proliferation rate is. In contrast, AMOTL2 KO ROCKi(-) EBs continued growing throughout the whole course of the differentiation, becoming significantly bigger than WT EBs at days 7-9 (**Fig. 34A, B**). The addition of ROCKi affected the size of both WT and AMOTL2 EBs. The WT EBs differentiated with ROCKi were significantly smaller than WT ROCKi(-) EBs from day 3 onwards, yet they followed a highly similar pattern of growth until day 6 and not increasing in size after day 6. Surprisingly, AMOTL2 KO ROCKi(+) EBs increased in size only marginally throughout the 9 days of the differentiation. The AMOTL2 KO ROCKi(+) EBs were significantly smaller than WT ROCKi(-) and AMOTL2 KO ROCKi(-) EBs from day 3 and 2 onwards, respectively, and smaller than WT ROCKi(+) EBs from day 5 onwards (**Fig. 34A, B**). On the graph only significant p-values compared to the WT ROCKi(-) conditions are shown, the full list of comparisons can be found in **Table 4**.

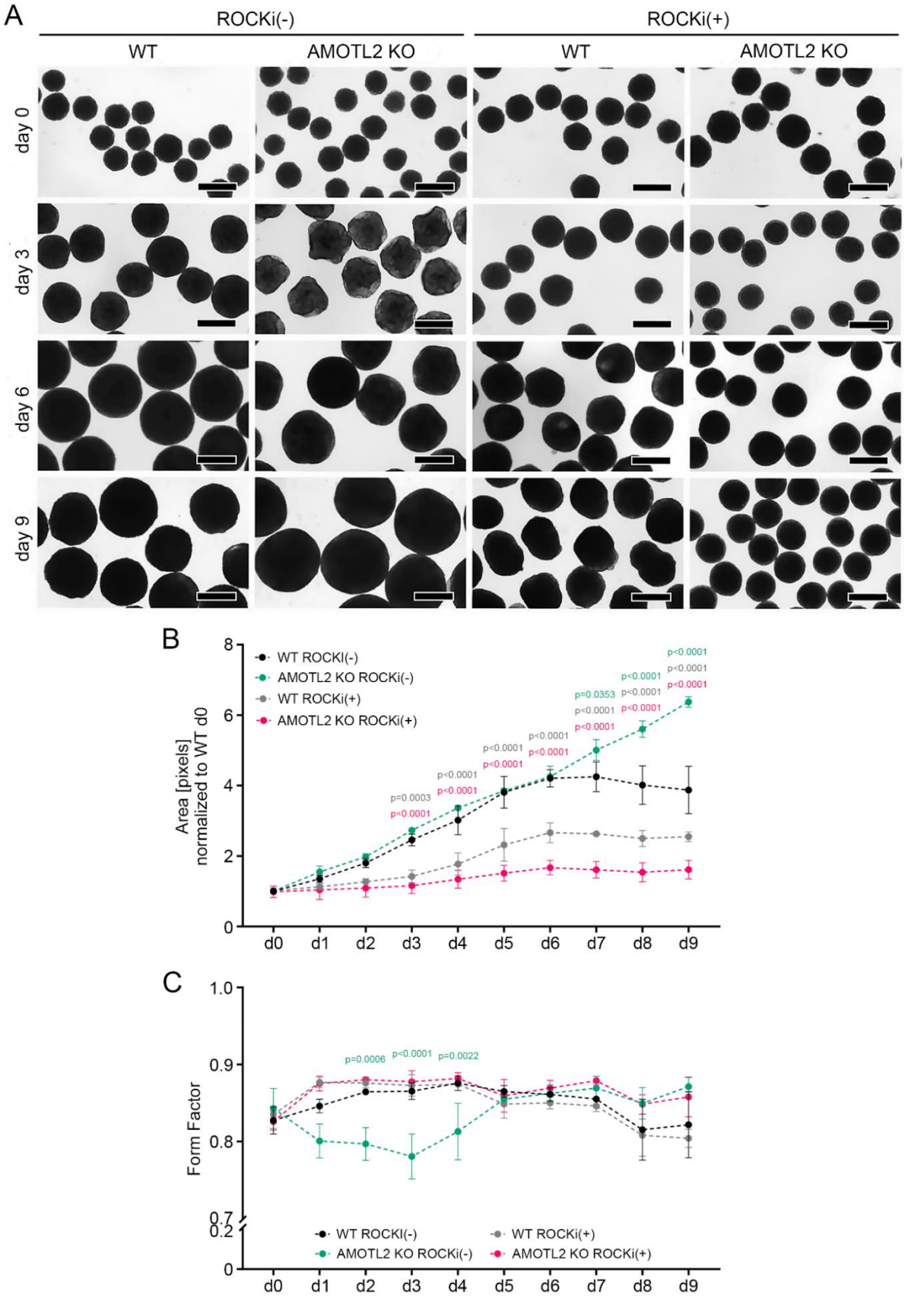

Fig. 34: Spontaneous differentiation of WT and AMOTL2 KO EBs with and without ROCKi. A. Representative images of the differentiating WT and AMOTL2 KO EBs at day 0, day 3, day 6, and day 9 of the culture. Scale bar = 500 µm. N=3 **B.** Size (Area) of WT and AMOTL2 KO EBs during spontaneous differentiation, normalized to day 0 WT. **C.** Form Factor of WT and AMOTL2 KO EBs during spontaneous differentiation. **B-C.** N=3 Statistics: 2-way Anova. P-values compared to WT, shown only when significant, remaining p-values shown in **Table 4** and **Table 5**.

Table 4: Multiple comparisons of 2-way Anova statistical analysis of the size of WT and AMOTL2 KO EBs treated and not treated with ROCKi.

Comparison	p-value (2-way Anova)
d0	
WT ROCKi(-) vs AMOTL2 KO ROCKi(-)	>0.9999
WT ROCKi(-) vs WT ROCKi(+)	>0.9999
WT ROCKi(-) vs AMOTL2 KO ROCKi(+)	>0.9999
AMOTL2 KO ROCKi(-) vs WT ROCKi(+)	>0.9999
AMOTL2 KO ROCKi(-) vs AMOTL2 KO ROCKi (+)	>0.9999
WT ROCKi(+) vs AMOTL2 KO ROCKi (+)	>0.9999
d1	
WT ROCKi(-) vs AMOTL2 KO ROCKi(-)	>0.9999
WT ROCKi(-) vs WT ROCKi(+)	>0.9999
WT ROCKi(-) vs AMOTL2 KO ROCKi(+)	>0.9999
AMOTL2 KO ROCKi(-) vs WT ROCKi(+)	0.9855
AMOTL2 KO ROCKi(-) vs AMOTL2 KO ROCKi (+)	0.8185
WT ROCKi(+) vs AMOTL2 KO ROCKi (+)	>0.9999
d2	
WT ROCKi(-) vs AMOTL2 KO ROCKi(-)	>0.9999
WT ROCKi(-) vs WT ROCKi(+)	0.5890
WT ROCKi(-) vs AMOTL2 KO ROCKi(+)	0.0728
AMOTL2 KO ROCKi(-) vs WT ROCKi(+)	0.1366
AMOTL2 KO ROCKi(-) vs AMOTL2 KO ROCKi (+)	0.0108
WT ROCKi(+) vs AMOTL2 KO ROCKi (+)	>0.9999
d3	
WT ROCKi(-) vs AMOTL2 KO ROCKi(-)	>0.9999
WT ROCKi(-) vs WT ROCKi (+)	0.0003
WT ROCKi(-) vs AMOTL2 KO ROCKi(+)	<0.0001
AMOTL2 KO ROCKi(-) vs WT ROCKi(+)	<0.0001
AMOTL2 KO ROCKi(-) vs AMOTL2 KO ROCKi (+)	<0.0001
WT ROCKi(+) vs AMOTL2 KO ROCKi (+)	>0.9999
d4	
WT ROCKi(-) vs AMOTL2 KO ROCKi(-)	0.9989
WT ROCKi(-) vs WT ROCKi(+)	<0.0001
WT ROCKi(-) vs AMOTL2 KO ROCKi(+)	<0.0001
AMOTL2 KO ROCKi(-) vs WT ROCKi(+)	<0.0001
AMOTL2 KO ROCKi(-) vs AMOTL2 KO ROCKi (+)	<0.0001
WT ROCKi(+) vs AMOTL2 KO ROCKi (+)	0.9762
d5	
WT ROCKi(-) vs AMOTL2 KO ROCKi(-)	>0.9999
WT ROCKi(-) vs WT ROCKi(+)	<0.0001

WT ROCKi(-) vs AMOTL2 KO ROCKi(+)	<0.0001
AMOTL2 KO ROCKi(-) vs WT ROCKi(+)	<0.0001
AMOTL2 KO ROCKi(-) vs AMOTL2 KO ROCKi (+)	<0.0001
WT ROCKi(+) vs AMOTL2 KO ROCKi (+)	0.0390
d6	
WT ROCKi(-) vs AMOTL2 KO ROCKi(-)	>0.9999
WT ROCKi(-) vs WT ROCKi(+)	<0.0001
WT ROCKi(-) vs AMOTL2 KO ROCKi(+)	<0.0001
AMOTL2 KO ROCKi(-) vs WT ROCKi(+)	<0.0001
AMOTL2 KO ROCKi(-) vs AMOTL2 KO ROCKi (+)	<0.0001
WT ROCKi(+) vs AMOTL2 KO ROCKi (+)	0.0022
d7	
WT ROCKi(-) vs AMOTL2 KO ROCKi(-)	0.0353
WT ROCKi(-) vs WT ROCKi(+)	<0.0001
WT ROCKi(-) vs AMOTL2 KO ROCKi(+)	<0.0001
AMOTL2 KO ROCKi(-) vs WT ROCKi(+)	<0.0001
AMOTL2 KO ROCKi(-) vs AMOTL2 KO ROCKi (+)	<0.0001
WT ROCKi(+) vs AMOTL2 KO ROCKi (+)	0.0013
d8	
WT ROCKi(-) vs AMOTL2 KO ROCKi(-)	<0.0001
WT ROCKi(-) vs WT ROCKi(+)	<0.0001
WT ROCKi(-) vs AMOTL2 KO ROCKi(+)	<0.0001
AMOTL2 KO ROCKi(-) vs WT ROCKi(+)	<0.0001
AMOTL2 KO ROCKi(-) vs AMOTL2 KO ROCKi (+)	<0.0001
WT ROCKi(+) vs AMOTL2 KO ROCKi (+)	0.0036
d9	
WT ROCKi(-) vs AMOTL2 KO ROCKi(-)	<0.0001
WT ROCKi(-) vs WT ROCKi(+)	<0.0001
WT ROCKi(-) vs AMOTL2 KO ROCKi(+)	<0.0001
AMOTL2 KO ROCKi(-) vs WT ROCKi(+)	<0.0001
AMOTL2 KO ROCKi(-) vs AMOTL2 KO ROCKi (+)	<0.0001
WT ROCKi(+) vs AMOTL2 KO ROCKi (+)	0.0052

I assessed the shape of the organoids using Form Factor (**Fig. 26C**). At day 0, I observed no statistically significant differences in the Form Factor of the WT and AMOTL2 KO EBs (**Fig. 34A, C**). Differentiating WT ROCKi(-) EBs became more round through days 1-4 and more irregular from day 5 onwards. Conversely, AMOTL2 KO ROCKi(-) EBs showed an opposite pattern with highly pronounced rosette-like irregular shape during days 1-4 (significantly different from WT ROCKi(-) at days 2-4), and becoming round again from day 5 onwards. The addition of ROCKi did not affect the shape of WT EBs, as they followed a pattern highly similar to WT ROCKi(-) EBs, becoming more regularly shaped during days 1-4 and less regular during days 5-9. In contrast, ROCKi treatment induced dramatic changes in AMOTL2 KO EBs, which maintained their round shape through the whole course of the differentiation without any major irregularities (**Fig. 34A, C**). Of note, the irregularities of WT ROCKi(-) and WT ROCKi(+) EBs on days 8 and 9 were different from those observed in AMOTL2 KO ROCKi(-) EBs during days 1-4 (cysts vs rosettes, respectively). On day 9 both ROCKi(-) and ROCKi(+) WT EBs were more irregular than either ROCKi(-) or ROCKi(+) AMOTL2 KO EBs. The differences reached the statistical significance for WT ROCKi(+) vs AMOTL2 KO ROCKi(+) and for WT ROCKi(+) vs AMOTL2 KO ROCKi(-), and almost for WT ROCKi(-) vs AMOTL2 KO ROCKi(-), with the p-value of 0.0534. On the graph only significant p-values compared to the WT ROCKi(-) conditions are shown, the full list of comparisons can be found in **Table 5**. Interestingly, it appears that AMOTL2 deficiency allows formation of the rosette-shaped organoids which is blocked by the addition of ROCKi. However, the cyst-like irregularities in WT organoids are ROCKi-independent.

Table 5: Multiple comparisons of 2-way Anova statistical analysis of the Form Factor of WT and AMOTL2 KO EBs treated and not treated with ROCKi.

Comparison	p-value (2-way Anova)
d0	
WT ROCKi(-) vs AMOTL2 KO ROCKi(-)	>0.9999
WT ROCKi(-) vs WT ROCKi(+)	>0.9999
WT ROCKi(-) vs AMOTL2 KO ROCKi(+)	>0.9999
AMOTL2 KO ROCKi(-) vs WT ROCKi(+)	>0.9999
AMOTL2 KO ROCKi(-) vs AMOTL2 KO ROCKi (+)	>0.9999
WT ROCKi(+) vs AMOTL2 KO ROCKi (+)	>0.9999
d1	
WT ROCKi(-) vs AMOTL2 KO ROCKi(-)	0.1248
WT ROCKi(-) vs WT ROCKi(+)	0.8882
WT ROCKi(-) vs AMOTL2 KO ROCKi(+)	0.9369
AMOTL2 KO ROCKi(-) vs WT ROCKi(+)	<0.0001
AMOTL2 KO ROCKi(-) vs AMOTL2 KO ROCKi (+)	<0.0001
WT ROCKi(+) vs AMOTL2 KO ROCKi (+)	>0.9999
d2	

WT ROCKi(-) vs AMOTL2 KO ROCKi(-)	0.0006
WT ROCKi(-) vs WT ROCKi(+)	>0.9999
WT ROCKi(-) vs AMOTL2 KO ROCKi(+)	>0.9999
AMOTL2 KO ROCKi(-) vs WT ROCKi(+)	<0.0001
AMOTL2 KO ROCKi(-) vs AMOTL2 KO ROCKi (+)	<0.0001
WT ROCKi(+) vs AMOTL2 KO ROCKi (+)	>0.9999
d3	
WT ROCKi(-) vs AMOTL2 KO ROCKi(-)	<0.0001
WT ROCKi(-) vs WT ROCKi (+)	>0.9999
WT ROCKi(-) vs AMOTL2 KO ROCKi(+)	>0.9999
AMOTL2 KO ROCKi(-) vs WT ROCKi(+)	<0.0001
AMOTL2 KO ROCKi(-) vs AMOTL2 KO ROCKi (+)	<0.0001
WT ROCKi(+) vs AMOTL2 KO ROCKi (+)	>0.9999
d4	
WT ROCKi(-) vs AMOTL2 KO ROCKi(-)	0.0022
WT ROCKi(-) vs WT ROCKi(+)	>0.9999
WT ROCKi(-) vs AMOTL2 KO ROCKi(+)	>0.9999
AMOTL2 KO ROCKi(-) vs WT ROCKi(+)	0.0030
AMOTL2 KO ROCKi(-) vs AMOTL2 KO ROCKi (+)	0.0005
WT ROCKi(+) vs AMOTL2 KO ROCKi (+)	>0.9999
d5	
WT ROCKi(-) vs AMOTL2 KO ROCKi(-)	>0.9999
WT ROCKi(-) vs WT ROCKi(+)	>0.9999
WT ROCKi(-) vs AMOTL2 KO ROCKi(+)	>0.9999
AMOTL2 KO ROCKi(-) vs WT ROCKi(+)	>0.9999
AMOTL2 KO ROCKi(-) vs AMOTL2 KO ROCKi (+)	>0.9999
WT ROCKi(+) vs AMOTL2 KO ROCKi (+)	>0.9999
d6	
WT ROCKi(-) vs AMOTL2 KO ROCKi(-)	>0.9999
WT ROCKi(-) vs WT ROCKi(+)	>0.9999
WT ROCKi(-) vs AMOTL2 KO ROCKi(+)	>0.9999
AMOTL2 KO ROCKi(-) vs WT ROCKi(+)	>0.9999
AMOTL2 KO ROCKi(-) vs AMOTL2 KO ROCKi (+)	>0.9999
WT ROCKi(+) vs AMOTL2 KO ROCKi (+)	>0.9999
d7	
WT ROCKi(-) vs AMOTL2 KO ROCKi(-)	>0.9999
WT ROCKi(-) vs WT ROCKi(+)	>0.9999
WT ROCKi(-) vs AMOTL2 KO ROCKi(+)	0.9981
AMOTL2 KO ROCKi(-) vs WT ROCKi(+)	0.9991
AMOTL2 KO ROCKi(-) vs AMOTL2 KO ROCKi (+)	>0.9999
WT ROCKi(+) vs AMOTL2 KO ROCKi (+)	0.7762

d8	
WT ROCKi(-) vs AMOTL2 KO ROCKi(-)	0.6912
WT ROCKi(-) vs WT ROCKi(+)	>0.9999
WT ROCKi(-) vs AMOTL2 KO ROCKi(+)	0.7669
AMOTL2 KO ROCKi(-) vs WT ROCKi(+)	0.2602
AMOTL2 KO ROCKi(-) vs AMOTL2 KO ROCKi (+)	>0.9999
WT ROCKi(+) vs AMOTL2 KO ROCKi (+)	0.3187
d9	
WT ROCKi(-) vs AMOTL2 KO ROCKi(-)	0.0534
WT ROCKi(-) vs WT ROCKi(+)	>0.9999
WT ROCKi(-) vs AMOTL2 KO ROCKi(+)	0.5610
AMOTL2 KO ROCKi(-) vs WT ROCKi(+)	0.0007
AMOTL2 KO ROCKi(-) vs AMOTL2 KO ROCKi (+)	>0.9999
WT ROCKi(+) vs AMOTL2 KO ROCKi (+)	0.0201

3.10. AMOTL2 KO promotes YAP activity in hPSCs yet the lineage bias in AMOTL2 KO is YAP-independent

Hippo is an inhibitory pathway regulating YAP activity. While YAP itself was not changed in our bulk RNA-seq data, the Hippo pathway GO term was downregulated (**Fig. 24D**). The downregulation of the Hippo pathway decreases YAP phosphorylation, which is synonymous with its cytoplasmic localization, and consequently, promotes nuclear localization synonymous with higher YAP activity. AMOTL2 supports Hippo pathway in its inhibitory role against YAP (**Fig. 6**), and therefore, its knockout would be expected to promote YAP nuclear localization and activity. To assess YAP subcellular localization at the protein level, I stained WT and AMOTL2 KO hPSCs against YAP (**Fig. 35A**). Next, I identified the nuclear and cytoplasmic compartments using a custom Cell Profiler pipeline and calculated the ratio of nuclear vs cytoplasmic YAP mean intensity, revealing increased nuclear localization of YAP in AMOTL2 KO hPSCs (**Fig. 35B**). YAP was previously reported to affect cell fate, especially ICM vs trophectoderm determination (Alarcon & Marikawa, 2018; Hirate et al., 2013; Leung & Zernicka-Goetz, 2013), and self-renewal vs differentiation decision, with YAP repression being permissible for the latter (Estarás et al., 2017; Meyer et al., 2023). To assess whether AMOTL2 KO phenotype in lineage bias is dependent on YAP, I performed EB spontaneous differentiation with verteporfin. Verteporfin inhibits YAP activity by increasing the level of 14-3-3σ protein, which in turn sequestrates YAP in the cytoplasm and targets it for proteasomal degradation (Chao Wang et al., 2016). Therefore, if AMOTL2 KO cell fate bias was dependent on YAP, verteporfin should reverse it, meaning upregulate endoderm-related genes and downregulate ectoderm-related genes. After 2 days of spontaneous differentiation, I collected the RNA from control and verteporfin-treated EBs to examine the gene expression of the previously used lineage markers (**Fig. 35C, D**). Treatment of AMOTL2 KO EBs with verteporfin did not influence the cell fate bias, since AMOTL2 KO verteporfin(+) EBs still

preferentially differentiated into ectoderm, similarly to untreated AMOTL2 KO EBs (**Fig. 35D**). In contrast, in WT EBs, verteporfin treatment inhibited endoderm and mesoderm formation, compared to untreated WT, yet without ectoderm induction (**Fig. 35D**). This indicates that AMOTL2 deficiency overrides the sole effect of YAP inhibition, strongly suggesting that there are other players by which AMOTL2 controls cell fate.

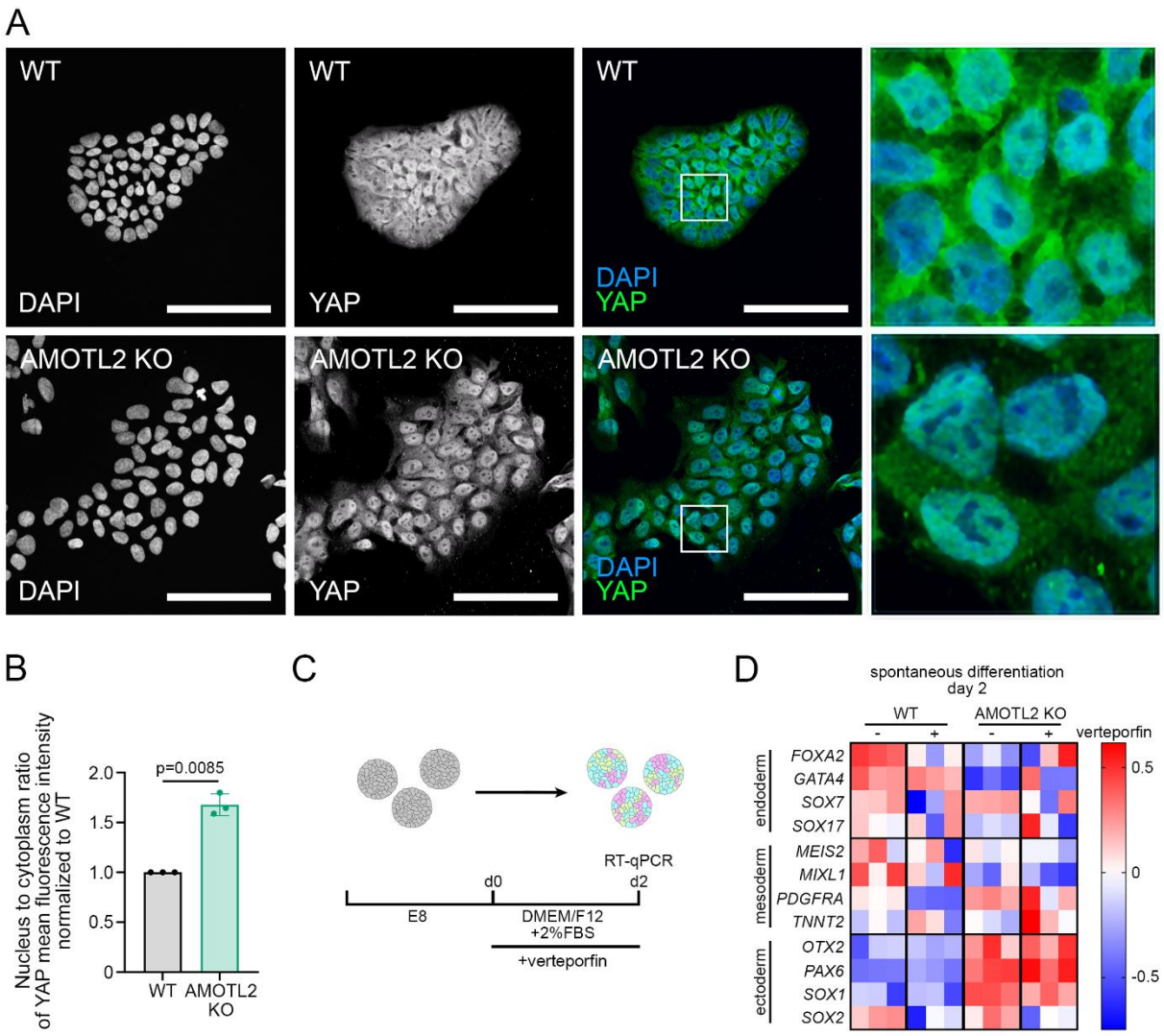

Fig. 35: AMOTL2 KO promotes YAP activity in hPSCs yet the lineage bias in AMOTL2 KO is YAP-independent. A. Representative images of immunofluorescent staining against YAP (green). Nuclei stained in blue with DAPI. Scale bar = 100 µm. N=3. The last panel is a zoom in from the marked square. **B.** Quantification of the nucleus to cytoplasm ratio of YAP mean fluorescence intensity. Statistics: t-Student test with Welch's correction. N=3. **C.** Schematic illustration of the protocol used for spontaneous EB differentiation with verteporfin. **D.** Gene expression analysis of day 2 spontaneously differentiating EBs with verteporfin. N=3 Statistics: t-Student test with Welch's correction.

3.11. Calcium channel PIEZO1 is decreased in AMOTL2 KO

Hippo pathway is a mechanosensing pathway, meaning that it integrates the outside mechanical cues into gene expression. In AMOTL2 KO hPSCs I observed downregulation of the mechanosensing Ca^{2+} channel PIEZO1 mRNA expression, with simultaneous upregulation of PIEZO2 (**Fig. 36A**). Based on bulk RNA-seq, PIEZO1 is a dominant family member in hPSC (**Fig. 36B**). I further confirmed PIEZO1 protein presence in hPSCs and its decreased level in AMOTL2 KO (**Fig. 36C, D**).

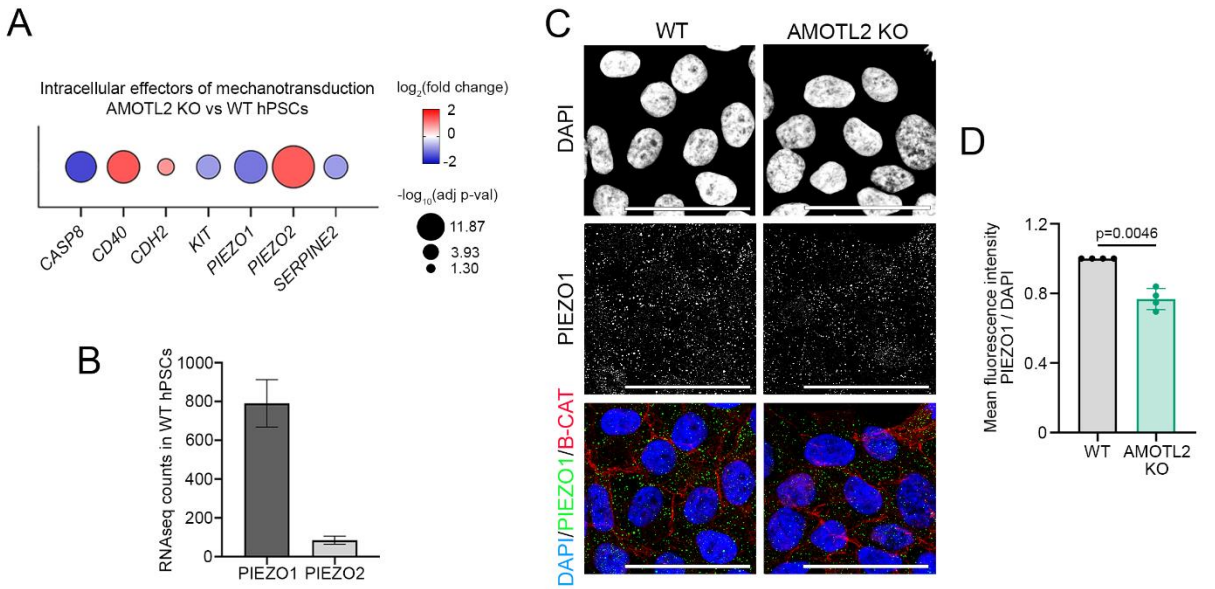

Fig. 36: Mechanosensing channel PIEZO1 in AMOTL2 KO hPSCs. A. Selected genes connected with mechanotransduction from RNA-seq. N=2. Note that genes with -$\log_{10}$ (adj p-val)$<$1.3 are not significantly changed. Statistical significance calculated with DESeq2. **B.** PIEZO mRNA expression in WT hPSCs assessed by bulk RNA-seq. Statistics: t-Student test N=2 **C.** Representative images of immunostaining against β-CAT (red) and PIEZO1 (green). Nuclei stained in blue with DAPI. N=3 Scale bar = 50 µm. **D.** Quantification PIEZO1 mean fluorescence intensity. Statistics: t-Student test with Welch's correction. N=3.

4. Discussion

4.1. AMOTL2 expression in human

This thesis includes a first comprehensive analysis of AMOTL2 expression patterns in human pluripotency and pancreatic development. AMOTL2 expression was previously reported in several human cell lines, including HEK293A, HEK293T, MCF10A (Kim et al., 2016; Z. Li et al., 2012; S. Mana-Capelli et al., 2014; Sebastian Mana-Capelli & McCollum, 2018; Paramasivam et al., 2011; W. Wang et al., 2015; Y. Wang et al., 2011), HeLa (Z. Li et al., 2012; S. Mana-Capelli et al., 2014; Sebastian Mana-Capelli & McCollum, 2018), HUVEC (Y. Wang et al., 2011), U87 and U251 glioblastoma cell lines (Artinian et al., 2015; X. Chen et al., 2021), and HepG2 (Han et al., 2017).

Here, I showed by the analysis of the publicly available scRNA-seq data, that *AMOTL2* earliest expression during development was found at the morula stage of preimplantation embryos, and it continued to be expressed in ICM *in vivo* and four independent lines of hPSCs cultured *in vitro*, proving that *AMOTL2* expression is not line-specific. I also confirmed the presence of AMOTL2 protein in hPSCs. This is consistent with the reports that identified AMOTL2 expression in human blastocyst, and in hPSCs (Hildebrand et al., 2017; Pagliari et al., 2021; Zaltsman et al., 2019).

Further, I showed that as we progress into pancreatic differentiation, *AMOTL2* mRNA expression was widespread at the DE stage, with varying levels, depending on the dataset. Next, *AMOTL2* mRNA could be found in a fraction of PP and EP cells during *in vitro* differentiation, and in a population of EP/early endocrine cells in developing human pancreas from 8-20 wpc. I confirmed the presence of AMOTL2 protein in human fetal pancreatic tissue from 10 wpc and 13 wpc. The expression pattern of known EP/early endocrine markers suggested that *AMOTL2* mRNA was expressed in early EPs and its expression diminished as they progressed into endocrine cells. *AMOTL2* mRNA was also detected in mesenchymal and ductal cells, as well as in a fraction of acinar, endothelial, and pancreatic stellate cells in both embryonic and adult tissues. In adult pancreas *AMOTL2* was not expressed in the endocrine cells. AMOTL2 expression was not previously explored in human pancreatic differentiation, except for the article by Scavuzzo et al. (Scavuzzo et al., 2018) from previous prof. Borowiak lab. There, AMOTL2 downregulation in the hPSC-derived EPs increased α-cell differentiation efficiency at the expense of β-cells (Scavuzzo et al., 2018).

Importantly, here, for the first time, I show the existence of the *NGN3*(+) / *AMOTL2*(+) endocrine progenitor population in human, in both *in vitro* directed pancreatic differentiation and *in vivo* pancreatic development. This specific population was earlier identified only in mice (Scavuzzo et al., 2018; van Gurp et al., 2019).

In this thesis, AMOTL2 protein was identified in 10 wpc and 13 wpc human fetal pancreatic tissue. The specimens were not stained against NGN3 for the following reasons: 1) the majority of the antibodies against NGN3 for immunofluorescence developed up to date are not of satisfactory

quality. 2) NGN3 expression in EPs is transient. Considering that the NGN3(+) population at a given timepoint is extremely small, accounting for up to 2% of all cells in the pancreas (Olaniru et al., 2023), there was a high probability that we would not detect NGN3(+) cells in the single tissue slides. 3) The NGN3(+) cells quickly progress into early endocrine cells, marked by the expression of CHGA. Since 93% of the *NGN3*(+) EPs in the developing human pancreas already co-express *CHGA* (Olaniru et al., 2023) and antibodies against CHGA produce a strong and specific signal, we decided to use this marker.

4.2. AMOTL2 in colony architecture

Here, I showed that AMOTL2 deficiency influences hPSC colony morphology, making them more irregular in shape as opposed to the classical hPSC colonies with well-defined smooth edges. Additionally, AMOTL2 KO colonies had more holes which are generally not found in WT hPSC colonies. While it is not direct evidence, these morphology changes might be a sign of increased mesenchymal phenotype of AMOTL2 KO hPSCs. This is supported by a clear dysregulation of the EMT- and migration-related genes in AMOTL2 KO in our bulk RNA-seq data, including upregulation of canonical EMT markers, such as *CDH2*, *VIM*, *FN1*, and *MMP2* (Matrix Metallopeptidase 2). Additionally, in our lab, we assessed the level of several adhesion proteins, which revealed decrease in the VCL and CDH1 levels, increase of CDH2 and VIM levels and unchanged levels of β-CAT, PXN (Paxilin), and ITGA5 (**Fig. 37**).

I attempted to assess the AMOTL2 KO hPSC motility, with a classical wound-healing migration assay, yet it was not best-suited for hPSCs. In wound-healing assay, the cells are grown into a confluent monolayer and a cell-free area is created either by scratch or by removing an insert that was preventing cells from growing in the particular area. However, hPSCs require coating for adherence, which was most probably disrupted while removing insert, since in my experiments neither WT nor AMOTL2 KO hPSCs have grown into the wound. I also tested time-lapse imaging paired with single-cell movement tracking as proposed by several groups (Chang et al., 2019; L. Li et al., 2010; Phadnis et al., 2015; Wadkin et al., 2017; Yamamoto et al., 2018) with the ImageJ TrackMate plugin. While the initial data suggest an increase in the speed (μm/h) of AMOTL2 KO hPSCs movement compared to WT, more technical and biological replicates would be needed to ensure the reliability. There are several factors to consider when examining hPSC motility: 1) hPSC movement is influenced by the proximity of the other cells, with more random-walk type and less directional movement as the distance between cells increases (L. Li et al., 2010); 2) Passaging hPSCs as single cells and seeding them sparsely is detrimental for their wellbeing and results in dissociation-induced apoptosis (Watanabe et al., 2007) unless treated with ROCKi. However, ROCKi increases hPSC migration (L. Li et al., 2010) and therefore might influence the results; 3) Tracking cells with brightfield images is challenging, hence the desire to use live cell stains, which however can also influence the migration rate (Wadkin et al., 2017).

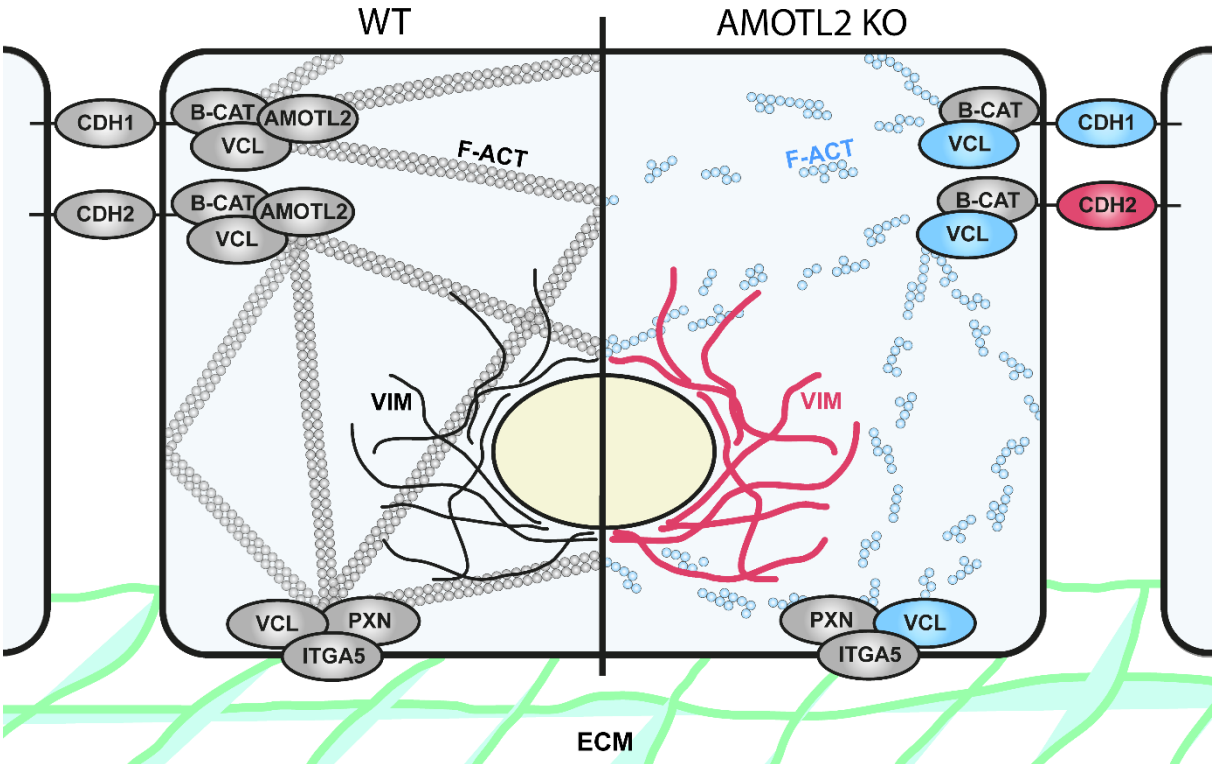

Fig. 37: Schematic summary of the changes in adhesion molecules in AMOTL2 KO compared to WT hPSCs. Black/gray indicate no changes in protein level, blue - decreased level, red - increased level.

Based on literature, AMOTL2 indeed has a role in cell motility, yet the results remain inconclusive. AMOTL2 KD resulted in the increase in cell migration in human epithelial cell lines, more spindle-like cell shape, and lower expression of the epithelial marker CDH1 with increased mesenchymal markers VIM and CDH2 (Artinian et al., 2015; X. Chen et al., 2021; Kim et al., 2016; W. Wang et al., 2011), which is also the most similar to our data on AMOTL2 KO in hPSCs (**Fig. 37**). Further, Amotl2 KD in canine epithelial cells led to the loss of contact inhibition (Zhao et al., 2011). The overexpression of AMOTL2 p60 isoform, which was reported to mimic AMOTL2 p100 isoform knockdown did not affect invasion in the study by Mojallaj et al. but increased invasiveness in the study by Subramani et al. (Mojallal et al., 2014; Subramani et al., 2023). AMOTL2 overexpression increased epithelial cell migration in Huang et. al (H. Huang et al., 2007) yet decreased it in (X. Chen et al., 2021). In human endothelial cells AMOTL2 deficiency inhibited migration (Y. Wang et al., 2011), similarly as in zebrafish embryo (H. Huang et al., 2007).

While experimentally beyond the scope of this thesis, the potentially upregulated migration of AMOTL2-deficient cells might become crucial during differentiation towards pancreatic cells, at the EP stage. I selected *Amotl2* as a gene specifically upregulated in the EP subtype 2, which was identified as EPs delaminating from epithelial cords into surrounding mesenchyme (Scavuzzo et al., 2018). This process is crucial for the formation of Langerhans islets. The mechanism behind EP exit from epithelial cords is still vague, yet it is strongly suggested to rely on the increased mesenchymal EP phenotype. According to the traditional, yet currently questioned, dispersal-aggregation model,

NGN3(+) EPs would undergo the EMT, which would allow them to leave epithelial cords and migrate into mesenchyme. Then, by the unknown mechanism, the dispersed cells would aggregate into islets and regain epithelial features (Benitez et al., 2012; Pan & Wright, 2011). Another model of EP exit from epithelial cords, a peninsular model, was first proposed in 1944 by Hard (Hard, 1944) and recently revisited by Sharon et al. (Sharon, Chawla, et al., 2019). There, EPs would undergo only partial EMT, where the upregulation of the mesenchymal genes is accompanied by the sustained expression of epithelial genes. As a result, the epithelial cord architecture becomes loosened, yet the cell-cell contacts are not entirely disrupted. Consequently, newly born EPs delaminate and form bud-like structures, called peninsulas, which eventually detach from cords to form islets. It is currently unknown if this model is applicable also in humans, however, peninsula-like buds were previously observed in hPSC pancreatic differentiation (Sharon, Chawla, et al., 2019).

It remains unclear how AMOTL2 would regulate EP delamination, yet it appears to be an exciting direction to explore. Since AMOTL2 KO results in the more mesenchymal phenotype in hPSCs, it is possible that not the increase in AMOTL2 expression in EP2 but AMOTL2 loss that happens between EP2 and EP3 is crucial for EP delamination. This remains to be studied in depth during hPSC pancreatic differentiation, however, we would need different tools, preferably inducible KO and OE constructs, since we showed that AMOTL2 KO hinders an efficient DE formation, which is a crucial step before EP formation.

4.3. AMOTL2 in proliferation and apoptosis

In this thesis I showed that AMOTL2 deficiency results in the increased proliferation and decreased apoptosis in hPSCs. The influence of AMOTL2 manipulation on the proliferation was previously studied in different models, with fairly consistent results. In epithelial cells AMOTL2 expression inhibits proliferation in both mouse and human (X. Chen et al., 2021; Cui et al., 2021; P. Fang et al., 2021), while AMOTL2 deficiency promotes proliferation in zebrafish, mouse, and human (Agarwala et al., 2015; Artinian et al., 2015; X. Chen et al., 2021; P. Fang et al., 2021). In contrast, AMOTL2 KD in endothelial cells resulted in decreased proliferation in both zebrafish and human (Y. Wang et al., 2011). AMOTL2 influence on proliferation was not yet studied in hPSCs. The apoptosis in the context of AMOTL2 was generally not studied previously. The influence on the proliferation and apoptosis is most probably connected with increased YAP activity in AMOTL2 KO, since YAP and Hippo pathway have a well-established role in those processes (Fu et al., 2022; Liu et al., 2012), and YAP overexpression in hESC induces proliferation (Choe et al., 2022).

4.4. AMOTL2 and lineage bias

Here, I showed that pluripotency factor expression was not impaired in AMOTL2 KO - SOX2 and NANOG levels were unchanged, while OCT3/4 was increased. Confronted with literature, both overexpression and KD of OCT3/4 in hESC promoted the endodermal fate in study by Rodriguez et al.

(Rodriguez et al., 2007). Further, Wang et al. (Z. Wang et al., 2012) showed that OCT3/4 overexpression stimulates endoderm formation, while inhibiting ectoderm. This seemingly stands in opposition to our data, however, might be connected with the OCT3/4 dosage, since in AMOTL2 KO OCT3/4 was 1.25-fold upregulated, in contrast to 4-fold increase in Wang et al. (Z. Wang et al., 2012). Additionally, OCT3/4 might regulate the expression of BMP4 (Z. Wang et al., 2012), the endoderm-related gene which is downregulated in our RNA-seq data from AMOTL2 KO.

In this thesis, I proved that AMOTL2 KO promotes ectoderm formation and hinders endoderm differentiation in spontaneous differentiation, also confirming ectoderm acceleration with directed differentiation. Both methods have their strengths and weaknesses and should be considered complementary. The spontaneous differentiation performed in the differentiation-permissive medium without any small molecules provides the most unbiased results, however it might suffer from the high variability between biological replicates. While the ectoderm dominance was consistently present with every round of the spontaneous differentiation that I performed, the gene expression levels varied, in some cases making it challenging to reach statistical significance. We also attempted to use another spontaneous differentiation assay, relying on micropatterned colonies in cooperation with the protocol authors (Warmflash et al., 2014). Two issues arose: 1) the protocol was originally applied to H1 cells and Hues8-iCas9 cell line did not follow the same differentiation patterns; and 2) in this system there were no significant differences between WT and AMOTL2 KO differentiating cells, which might be attributed to the fact that micropatterned colonies are treated with BMP4 to induce differentiation.

Directed differentiation, while more reproducible, is frequently performed with the excess of small molecules to achieve the desired efficiency in various hPSC lines. If the cell fate bias is more subtle, this excess can mask the existing phenotype.

In the directed differentiation towards ectoderm, I demonstrated the existence of the dominant double-positive SOX1(+) / OCT3/4(+) and OTX2(+) / OCT3/4(+) populations in differentiating WT cells. Instead in AMOTL2 cells this population was dramatically reduced and replaced by ectoderm marker(+) / OCT3/4(-) populations. Similar pattern was also observed by Noisa et al. (Noisa et al., 2012) in H1 and H7 hPSC lines with the intermediate neural progenitor population co-expressing pluripotency markers and ectodermal markers, OCT3/4 and PAX6 respectively. The pluripotency factors would further diminish, and ectodermal markers increase as the differentiation progressed (Noisa et al., 2012). This indicates that AMOTL2 KO neural progenitors are more mature than in WT.

AMOTL2 was not previously studied in the context of tri-lineage specification. Angiomotin family members were shown to be involved in the first cell fate decision between TE and ICM in mouse blastocyst. *Amot* was enriched in the ICM vs TE, where it prevented the expression of TE marker, Cdx2, in F-actin, Yap, and Rho-dependent manner. Depletion of *Amot* or its co-depletion with *Amotl2* resulted in the Hippo pathway activation, exclusion of Yap form the nucleus, downregulation of pluripotency markers, differentiation towards TE and compromised embryo development (Hirate et al., 2013; Leung

& Zernicka-Goetz, 2013; Shi et al., 2017). The Cdx2 was not upregulated in Amotl2-deficient mouse blastocyst, indicating no Amotl2 involvement in TE vs ICM determination (Hildebrand et al., 2017). The *Amotl2* mRNA was upregulated in TE vs ICM in both mouse and human blastocyst, suggesting a differential functions of Amot and Amotl2 in this cell fate decision (Hildebrand et al., 2017). However, I showed that in human the expression of *AMOT* in hPSCs is 22-fold lower than of *AMOTL2*, and therefore it seems unlikely that AMOT could be involved in tri-lineage determination.

4.5. AMOTL2 and F-actin cytoskeleton

AMOTL2 involvement in cytoskeleton changes was previously reported by several groups in different systems, however not in hPSCs. Both overexpression and knockdown of AMOTL2 result in changes in F-actin. AMOTL2 overexpression in human epithelial cells disrupted peripheral F-actin fibers (H. Huang et al., 2007). AMOTL2 knockdown or overexpression of the p60 isoform caused the loss of radial F-actin fibers in canine and human epithelial cells, and in mouse blastocyst (Hildebrand et al., 2017; Subramani et al., 2023). Studies in zebrafish also showed less abundant and disrupted F-actin fibers following Amotl2 knockdown (H. Huang et al., 2007; Hultin et al., 2014, 2017).

F-actin depolymerization with ROCKi (Y-27632) in WT did not mimic the ectodermal cell fate bias of AMOTL2 KO. ROCKi treatment appeared to generally improve the differentiation efficiency but without particular direction. Boraas et al. (Boraas et al., 2018) performed a similar experiment, where they treated spontaneously differentiating EBs with cytochalasin D, as F-actin depolymerization agent, and jasplakinolide for the opposite effect. F-actin depolymerization resulted in increase in endoderm differentiation efficiency, and mixed results for mesoderm efficiency. Ectoderm was not studied by authors. While I could see an improvement in endoderm formation efficiency in WT ROCKi(+) vs WT ROCKi(-) EBs, this effect was not visible in AMOTL2 KO (**Fig. 33E, F**), suggesting that there is a dominant factor over F-actin depolymerization in AMOTL2 deficiency-related cell bias.

Additional experiments could be performed, with other F-actin depolymerizing agents, such as latrunculin A (Coue et al., 1987; Fujiwara et al., 2018) or cytochalasin D (Casella et al., 1981; Goddette & Frieden, 1986) to further confirm this phenotype.

4.6. AMOTL2 and YAP

In this thesis, we showed that AMOTL2 deficiency activates YAP in hPSCs, which is in line with AMOTL2 being a known YAP and Hippo pathway regulator in other systems. AMOTL2 KD in murine and human epithelial cells resulted in increased YAP/TAZ activity, as designated by the increase in the nuclear localization of YAP/TAZ, decrease in their phosphorylation, and decreased LATS1/2 phosphorylation/activity (P. Fang et al., 2021; Paramasivam et al., 2011; Zhao et al., 2011). AMOTL2 overexpression caused cytoplasmic localization of YAP/TAZ and increase in YAP/TAZ phosphorylation in both human and mice (P. Fang et al., 2021; Lucci et al., 2013; Paramasivam et al.,

2011). Of note, in the studies by Mana-Capelli et al. the knockdown or overexpression of individual angiomotin family members did not induce significant changes in Hippo pathway, yet modulation of all three angiomotins mimicked the results obtained by other groups (S. Mana-Capelli et al., 2014; Sebastian Mana-Capelli & McCollum, 2018). Similarly, in mouse preimplantation embryo, Amotl2 and Amot simultaneous knockdown promoted Yap nuclear localization, as opposed to Amotl2 knockdown only (Hirate et al., 2013).

YAP has a relatively well documented role in cell fate decisions at the different stages of differentiation. For instance, YAP is involved in the fate specification between TE and ICM. In mouse blastocyst, nuclear active Yap is present in the outer cells where it is required for the expression of the trophectoderm-related gene Cdx2, while in the ICM cells YAP is sequestered in cytoplasm (Hirate et al., 2013; Leung & Zernicka-Goetz, 2013; Shi et al., 2017). This YAP expression pattern and TE vs ICM determination mechanism appears to be conserved in human (Gerri et al., 2020). Along this line, the stable self-renewal of naive hPSCs requires YAP inhibition, while YAP induction results in the activation of the trophectodermal fate (Dattani et al., 2022). After this first cell fate decision, Yap is activated in the murine ICM cells and is necessary for the high expression of the pluripotency factors (Hashimoto & Sasaki, 2019). YAP is also predominantly active (nuclear) in primed hPSC lines (Beyer et al., 2013; Pagliari et al., 2021; Qin et al., 2012; Varelas et al., 2008), however it is not indispensable for pluripotency, since neither upregulation nor downregulation of YAP impairs hPSC colony morphology and pluripotency marker levels (Estarás et al., 2017; Laowtammathron et al., 2023; Quan et al., 2022; Zeevaert et al., 2023).

The influence of YAP was also previously studied in the tri-lineage specification. In directed differentiation YAP OE hinders mesoderm formation (Pagliari et al., 2021; Quan et al., 2022), while YAP deficiency generally promotes endoderm and mesoderm differentiation, and inhibits ectodermal fate (Estarás et al., 2017; Pagliari et al., 2021; Quan et al., 2022; Stronati et al., 2022; Zeevaert et al., 2023), however the effect on mesoderm and ectoderm formation was not always present (Pagliari et al., 2021; Zeevaert et al., 2023). In the EB spontaneous differentiation performed by Laowtammathron et al. (Laowtammathron et al., 2023) YAP KO promotes mesoderm but do not influence endoderm formation, while YAP OE upregulates endoderm and inhibits mesoderm. None influences the ectoderm specification (Laowtammathron et al., 2023). In contrast, another group performed a semi-spontaneous differentiation with the addition of SB431542, where the YAP KO EBs did not differentiate and retained the high levels of pluripotency markers (Zeevaert et al., 2023). The 2D self-patterning YAP KO organoids primed with BMP4 upregulated endoderm and mesoderm at the expense of ectoderm (Stronati et al., 2022).

Interestingly, this YAP KO phenotype appears to be the opposite of our AMOTL2 KO phenotype, which would suggest that AMOTL2 KO cell fate bias could be YAP-dependent. However, I showed that treatment with YAP inhibitor, verteporfin, does not promote mesendodermal fate. Manipulation with YAP activity did not result in the reversal of AMOTL2 KO differentiation bias towards ectoderm

(**Fig. 35D**). In WT, verteporfin treatment resulted in decreased efficiency of endoderm and mesoderm formation, which appears to be opposite to what was expected. This indicates, that while YAP could be partially responsible for the mesendodermal part of the phenotype, AMOTL2 KO cell fate bias phenotype is not entirely YAP-dependent and there are more potent players in the game.

4.7. AMOTL2 influences size and shape of spontaneously differentiating EBs

This thesis demonstrates that AMOTL2 KO spontaneously differentiating EBs differ from WT EBs in size and shape. The addition of ROCKi affects the size of WT EBs but not their growth or shape pattern. In contrast, the ROCKi treatment of AMOTL2 KO EBs induces dramatic changes compared to the untreated AMOTL2 KO EBs, with growth and shape patterns more similar to WT and almost no increase in the size during culture. AMOTL2 KO EBs show differentiation bias towards ectodermal lineages, and inhibited endoderm and mesoderm fate, compared to WT EBs. The addition of ROCKi does not significantly affect the cell fate. This suggests that EB morphological changes are not coupled with the cell fate decisions in this setting. On the other hand, in the rare cases when I did not observe the characteristic rosette-like structure formation, I also did not observe the differences in cell fate. This is an intriguing phenomenon, however it would require further research, which is beyond the scope of this thesis.

4.8. Future directions

The previous research on angiomotin family members in the TE vs ICM cell fate decisions implied a heavy involvement of both cytoskeleton and YAP in the process. While I can clearly see the dysregulation of the cytoskeleton and YAP in the AMOTL2 KO hPSCs, the experimental data indicate that neither of them is a main player in AMOTL2-dependent ectoderm bias during differentiation.

In the future, it would be exciting to explore the YAP-independent modes of AMOTL2 action. The preliminary data points to the possible directions:

1) In AMOTL2 KO hPSCs I observed downregulation of the mechanosensing Ca^{2+} channel PIEZO1. Consequently, the intracellular Ca^{2+} levels are also changed in AMOTL2 KO. Ca^{2+} is an important intracellular messenger that influences various cellular functions. There are also implications that Ca^{2+} levels might be involved in the cell fate regulation (Bikle et al., 2012; Hao et al., 2016; Sinha et al., 2022). Treatment with PIEZO1 activator, YODA1 (Botello-Smith et al., 2019), or alternatively, activation of another calcium channel during spontaneous differentiation could shed a light on Ca^{2+} importance for lineage determination.
2) The RNA-seq showed significant changes in the cellular metabolism and energy production mechanisms in AMOTL2 KO compared to WT. The preliminary functional assays confirmed changes in mitochondria activity in AMOTL2 KO. Both mitochondria status and metabolism

can be involved in the differentiation or change as cells differentiate, which sets an interesting course for future research (Lv et al., 2022; Qi et al., 2022; Seo et al., 2018).

Last but not least, it is compelling to investigate AMOTL2 role in human pancreatic differentiation. I first identified *Amotl2* in the specific population of mouse EPs biased towards β-cell production. Here, I showed that the *AMOTL2*(+) EP population exists also in human, raising the question if AMOTL2 can be a regulator of β-cell differentiation in human. In support of this, AMOTL2 KD in hPSC-derived PPs resulted in the decreased number of β-cells (Scavuzzo et al., 2018), however the underlying mechanisms were not explored. Since *Amotl2* expression in mice was specific for the delaminating EPs, and AMOTL2 is known to have a role in cell migration in several systems, it would be super interesting to explore if and how these two processes are interconnected.

5. Materials and methods

5.1. scRNA-seq atlases analyzed in the thesis

Table 6: List of scRNA-seq atlases used in the thesis

AUTHOR & YEAR	CELL TYPE	PUBLICATION	LINK TO THE ATLAS
(Baron et al., 2016)	● adult pancreas	A Single-Cell Transcriptomic Map of the Human and Mouse Pancreas Reveals Inter- and Intra-cell Population Structure	https://human-pancreas.cells.ucsc.edu
(Enge et al., 2017)	● adult pancreas: mixed ages, from 1 month to 54 years	Single-Cell Analysis of Human Pancreas Reveals Transcriptional Signatures of Aging and Somatic Mutation Patterns	https://adultPancreas.cells.ucsc.edu
(Z. Fang et al., 2019)	● hESC (H1, H9) ● human primary islets	Single-Cell Heterogeneity Analysis and CRISPR Screen Identify Key β-Cell-Specific Disease Genes	Beta cell Hub (case.edu)
GRAPPA (Boroviak et al., 2018)	● preimplantation embryos	Single cell transcriptome analysis of human, marmoset and mouse embryos reveals common and divergent features of preimplantation development	https://boroviaklab.pdn.cam.ac.uk/resources/ https://app.stemcells.cam.ac.uk/GRAPPA/ (currently unavailable)
(Olaniru et al., 2023)	● fetal pancreas: 8-20 wpc	Single-cell transcriptomic and spatial landscapes of the developing human pancreas	Human fetal pancreas (shinyapps.io)
(Petropoulos et al., 2016)	● preimplantation embryos: days 3-7	Single-Cell RNA-Seq Reveals Lineage and X Chromosome Dynamics in Human Preimplantation Embryos	https://cells.ucsc.edu/?ds=preimplant-embryos&layout=0&gene=NANOG&pal=tol-dv#
(Sharon, Vanderhooft, et al., 2019)	● pancreatic differentiation: from ES to endocrine cells (H8)	Wnt Signaling Separates the Progenitor and Endocrine Compartments during Pancreas Development	https://ifx.rc.fas.harvard.edu/invitrobetacells/

(Weng et al., 2020)	● pancreatic differentiation: from ES to endocrine cells	Single-cell lineage analysis reveals extensive multimodal transcriptional control during directed beta-cell differentiation	http://hiview.case.edu/public/BetaCellHub/differentiation.php
(Yan et al., 2013)	● preimplantation embryos ● hESC	Single-cell RNA-Seq profiling of human preimplantation embryos and embryonic stem cells	https://www.ebi.ac.uk/gxa/sc/experiments/E-GEOD-36552/results?colourBy=developmental+stage&plotOption=20&plotType=umap&geneId=ENSG00000126016
(Yiangou et al., 2019)	● hESC (H9) ● iPSC ● pluripotent vs DE	Method to Synchronize Cell Cycle of Human Pluripotent Stem Cells without Affecting Their Fundamental Characteristics	https://www.ebi.ac.uk/gxa/sc/experiments/E-MTAB-7008/results?colourBy=sampling+time+point&plotType=umap&plotOption=20&geneId=ENSG00000126016
Ziojła Natalia, 2022 (Borowiak Lab)	● pancreatic differentiation: day 12	Rola czynnika transkrypcyjnego ETV1 w adhezji ludzkich pluripotencjalnych komórek macierzystych i rozwoju in vitro ludzkiej endokrynnej trzustki (PhD thesis)	-

5.2. scRNA-seq data analysis

The scRNA-seq data obtained in our laboratory were analyzed using Loupe Browser 6.4.1. Gene/Feature Expression and Filter functions were used to visualize the expression of selected genes and define clusters. The *NGN3*(+) / *AMOTL2*(-) vs *NGN3*(+) / *AMOTL2*(+) differentially expressed genes were identified using the Globally Distinguish option in Significant Feature Comparison. The analysis excluded the genes with low average count - genes with an average occurrence greater than 1 count per cell across the entire dataset. The pathways were identified using Gene Codis (Garcia-Moreno et al., 2022).

5.3. Development of AMOTL2 KO hPSC line

5.3.1. sgRNA

AMOTL2 KO was generated in the hPSC line Hue8-iCas9, with a doxycycline-inducible expression of iCas9 protein (González et al., 2014). Two sets of three sgRNAs were designed, one set targeting the region of exon 2 with the highest overlap in AMOTL2 isoforms, and second, with sgRNAs targeting exon 1, unique for 837 aa isoform. The sgRNA sequences were designed using the Benchling CRISPR tool. Benchling CRISPR tool provides "on-target" score, which is a predicted efficiency and "off-target" score that is a measure of the specificity. The sgRNAs with the highest scores possible (the higher the scores, the better) were selected, prioritizing specificity over efficiency. The sgRNA sequences were flanked with T7 promoter sequence at the beginning and Tracr sequence at the end (**Table 7**).

Table 7: The sgRNAs used for AMOTL2 KO in hPSCs

ISOFORM	sgRNA	RNA SEQUENCE (5' TO 3') T7 - gRNA - TRACR
ALL ISOFORMS	AMOTL2_sgRNA_A	TAATACGACTCACTATAGGG**CTGTGGGCATAGCCGGTAGA**GTTTTAGAGCTAGAAATAGCAAGTTAAAATAAGGCTAGTCCGTTATCAACTTGAAAAAGTGGCACCGAGTCGGTGCTTTT
	AMOTL2_sgRNA_B	TAATACGACTCACTATAGGG**AGCCCACTCGCAGTACTATG**GTTTTAGAGCTAGAAATAGCAAGTTAAAATAAGGCTAGTCCGTTATCAACTTGAAAAAGTGGCACCGAGTCGGTGCTTTT
	AMOTL2_sgRNA_C	TAATACGACTCACTATAGGG**CGGGGGACCGAGATCCCCGT**GTTTTAGAGCTAGAAATAGCAAGTTAAAATAAGGCTAGTCCGTTATCAACTTGAAAAAGTGGCACCGAGTCGGTGCTTTT
837 AA	AMOTL2_sgRNA_1A	TAATACGACTCACTATAGGG**ACTGGGCGAAAAGCCAGCGG**GTTTTAGAGCTAGAAATAGCAAGTTAAAATAAGGCTAGTCCGTTATCAACTTGAAAAAGTGGCACCGAGTCGGTGCTTTT
	AMOTL2_sgRNA_1B	TAATACGACTCACTATAGGG**GGGCGCCTATTATCACCTTG**GTTTTAGAGCTAGAAATAGCAAGTTAAAATAAGGCTAGTCCGTTATCAACTTGAAAAAGTGGCACCGAGTCGGTGCTTTT
	AMOTL2_sgRNA_1C	TAATACGACTCACTATAGGG**TGGCGGCGGGTGATTCAGTT**GTTTTAGAGCTAGAAATAGCAAGTTAAAATAAGGCTAGTCCGTTATCAACTTGAAAAAGTGGCACCGAGTCGGTGCTTTT

5.3.2. AMOTL2 KO procedure

The sgRNA oligonucleotides were multiplied in PCR reaction using Q5 polymerase. The PCR products were purified with DNA Purification GeneJet Kit (Invitrogen) according to the manufacturer instructions. Next, the PCR products were used for *in vitro* transcription reaction with MEGA shortscript

kit (Invitrogen) according to the manufacturer instructions, to obtain RNA molecules. The quantity and quality of RNA was assessed with NanoDrop.

The hPSCs were cultured with 2 μg/ml doxycycline for 24 h before lipofection to activate the expression of iCas9 protein. The reverse transfection method was used - cells were dissociated from the plate, counted and 1.5 x 10^5 cells (per 24-well) were seeded onto new plate in E8 medium with 10 μM Y-27632, 2 μg/ml doxycycline, lipofectamine RNAiMAX, and the mix of sgRNAs in various configurations. After 24 h the medium was changed to StemFlex without Y-27632 and cells were cultured for the additional 24 h. Further, the fraction of the cells was collected, and DNA was isolated using A&A Biotechnology Genomic Mini Kit, according to the manufacturer instructions. The PCR reaction with the primers flanking the CRISPR/Cas9 edition sites was performed and PCR products were Sanger sequenced. Primer sequences are listed in **Table 8**. The sequencing results were analyzed using ICE CRISPR Analysis Tool for a bioinformatic analysis of knockout efficiency. The transfected cells with the higher knockout efficiency were dispersed and seeded as single cells to ensure clonal cell lines. DNA from single-cell colonies was isolated and the PCR reaction primers flanking the CRISPR/Cas9 edition sites was performed. The PCR products were visualized on the 1% agarose gel electrophoresis and Sanger sequenced. The exact mutations were identified using Benchling and INDIGO Gear Genomics (Rausch et al., 2020) platforms.

Table 8: Primers used for the sequencing of sgRNA-targeted regions

ISOFORM	sgRNA	SEQUENCE (5' TO 3')
all	AMOTL2_seq_F	CATCCAGGAGCAGCTGCGCTAC
	AMOTL2_seq_R	TTCAGCATGCTGGAAGTGCGGG
837 aa	AMOTL2_seq1_F	TGGAAGTGTCCTGGGGGCAGAG
	AMOTL2_seq1_R	TGCTTCCAGCCACAGAGCCTCT

5.4. hPSC culture

The hPSCs were cultured at the vitronectin-coated plates in StemFlex medium with supplement in a 37°C incubator with 5% CO_2. Cells were passaged as clusters with PBS-EDTA (0.5 mM EDTA in 1 × PBS) every 3-5 days after reaching 80% confluency. Whenever the experiment required seeding a defined number of cells, hPSCs were passaged as single cells with TrypLE, counted using CellCountess ThermoFischer Scientific), and seeded in the StemFlex medium with the addition of 10 μM ROCKi (Y-27632) for the first 24 h. The hPSCs Hues8-iCas9 cell line was obtained from Prof. Huangfu laboratory (MSCK, NYC, USA). Cell lines were routinely tested for mycoplasma and found negative.

5.5. Immunofluorescent staining

5.5.1. Adherent cells

Cells from adherent cultures were fixed with 4% paraformaldehyde (PFA) for 15 min in room temperature (RT). For the staining against nuclear proteins, fixed cells were permeabilized with 0.5% TritonX100 in PBS for 15 min at RT (room temperature) and washed three times with PBS. Cells were blocked for 1 h at RT with 3% BSA (bovine albumin serum) + 0.1% Tween20 in PBS. Cells were stained with primary antibodies diluted in 5% NDS (normal donkey serum) + 0.1% Tween20 + PBS overnight at 4°C. The following day, the cells were washed three times with 0.1% Tween20 in PBS and stained with secondary antibodies diluted in 5% NDS + 0.1% Tween20 + PBS for 1h at RT. Next, cells were washed two times with 0.1% Tween20 in PBS and incubated with DAPI (1: 10 000) for 5 min in RT.

5.5.2. Human fetal pancreas tissues

The human 10 and 13 wpc fetal pancreas sections were processed at Baylor College of Medicine in Houston (Texas, USA) with the approval to Malgorzata Borowiak (IRB-3097). The donor identities were encrypted, and the data were analyzed anonymously. Pancreata were fixed with 4% PFA for 4 h, washed with PBS and soaked in 30% sucrose. Next, tissues were embedded in TissueTek and cut into 12 µm-thick sections, which were placed onto SuperFrost Plus coated glass slides and stored at -80°C.

For immunostaining, slides were warmed up in RT for 30 min, then washed in PBS two times for 10 min to remove TissueTek residue. Sections were blocked for 45 min in RT in 5% NDS + 0.1% Tween20 + PBS. Slides were stained with primary antibodies diluted in 5% NDS + 0.1% Tween20 + PBS overnight at 4°C.

The following day the tissue was washed three times (10 min each) with 0.1% Tween20 in PBS and stained with secondary antibodies diluted in 5% NDS + 0.1% Tween20 + PBS for 1h at RT. Next, cells were washed two times (10 min each) with 0.1% Tween20 in PBS and incubated with DAPI (1: 10 000) for 5 min in RT.

5.5.3. Antibodies

Table 9: Antibodies used for immunofluorescent staining. Hu = human, Mus = mouse, Mk = monkey

ANTIBODY NAME	COMPANY	CATALOG #	DILUTION	PRIMARY / SECONDARY	HOST	REACTIVITY
CHGA	Santa Cruz, CA	sc-393941	1:200	Primary	Mouse	Hu, Mus, Rat
C-PEP	DSHB	GN-ID4	1:20	Primary	Rat	Hu
GCG	Santa Cruz, CA	sc-514592	1:100	Primary	Mouse	Hu, Mus, Rat
pHH3	Millipore	06-570	1:100	Primary	Rabbit	Hu, Mus
cleaved CASP3	Cell Signaling	9664	1:400	Primary	Rabbit	Hu, Mus, Rat, Mk

AMOTL2	US Biological	KIAA0989	1:400	Primary	Rabbit	Hu
SST	Santa Cruz, CA	sc-55565	1:100	Primary	Mouse	Hu
NANOG	R&D	AF1997	1:100	Primary	Goat	Hu
OCT3/4	Santa Cruz, CA	sc-5279	1:100	Primary	Mouse	Hu, Mus, Rat
SOX2	R&D	MAB2018	1:100	Primary	Mouse	Hu, Mus, Rat
β-CAT	Santa Cruz, CA	sc-7963	1:100	Primary	Mouse	Hu, Mus, Rat
AlexaFluor488	Jackson Immunoresearch	715-545-150	1:400	Secondary	Donkey	anti-Mouse IgG (H+L)
AlexaFluor488	Jackson Immunoresearch	711-545-152	1:400	Secondary	Donkey	anti-Rabbit IgG (H+L)
TRITC	Jackson Immunoresearch	705-025-147	1:400	Secondary	Donkey	anti-Goat IgG (H+L)
TRITC	Jackson Immunoresearch	715-025-150	1:400	Secondary	Donkey	anti-Mouse IgG (H+L)
TRITC	Jackson Immunoresearch	711-025-152	1:400	Secondary	Donkey	anti-Rabbit IgG (H+L)
TRITC	Jackson Immunoresearch	712-025-153	1:400	Secondary	Donkey	anti-Rat IgG (H+L)
AlexaFluor647	Jackson Immunoresearch	711-605-152	1:400	Secondary	Donkey	anti-Rabbit IgG (H+L)
AlexaFluor647	Jackson Immunoresearch	715-605-151	1:400	Secondary	Donkey	anti-Mouse IgG (H+L)

5.6. Imaging

Epifluorescence microscopy was performed using Leica DM IL-Led microscope with N Plan Fluor 4x/0.12, N Plan Fluor 10x/0.30, N Plan Fluor 20x/0.40 and N Plan Fluor 40x/0.60 lenses with JENOPTIK Progres Gryphax camera. Confocal microscopy was performed using 1) Nikon A1Rsi microscope with Plan Fluor 4x/0.13, Plan Apo 10x/0.45 DIC N1, Plan Apo VC 20x/0.75 DIC N2, Apo 40x/1.25 WI λS DIC N2, and Plan Apo VC 60x/1.4 Oil DIC N2 lenses, with Nikon NIS Elements AR software; and 2) Leica Stellaris 8 microscope with HC PL FLUOTAR 10x/0.20 Air, HC PL APO 20x/0.75 CS2 Air, HC PL IRAPO 40x/1.10 W CORR, PL APO 63x/1.20 W CORR CS2, and HC PL APO 63x-1.40 OIL CS2 lenses, with Leica LAS X software.

5.7. RNA isolation and real time quantitative PCR (RT-qPCR)

The total RNA was isolated using TRIzol Reagent and phenol/chloroform method, according to the manufacturer's instructions. The RNA was dissolved in RNase-free water and subjected to the DNase treatment. Quality and concentration of RNA was analyzed spectrophotometrically at A260/230 and A260/280. For cDNA synthesis, 1 ng of DNA-free RNA was reverse-transcribed with RevertAid First Strand cDNA Synthesis kit, using random hexamer primers. The qPCR was performed with Power SYBR Green qPCR MasterMix at QuantStudio 7 Flex Real-Time PCR System.

The sequences of the primers are listed in **Table 10**. Gene expression was calculated in QuantStudio 7 software using the ΔΔCT quantification method (Willems et al., 2008) and double-normalized by algorithmically incorporating multiple endogenous controls - GAPDH and ACTB.

Table 10: RT-qPCR primers

PRIMER NAME	SEQUENCE (5' TO 3')
GAPDH_F	AAGGTGAAGGTCGGAGTCAA
GAPDH_R	AATGAAGGGGTCATTGATGG
ACTB_F	ACAGAGCCTCGCCTTTGCCGAT
ACTB_R	ATCATCCATGGTGAGCTGGCGG
FOXA2_F	GGTCGTTTGTTGTGGCTGTTA
FOXA2_R	GTTCATGTTGCTCACGGAGGA
GATA4_F	CGACACCCCAATCTCGATATGT
GATA4_R	ACAGATAGTGACCCGTCCCA
SOX7_F	TTTGGGCCAAGGACGAGAGG
SOX7_R	CTTCCACGACTTTCCCAGCAT
SOX17_F	CGCTTTCATGGTGTGGGCTA
SOX17_R	CTTCCACGACTTGCCCAGC
MEIS2_F	TCCAGCATCTCACACATCCG
MEIS2_R	ACTGGTCAATCATGGGCTGT
MIXL1_F	GGATCCAGCTTTTATTTTCTCCCC
MIXL1_R	TCCAGGAGCACAGTGGTTGA
PDGFRA_F	CTATGTGCCAGACCCAGATGT
PDGFRA_R	CAGGAGTCTCGGGATCAGTTG
TNNT2_F	GAATGAGCGGGAGAAGGAGC
TNNT2_R	TGCTTCTGGATGTAACCCCC
OTX2_F	CGAGGGTGCAGGTATGGTTTA
OTX2_R	GCCACTTGTTCCACTCTCTGA
PAX6_F	CGATAACATACCAAGCGTGTCA
PAX6_R	TGCCCGTTCAACATCCTTAGT
SOX1_F	GCAGGTCCAAGCACTTACAAG
SOX1_R	GGGTGGTGGTGGTAATCTCTT
SOX2_F	CATGCACCGCTACGACGT
SOX2_R	CTGCGAGTAGGACATGCTGTA
AMOTL2_seq_F	CATCCAGGAGCAGCTGCGCTAC
AMOTL2_seq_R	TTCAGCATGCTGGAAGTGCGGG

5.8. RNA-sequencing

Total RNA was extracted with the phenol-chloroform method. For the library preparation, 1 000 ng of total RNA from WT and AMOTL2 KO hPSCs were used. The RNA quality was checked on Bioanalyzer (Agilent) and samples with RNA integrity above 9.0 were used for cDNA library preparation. Libraries were prepared in duplicates, using Illumina TruSeq RNA Library Prep Kit v2, according to the manufacturer's protocol. Library quantification was performed using Qubit fluorometer (TFS) and quality assessment using Agilent High Sensitivity DNA kit (Agilent Technologies). The sequencing was performed at the outside facility.

RNA-seq raw paired-end reads were trimmed with fastp (S. Chen et al., 2018). Trimmed reads were aligned to the human genome (Ensembl GRCh38) using STAR (v2.7) (Dobin et al., 2013) and counts were obtained using featureCounts v1.6.3 (Liao et al., 2014). To establish the differentially expressed genes, the read counts were normalized and analyzed with iDEP.96 (Ge et al., 2018) and DESeq2 (Love et al., 2014) software. Genes differentially expressed between WT And AMOTL2 KO hPSCs with $p \leq 0.05$ and fold change ≥ 2.0 were used for further analysis. Cluster analysis was performed with Genesis (Sturn & Quackenbush, 2002) software, using the average linkage method for hierarchical clustering. Volcano plot was prepared with GraphPad Prism9. Functional enrichment analysis was performed using Gene Codis (Garcia-Moreno et al., 2022) web-based platform. The cut-off value for significant pathway results was $p<0.005$.

5.9. Live cell imaging (IncuCyte)

The analysis of the confluency and cell number was performed using IncuCyte Live Cell Imager (Sartorius). Photographs were automatically taken every 2 h. The confluency and cell number were analyzed using IncuCyte Base Analysis Software. For cell number analysis, the cells were cultured with 50 mM SiR-DNA and 100 nM verapamil for the nuclear staining of live cells.

5.10. Spontaneous differentiation

Spontaneous differentiation was performed as 3D organoids. Two days before the differentiation, adherent cultures were dissociated into single cells, counted, and 1 x 10^6 cells were plated onto a 10 cm dish. After 48 h, hPSCs were once more dissociated into single cells. Cells were counted and plated in E8 medium with Y-27632 onto low-attachment 6-well plates, 3x 10^6 cells per well. Cells were cultured on the orbital shaker that allows formation of the homogeneously sized organoids and prevents clumping. After 24 h, the medium was changed for E8 without Y-27632, and after next 24 h to the basal differentiation medium deprived of the pluripotency factors. For the first 48 h cells were cultured in S1 medium and then in S2 medium, up to 9 days. For the treatments, 10 μM Y-27632 or 350 nM verteporfin were added to the medium every two days, with the medium change. The components of the differentiation media are listed in **Table 11**.

Table 11: Component of the media for spontaneous differentiation.

	S1 MEDIUM	S2 MEDIUM
ADVANCED DMEM/F12	48 ml	43.5 ml
PEN/STREP (10 000 U/ML, 100X)	500 µl	500 µl
GLUTAMAX (100X)	500 µl	500 µl
FBS	2 ml (2 %)	5 ml (10 %)
NEAA (100X)	-	500 µl
TOTAL	50 ml	50 ml

5.11. Directed differentiation towards ectoderm

The hPSC directed differentiation into ectoderm lineage was performed using a modified Calvo-Garrido protocol (Calvo-Garrido et al., 2021). The hPSCs were dissociated into single cells, counted and seeded at the density of 3.5 x 10^4 cells per cm^2 on the GelTrex-coated plates. The cells were cultured for 24 h in E8 medium with Y-27632. During days 1-4 cells were differentiated in the KOSR medium supplemented with LDN193189, SB431542, and Chir99021. On day 5 differentiating cells were dissociated into single cells, counted and plated onto new GelTrex-coated plates at the density of 2.4 x 10^5 cells per cm^2. From day 5 till day 9 cells were cultured in the mix of KOSR and N2B27 medium supplemented with LDN193189 and CHIR99021. The media components are listed in **Table 12**. The proportions of the KOSR and N2B27 media for each day and small molecules are stated in **Table 13**.

Table 12: Composition of ectoderm differentiation media

	KOSR MEDIUM	N2B27 MEDIUM
DMEM/F12 + GLUTAMAX	39.5 ml	24 ml
KOSR	10 ml	-
NEAA	500 µl	-
2-MERCAPTOETHANOL	91 µl	91 µl
PEN/STREP	500 µl	500 µl
NEUROBASAL	-	24 ml
GLUTAMAX	-	250 µl
N2	-	250 µl
B27	-	500 µl

Table 13: Media composition and small molecules for each day of ectoderm differentiation

DAY	KOSR MEDIUM	N2B27 MEDIUM	SMALL MOLECULES	
1-4	100%	0%	LDN193189 SB431542 CHIR99021	1 : 1 250 1 : 5 000 1 : 3 000
5-6	75%	25%	LDN193189 CHIR99021	1 : 1 250 1 : 3 000
7-8	50%	50%	LDN193189 CHIR99021	1 : 1 250 1 : 3 000

5.12. Flow cytometry

Cells were dissociated into a single-cell suspension, washed with PBS, and fixed with 4% PFA + 0.1% saponin in PBS for 45 min at 4°C, followed by wash with SBP solution: 0.1% saponin + 1% BSA in PBS (SBP). Fixed cells were permeabilized for 15 min at 4°C using 1% TritonX100 in PBS, followed by two washes with SBP. Next, samples were incubated with primary antibodies diluted in SBP overnight at 4 °C on a roller. The cells were then washed twice with SBP and incubated with secondary antibodies diluted in SBP, for 1 hour at 4°C. Subsequently, cells were centrifuged at 2,000 × g for 5 min, washed with SBP, and filtered through a 40 μm cell strainer before flow cytometry. Flow cytometry data were acquired using NovoCyte (Agilent Technologies, USA). Flow cytometry data analysis was performed with NovoCyte software. The primary and secondary antibodies used in the study are listed in Table 14.

Table 14: Antibodies used for flow cytometry. Hu = human, Mus = mouse

ANTIBODY NAME	COMPANY	CATALOG #	DILUTION	PRIMARY / SECONDARY	HOST	REACTIVITY
OTX2	R&D	AF1979	1:300	Primary	goat	Hu
SOX1	Cell Signaling	4194s	1:150	Primary	mouse	Hu, Mus, Rat
OCT3/4	Santa Cruz, CA	sc-5279	1:300	Primary	mouse	Hu, Mus, Rat
AlexaFluor647	Jackson Immunoresearch	705-605-147	1:1000	Secondary	donkey	anti-Goat IgG (H+L)
AlexaFluor647	Jackson Immunoresearch	705-605-151	1:1000	Secondary	donkey	anti-Mouse IgG (H+L)

5.13. Statistical analysis

Graphs were prepared using GraphPad Prism 9. For statistical analysis, the t-Student test with Welch's correction was used in the majority of experiments. In some cases, the 2-way Anova or paired t-Student test were used. The statistical tests used for the particular experiments are stated in the figure legend.

5.14. Figure preparation

Graphs, heatmaps, and bubble plots were prepared using GraphPad Prism 9. Figures were prepared using Adobe Photoshop, and illustrations were created with Adobe Illustrator.

5.15. Software

Table 15: Software used in the thesis

SOFTWARE	SOURCE	CITATION
Ensembl Genome Browser	https://www.ensembl.org/index.html	(Zerbino et al., 2018)
GeneCards Human Gene Database	https://www.genecards.org/	(Stelzer et al., 2016)
Prism GraphPad 9	https://www.graphpad.com/scientific-software/prism/	-
ImageJ (FiJi), ScientiFig plugin	https://imagej.net/Welcome	(Aigouy & Mirouse, 2013; Rueden et al., 2017; Schindelin et al., 2012)
QuantStudio TM Real-Time PCR Software (Applied Biosystems by ThermoFisher Scientific)	https://www.thermofisher.com/pl/en/home/technical-resources/software-downloads/quantstudio-flex-real-time-pcr-system.html	-
ClustalW	https://www.genome.jp/tools-bin/clustalw	(Thompson et al., 1994)
Loupe Browser	https://www.10xgenomics.com/products/loupe-browser	-
fastp	https://bioinformaticshome.com/tools/rna-seq/descriptions/fastp.html#gsc.tab=0	(S. Chen et al., 2018)
STAR	https://github.com/alexdobin/STAR/releases	(Dobin et al., 2013)
featureCounts	https://subread.sourceforge.net/featureCounts.html	(Liao et al., 2014)
iDEP.96	http://bioinformatics.sdstate.edu/idep96/	(Ge et al., 2018)
DESeq2	https://bioconductor.org/packages/release/bioc/html/DESeq2.html	(Love et al., 2014)
Genesis	https://genome.tugraz.at/genesisclient/genesisclient_description.shtml	(Sturn & Quackenbush, 2002)
Gene Codis	https://genecodis.genyo.es/	(Garcia-Moreno et al., 2022)
CellProfiler	https://cellprofiler.org/	(Stirling et al., 2021)
UCSC Browser	https://cells.ucsc.edu/	(Speir et al., 2021)
ICE CRISPR Analysis Tool, Synthego	https://www.synthego.com/products/bioinformatics/crispr-analysis	(Conant et al., 2022)
Chromas	https://technelysium.com.au/wp/chromas/	-
Benchling	https://www.benchling.com/	-
INDIGO Gear Genomics	https://www.gear-genomics.com/indigo/	(Rausch et al., 2020)

Nikon NIS Elements AR	https://www.microscope.healthcare.nikon.com/en_EU/products/software/nis-elements/nis-elements-advanced-research	
Leica LAS X	https://www.leica-microsystems.com/products/microscope-software/p/leica-las-x-ls/	-

5.16. Image analysis

Fluorescent and bright field images were processed and analyzed using custom Cell Profiler pipelines, in some cases ImageJ or Leica LAS X software was used.

5.17. Reagents

Table 16: List of the reagents used in the thesis

REAGENT	MANUFACTURER	CATALOG #
6x DNA loading buffer	ThermoFisher Scientific	R0611
Advanced DMEM/F12 medium	ThermoFisher Scientific	12634-010
Agarose	Sigma Aldrich	A9539
Agilent High Sensitivity DNA Kit	Agilent	5067-4626
B27 supplement	ThermoFisher Scientific	17504044
CHIR99021	Peprotech	2520691
Chloroform CZDA 98.5%	Chempur	363-112344306
DAPI	Sigma Aldrich	D9542
DMEM/F12 medium	ThermoFisher Scientific	10-090-CV
DMSO	Bioshop	DMS555.1
DNA Marker 1	A&A Biotechnology	3000-500
DNase I, RNase-free (1 U/µL)	ThermoFisher Scientific	EN0521
dNTP	ThermoFisher Scientific	R0182
Doxycycline	Sigma Aldrich	D9891
E8 (Essential 8) medium	ThermoFisher Scientific	A1516901
EDTA	Sigma Aldrich	D2650
Ethanol CZDA 99.8%	Chempur	363-113964800
FBS	Sigma Aldrich	F7524
Geltrex (for hPSCs)	ThermoFisher Scientific	A1413302
GeneJET PCR Purification Kit	ThermoFisher Scientific	K0702
Genomic Mini DNA isolation Kit	A&A Biotechnology	116-250
Glutamax	ThermoFisher Scientific	35050038
GoTaq G2 Hot Start	Promega	M7405
Illumina TruSeq RNA Library Prep Kit v2	Illumina	RS-122-2001

Izopropanol CZDA 99.7%	Chempur	363-117515002
KOSR	ThermoFisher Scientific	10828010
LDN193189	Peprotech	1066208
Lipofectamine RNAiMax	ThermoFisher Scientific	13778-100
MEGAshortscript™ T7 Transcription Kit	ThermoFisher Scientific	AM1354
N2 supplement	ThermoFisher Scientific	17502048
NDS (normal donkey serum)	Jackson Immunoresearch	017-000-121
NEAA (100x)	ThermoFisher Scientific	11140035
Neurobasal medium	ThermoFisher Scientific	21103-049
OptiMEM medium	ThermoFisher Scientific	11058021
Paraformaldehyde	Sigma Aldrich	158127
PBS	Invitrogen	3002
penicillin/streptomycin (10,000 U/mL, 100×)	ThermoFisher Scientific	15140122
Power SYBR Green qPCR MasterMix	ThermoFisher Scientific	4367659
Probumin Bovine Serum Albumin	Merck Millipore	810685
ProLong Diamond	Invitrogen	P36961
Q5 start high-fidelity	NEB	M0493L
Qubit™ dsDNA HS Assay Kit	Invitrogen	Q32850
Qubit™ dsDNA standards	Invitrogen	Q32854
RevertAid First Strand cDNA Synthesis Kit	ThermoFisher Scientific	K1622
Saponin	Carl Roth	ROTH-4185.1
SB431542	Peprotech	3014193
SiR-DNA	Tebubio	251SC007
StemFlex medium	ThermoFisher Scientific	A3349301
Triton X-100	Bioshop	TRX777.100
TRIzol™	ThermoFisher Scientific	15596026
Trypan blue (0.4%)	ThermoFisher Scientific	15250061
TrypLE Express	ThermoFisher Scientific	12604021
Tween20	Bioshop	WN510.100
UltraPure™ DNase/RNase-Free Distilled Water	ThermoFisher Scientific	10977035
Verteporfin	Sigma Aldrich	SML0534
Vitronectin	ThermoFisher Scientific	A14700
Y-27632	Peprotech	1293823

6. Figure list

7. Literature

Adachi, K., Suemori, H., Yasuda, S. ya, Nakatsuji, N., & Kawase, E. (2010). Role of SOX2 in maintaining pluripotency of human embryonic stem cells. *Genes to Cells*, *15*(5), 455–470. https://doi.org/10.1111/j.1365-2443.2010.01400.x

Agarwala, S., Duquesne, S., Liu, K., Boehm, A., Grimm, L., Link, S., König, S., Eimer, S., Ronneberger, O., & Lecaudey, V. (2015). Amotl2a interacts with the hippo effector yap1 and the Wnt/β-catenin effector lef1 to control tissue size in zebrafish. *eLife*, *4*(September 2015), 1–26. https://doi.org/10.7554/eLife.08201

Aigouy, B., & Mirouse, V. (2013). ScientiFig: a tool to build publication-ready scientific figures. *Nature Methods*, *10*(11), 1048. https://doi.org/10.1038/nmeth.2692

Alarcon, V. B., & Marikawa, Y. (2018). ROCK and RHO Playlist for Preimplantation Development: Streaming to HIPPO Pathway and Apicobasal Polarity in the First Cell Differentiation. In *Chromatin Regulation of Early Embryonic Lineage Specification* (Vol. 229, pp. 47–68). https://doi.org/10.1007/978-3-319-63187-5

Alva, J. A., Lee, G. E., Escobar, E. E., & Pyle, A. D. (2011). Phosphatase and tensin homolog regulates the pluripotent state and lineage fate choice in human embryonic stem cells. *Stem Cells*, *29*(12), 1952–1962. https://doi.org/10.1002/stem.748

Anderson, S. J., Seeberger, K. L., Ellis, C. E., Eshpeter, A., & Korbutt, G. S. (2013). Immunohistochemical Characterization of Insulin, Glucagon, PDX1, SOX17 and NGN3 Expression in Human Fetal Pancreatic Development. *Journal of Stem Cell Research & Therapy*, *03*(04). https://doi.org/10.4172/2157-7633.1000148

Angers, S., & Moon, R. T. (2009). Proximal events in Wnt signal transduction. *Nature Reviews Molecular Cell Biology*, *10*(7), 468–477. https://doi.org/10.1038/nrm2717

Anton, E. S., Ghashghaei, H. T., Weber, J. L., McCann, C., Fischer, T. M., Cheung, I. D., Gassmann, M., Messing, A., Klein, R., Schwab, M. H., Lloyd, K. C. K., & Lai, C. (2004). Receptor tyrosine kinase ErbB4 modulates neuroblast migration and placement in the adult forebrain. *Nature Neuroscience*, *7*(12), 1319–1328. https://doi.org/10.1038/nn1345

Armstrong, L., Hughes, O., Yung, S., Hyslop, L., Stewart, R., Wappler, I., Peters, H., Walter, T., Stojkovic, P., Evans, J., Stojkovic, M., & Lako, M. (2006). The role of PI3K/AKT, MAPK/ERK and NFκβ signalling in the maintenance of human embryonic stem cell pluripotency and viability highlighted by transcriptional profiling and functional analysis. *Human Molecular Genetics*, *15*(11), 1894–1913. https://doi.org/10.1093/hmg/ddl112

Arthur, T. D., Nguyen, J. P., D'Antonio-Chronowska, A., Matsui, H., Silva, N. S., Joshua, I. N., Luchessi, A. D., Greenwald, W. W. Y., D'Antonio, M., Pera, M. F., & Frazer, K. A. (2024). Complex regulatory networks influence pluripotent cell state transitions in human iPSCs. *Nature Communications*, *15*(1), 1664. https://doi.org/10.1038/s41467-024-45506-6

Artinian, N., Cloninger, C., Holmes, B., Benavides-Serrato, A., Bashir, T., & Gera, J. (2015). Phosphorylation of the Hippo pathway component AMOTL2 by the mTORC2 kinase promotes YAP signaling, resulting in enhanced glioblastoma growth and invasiveness. *Journal of Biological Chemistry*, *290*(32), 19387–19401. https://doi.org/10.1074/jbc.M115.656587

Babaie, Y., Herwig, R., Greber, B., Brink, T. C., Wruck, W., Groth, D., Lehrach, H., Burdon, T., & Adjaye, J. (2007). Analysis of Oct4-Dependent Transcriptional Networks Regulating Self-Renewal and Pluripotency in Human Embryonic Stem Cells. *Stem Cells*, *25*(2), 500–510. https://doi.org/10.1634/stemcells.2006-0426

Baron, M., Veres, A., Wolock, S. L., Faust, A. L., Gaujoux, R., Vetere, A., Ryu, J. H., Wagner, B. K., Shen-Orr, S. S., Klein, A. M., Melton, D. A., & Yanai, I. (2016). A Single-Cell Transcriptomic Map of the Human and Mouse Pancreas Reveals Inter- and Intra-cell Population Structure. *Cell Systems*, *3*(4), 346–360. https://doi.org/10.1016/j.cels.2016.08.011

Beattie, G. M., Lopez, A. D., Bucay, N., Hinton, A., Firpo, M. T., King, C. C., & Hayek, A. (2005). Activin A Maintains Pluripotency of Human Embryonic Stem Cells in the Absence of Feeder Layers. *Stem Cells*, *23*(4), 489–495. https://doi.org/10.1634/stemcells.2004-0279

Bendall, S. C., Stewart, M. H., Menendez, P., George, D., Vijayaragavan, K., Werbowetski-Ogilvie, T., Ramos-Mejia, V., Rouleau, A., Yang, J., Bossé, M., Lajoie, G., & Bhatia, M. (2007). IGF and FGF cooperatively establish the regulatory stem cell niche of pluripotent human cells in vitro. *Nature*, *448*(7157), 1015–1021. https://doi.org/10.1038/nature06027

Benitez, C. M., Goodyer, W. R., & Kim, S. K. (2012). Deconstructing pancreas developmental biology. *Cold Spring Harb Perspect Biol*, *4*(6). https://doi.org/10.1101/cshperspect.a012401

Beyer, T. A., Weiss, A., Khomchuk, Y., Huang, K., Ogunjimi, A. A., Varelas, X., & Wrana, J. L. (2013). Switch enhancers interpret TGF-β and hippo signaling to control cell fate in human embryonic stem cells. *Cell Reports*, *5*(6), 1611–1624. https://doi.org/10.1016/j.celrep.2013.11.021

Bica, C., Tirpe, A., Nutu, A., Ciocan, C., Chira, S., Gurzau, E. S., Braicu, C., & Berindan-Neagoe, I. (2023). Emerging roles and mechanisms of semaphorins activity in cancer. *Life Sciences*, *318*(February), 121499. https://doi.org/10.1016/j.lfs.2023.121499

Bikle, D. D., Xie, Z., & Tu, C. L. (2012). Calcium regulation of keratinocyte differentiation. *Expert Review of Endocrinology and Metabolism*, *7*(4), 461–472. https://doi.org/10.1586/eem.12.34

Boraas, L. C., Pineda, E. T., & Ahsan, T. (2018). Actin and myosin II modulate differentiation of pluripotent stem cells. *PLoS ONE*, *13*(4), 1–14. https://doi.org/10.1371/journal.pone.0195588

Boroviak, T., Stirparo, G. G., Dietmann, S., Hernando-Herraez, I., Mohammed, H., Reik, W., Smith, A., Sasaki, E., Nichols, J., & Bertone, P. (2018). Single cell transcriptome analysis of human, marmoset and mouse embryos reveals common and divergent features of preimplantation development. *Development*, *145*(21). https://doi.org/10.1242/dev.167833

Botello-Smith, W. M., Jiang, W., Zhang, H., Ozkan, A. D., Lin, Y. C., Pham, C. N., Lacroix, J. J., & Luo, Y. (2019). A mechanism for the activation of the mechanosensitive Piezo1 channel by the small molecule Yoda1. *Nature Communications*, *10*(1). https://doi.org/10.1038/s41467-019-12501-1

Boyer, L. A., Tong, I. L., Cole, M. F., Johnstone, S. E., Levine, S. S., Zucker, J. P., Guenther, M. G., Kumar, R. M., Murray, H. L., Jenner, R. G., Gifford, D. K., Melton, D. A., Jaenisch, R., & Young, R. A. (2005). Core transcriptional regulatory circuitry in human embryonic stem cells. *Cell*, *122*(6), 947–956. https://doi.org/10.1016/j.cell.2005.08.020

Bratt, A., Wilson, W. J., Troyanovsky, B., Aase, K., Kessler, R., Meir, E. G. V., & Holmgren, L. (2002). Angiomotin belongs to a novel protein family with conserved coiled-coil and PDZ binding domains. *Gene*, *298*(1), 69–77. https://doi.org/10.1016/S0378-1119(02)00928-9

Brissova, M., Fowler, M. J., Nicholson, W. E., Chu, A., Hirshberg, B., Harlan, D. M., & Powers, A. C. (2005). Assessment of human pancreatic islet architecture and composition by laser scanning confocal microscopy. *Journal of Histochemistry and Cytochemistry*, *53*(9), 1087–1097. https://doi.org/10.1369/jhc.5C6684.2005

Brown, S., Adrian, T. E. O., Pauklin, S., Hannan, N., Cho, C. H. H., Lim, B., Vardy, L., Dunn, N. R., Trotter, M., Pedersen, R., & Vallier, L. (2011). Activin/nodal signaling controls divergent transcriptional networks in human embryonic stem cells and in endoderm progenitors. *Stem Cells*, *29*(8), 1176–1185. https://doi.org/10.1002/stem.666

Byrnes, L. E., Wong, D. M., Subramaniam, M., Meyer, N. P., Gilchrist, C. L., Knox, S. M., Tward, A. D., Ye, C. J., & Sneddon, J. B. (2018). Lineage dynamics of murine pancreatic development at single-cell resolution. *Nature Communications*, *9*(3922). https://doi.org/10.1038/s41467-018-06176-3

Cai, L., Ye, Z., Zhou, B. Y., Mali, P., Zhou, C., & Cheng, L. (2007). Promoting human embryonic stem cell renewal or differentiation by modulating Wnt signal and culture conditions. *Cell Research*,

17(1), 62–72. https://doi.org/10.1038/sj.cr.7310138

Calvo-Garrido, J., Winn, D., Maffezzini, C., Wedell, A., Freyer, C., Falk, A., & Wredenberg, A. (2021). Protocol for the derivation, culturing, and differentiation of human iPS-cell-derived neuroepithelial stem cells to study neural differentiation in vitro. *STAR Protocols*, *2*(2), 100528. https://doi.org/10.1016/j.xpro.2021.100528

Casella, J. F., Flangan, M. D., & Lin, S. (1981). Cytochalasin D inhibits actin polymerization and induces depolymerization of actin filaments formed during platelet shape change. *Nature*, *293*(5830), 302–305. https://doi.org/10.1038/293302a0

Chan, S. W., Lim, C. J., Guo, F., Tan, I., Leung, T., & Hong, W. (2013). Actin-binding and cell proliferation activities of angiomotin family members are regulated by Hippo pathway-mediated phosphorylation. *Journal of Biological Chemistry*, *288*(52), 37296–37307. https://doi.org/10.1074/jbc.M113.527598

Chang, J., Kim, M. H., Agung, E., Senda, S., & Kino-oka, M. (2019). Effect of migratory behaviors on human induced pluripotent stem cell colony formation on different extracellular matrix proteins. *Regenerative Therapy*, *10*, 27–35. https://doi.org/10.1016/j.reth.2018.10.004

Chavez, L., Bais, A. S., Vingron, M., Lehrach, H., Adjaye, J., & Herwig, R. (2009). In silico identification of a core regulatory network of OCT4 in human embryonic stem cells using an integrated approach. *BMC Genomics*, *10*, 1–14. https://doi.org/10.1186/1471-2164-10-314

Chen, L., Shi, K., Frary, C. E., Ditzel, N., Hu, H., Qiu, W., & Kassem, M. (2015). Inhibiting actin depolymerization enhances osteoblast differentiation and bone formation in human stromal stem cells. *Stem Cell Research*, *15*(2), 281–289. https://doi.org/10.1016/j.scr.2015.06.009

Chen, S., Zhou, Y., Chen, Y., & Gu, J. (2018). Fastp: An ultra-fast all-in-one FASTQ preprocessor. *Bioinformatics*, *34*(17), i884–i890. https://doi.org/10.1093/bioinformatics/bty560

Chen, X., Lu, Y., Guo, G., Zhang, Y., Sun, Y., Guo, L., Li, R., Nan, Y., Yang, X., Dong, J., Jin, X., & Huang, Q. (2021). AMOTL2-knockdown promotes the proliferation, migration and invasion of glioma by regulating β-catenin nuclear localization. *Oncology Reports*, *46*(1), 1–11. https://doi.org/10.3892/or.2021.8090

Chng, Z., Teo, A., Pedersen, R. A., & Vallier, L. (2010). SIP1 Mediates Cell-Fate Decisions between Neuroectoderm and Mesendoderm in Human Pluripotent Stem Cells. *Cell Stem Cell*, *6*(1), 59–70. https://doi.org/10.1016/j.stem.2009.11.015

Choe, M. S., Bae, C. M., Kim, S. J., Oh, S. T., Kown, Y. J., Choi, W. young, Han, H. J., Baek, K. M., Chang, W., Kim, J. S., Lim, K. S., Yun, S. P., & Lee, M. Y. (2022). Human embryonic stem cell-specific role of YAP in maintenance of self-renewal and survival. *Cellular and Molecular Life Sciences*, *79*(11), 1–14. https://doi.org/10.1007/s00018-022-04558-x

Conant, D., Hsiau, T., Rossi, N., Oki, J., Maures, T., Waite, K., Yang, J., Joshi, S., Kelso, R., Holden, K., Enzmann, B. L., & Stoner, R. (2022). Inference of CRISPR Edits from Sanger Trace Data. *CRISPR Journal*, *5*(1), 123–130. https://doi.org/10.1089/crispr.2021.0113

Coue, M., Brenner, S. L., Spector, I., & Korn, E. D. (1987). Inhibition of actin polymerization by latrunculin A. *FEBS Letters*, *2*(2), 316–318. https://doi.org/https://doi.org/10.1016/0014-5793(87)81513-2

Cui, R., Jiang, N., Zhang, M., Du, S., Ou, H., Ge, R., Ma, D., & Zhang, J. (2021). AMOTL2 inhibits JUN Thr239 dephosphorylation by binding PPP2R2A to suppress the proliferation in non-small cell lung cancer cells. *Biochimica et Biophysica Acta - Molecular Cell Research*, *1868*(1), 118858. https://doi.org/10.1016/j.bbamcr.2020.118858

D'Amour, K. A., Agulnick, A. D., Eliazer, S., Kelly, O. G., Kroon, E., & Baetge, E. E. (2005). Efficient differentiation of human embryonic stem cells to definitive endoderm. *Nature Biotechnology*, *23*(12), 1534–1541. https://doi.org/10.1038/nbt1163

D'Amour, K. a, Bang, A. G., Eliazer, S., Kelly, O. G., Agulnick, A. D., Smart, N. G., Moorman, M. A., Kroon, E., Carpenter, M. K., & Baetge, E. E. (2006). Production of pancreatic hormone-expressing endocrine cells from human embryonic stem cells. *Nature Biotechnology*, *24*(11), 1392–1401. https://doi.org/10.1038/nbt1259

Das, S., Jena, S., Kim, E.-M., Zavazava, N., & Levasseur, D. N. (2012). Transcriptional Regulation of Human NANOG by Alternate Promoters in Embryonic Stem Cells. *Journal of Stem Cell Research & Therapy*, *01*(S10). https://doi.org/10.4172/2157-7633.s10-009

Dattani, A., Huang, T., Liddle, C., Smith, A., & Guo, G. (2022). Suppression of YAP safeguards human naïve pluripotency. *Development*, *149*(dev200988), 1–9. https://doi.org/10.1242/dev.200988

Davidson, K. C., Adams, A. M., Goodson, J. M., McDonald, C. E., Potter, J. C., Berndt, J. D., Biechele, T. L., Taylor, R. J., & Moon, R. T. (2012). Wnt/β-catenin signaling promotes differentiation, not self-renewal, of human embryonic stem cells and is repressed by Oct4. *Proceedings of the National Academy of Sciences of the United States of America*, *109*(12), 4485–4490. https://doi.org/10.1073/pnas.1118777109

Dietrich, J. E., & Hiiragi, T. (2007). Stochastic patterning in the mouse pre-implantation embryo. *Development*, *134*(23), 4219–4231. https://doi.org/10.1242/dev.003798

Dobin, A., Davis, C. A., Schlesinger, F., Drenkow, J., Zaleski, C., Jha, S., Batut, P., Chaisson, M., & Gingeras, T. R. (2013). STAR: Ultrafast universal RNA-seq aligner. *Bioinformatics*, *29*(1), 15–21. https://doi.org/10.1093/bioinformatics/bts635

Dravid, G., Ye, Z., Hammond, H., Chen, G., Pyle, A., Donovan, P., Yu, X., & Cheng, L. (2005). Defining the Role of Wnt/β-Catenin Signaling in the Survival, Proliferation, and Self-Renewal of Human Embryonic Stem Cells. *Stem Cells*, *23*(10), 1489–1501. https://doi.org/10.1634/stemcells.2005-0034

Eiselleova, L., Matulka, K., Kriz, V., Kunova, M., Schmidtova, Z., Neradil, J., Tichy, B., Dvorakova, D., Pospisilova, S., Hampl, A., & Dvorak, P. (2009). A complex role for FGF-2 in self-renewal, survival, and adhesion of human embryonic stem cells. *Stem Cells*, *27*(8), 1847–1857. https://doi.org/10.1002/stem.128

Enge, M., Arda, H. E., Mignardi, M., Beausang, J., Bottino, R., Kim, S. K., & Quake, S. R. (2017). Single-Cell Analysis of Human Pancreas Reveals Transcriptional Signatures of Aging and Somatic Mutation Patterns. *Cell*, *171*(2), 321-330.e14. https://doi.org/10.1016/j.cell.2017.09.004

Estarás, C., Hsu, H. T., Huang, L., & Jones, K. A. (2017). YAP repression of the WNT3 gene controls hESC differentiation along the cardiac mesoderm lineage. *Genes and Development*, *31*(22), 2250–2263. https://doi.org/10.1101/gad.307512.117

Fang, P., Deng, W. jing, Fan, N., Shi, J., Shi, H. yang, Ou, L., Pan, J. li, & Yang, S. ying. (2021). AMOTL2 restrains transforming growth factor-β1-induced proliferation and extracellular matrix deposition of airway smooth muscle cells via the down-regulation of YAP1 activation. *Environmental Toxicology*, *36*(11), 2225–2235. https://doi.org/10.1002/tox.23336

Fang, Z., Weng, C., Li, H., Tao, R., Mai, W., Liu, X., Lu, L., Lai, S., Duan, Q., Alvarez, C., Arvan, P., Wynshaw-Boris, A., Li, Y., Pei, Y., Jin, F., & Li, Y. (2019). Single-Cell Heterogeneity Analysis and CRISPR Screen Identify Key β-Cell-Specific Disease Genes. *Cell Reports*, *26*(11), 3132-3144.e7. https://doi.org/10.1016/j.celrep.2019.02.043

Fernandez-Borja, M., Janssen, L., Verwoerd, D., Hordijk, P., & Neefjes, J. (2005). RhoB regulates endosome transport by promoting actin assembly on endosomal membranes through Dia1. *Journal of Cell Science*, *118*(12), 2661–2670. https://doi.org/10.1242/jcs.02384

Fong, H., Hohenstein, K. A., & Donovan, P. J. (2008). Regulation of Self-Renewal and Pluripotency by Sox2 in Human Embryonic Stem Cells. *Stem Cells*, *26*(8), 1931–1938. https://doi.org/10.1634/stemcells.2007-1002

Fu, M., Hu, Y., Lan, T., Guan, K. L., Luo, T., & Luo, M. (2022). The Hippo signalling pathway and its

implications in human health and diseases. *Signal Transduction and Targeted Therapy*, *7*(1). https://doi.org/10.1038/s41392-022-01191-9

Fujimori, T. (2010). Preimplantation development of mouse: A view from cellular behavior. *Development Growth and Differentiation*, *52*(3), 253–262. https://doi.org/10.1111/j.1440-169X.2010.01172.x

Fujiwara, I., Zweifel, M. E., Courtemanche, N., & Pollard, T. D. (2018). Latrunculin A Accelerates Actin Filament Depolymerization in Addition to Sequestering Actin Monomers. *Current Biology*, *28*(19), 3183-3192.e2. https://doi.org/10.1016/j.cub.2018.07.082

Garcia-Moreno, A., López-Domínguez, R., Villatoro-García, J. A., Ramirez-Mena, A., Aparicio-Puerta, E., Hackenberg, M., Pascual-Montano, A., & Carmona-Saez, P. (2022). Functional Enrichment Analysis of Regulatory Elements. *Biomedicines*, *10*(3). https://doi.org/10.3390/biomedicines10030590

Ge, S. X., Son, E. W., & Yao, R. (2018). iDEP: An integrated web application for differential expression and pathway analysis of RNA-Seq data. *BMC Bioinformatics*, *19*(1), 1–24. https://doi.org/10.1186/s12859-018-2486-6

Gerri, C., McCarthy, A., Alanis-Lobato, G., Demtschenko, A., Bruneau, A., Loubersac, S., Fogarty, N. M. E., Hampshire, D., Elder, K., Snell, P., Christie, L., David, L., Van de Velde, H., Fouladi-Nashta, A. A., & Niakan, K. K. (2020). Initiation of a conserved trophectoderm program in human, cow and mouse embryos. *Nature*, *587*(7834), 443–447. https://doi.org/10.1038/s41586-020-2759-x

Geutskens, S. B., Andrews, W. D., Van Stalborch, A. M. D., Brussen, K., Holtrop-De Haan, S. E., Parnavelas, J. G., Hordijk, P. L., & Van Hennik, P. B. (2012). Control of human hematopoietic stem/progenitor cell migration by the extracellular matrix protein Slit3. *Laboratory Investigation*, *92*(8), 1129–1139. https://doi.org/10.1038/labinvest.2012.81

Goddette, D. W., & Frieden, C. (1986). Actin polymerization. The mechanism of action of cytochalasin D. *Journal of Biological Chemistry*, *261*(34), 15974–15980. https://doi.org/10.1016/s0021-9258(18)66662-1

González, F., Zhu, Z., Shi, Z. D., Lelli, K., Verma, N., Li, Q. V., & Huangfu, D. (2014). An iCRISPR platform for rapid, multiplexable, and inducible genome editing in human pluripotent stem cells. *Cell Stem Cell*, *15*(2), 215–226. https://doi.org/10.1016/j.stem.2014.05.018

Greber, B., Lehrach, H., & Adjaye, J. (2008). Control of early fate decisions in human ES cells by distinct states of TGFβ pathway activity. *Stem Cells and Development*, *17*(6), 1065–1077. https://doi.org/10.1089/scd.2008.0035

Haghighi, F., Dahlmann, J., Nakhaei-Rad, S., Lang, A., Kutschka, I., Zenker, M., Kensah, G., Piekorz, R. P., & Ahmadian, M. R. (2018). bFGF-mediated pluripotency maintenance in human induced pluripotent stem cells is associated with NRAS-MAPK signaling. *Cell Communication and Signaling*, *16*(1), 1–14. https://doi.org/10.1186/s12964-018-0307-1

Han, H., Yang, B., & Wang, W. (2017). Angiomotin-like 2 interacts with and negatively regulates AKT. *Oncogene*, *36*(32), 4662–4669. https://doi.org/10.1038/onc.2017.101

Hancili, S., Bonnefond, A., Philippe, J., Vaillant, E., Graeve, F. De, Sand, O., Busiah, K., Robert, J., Polak, M., Froguel, P., Güven, A., & Vaxillaire, M. (2017). *A novel NEUROG3 mutation in neonatal diabetes associated with a neuro-intestinal syndrome*. *August*, 1–7. https://doi.org/10.1111/pedi.12576

Hanley, N. (2014). Closing in on pancreatic beta cells. *Nat Biotech*, *32*(11), 1100–1102. https://doi.org/10.1038/nbt.3064

Hao, B., Webb, S. E., Miller, A. L., & Yue, J. (2016). The role of Ca2+ signaling on the self-renewal and neural differentiation of embryonic stem cells (ESCs). *Cell Calcium*, *59*(2–3), 67–74. https://doi.org/10.1016/j.ceca.2016.01.004

Hard, W. L. (1944). The origin and differentiation of the alpha and beta cells in the pancreatic islets of the rat. *American Journal of Anotomy*, *75*(3), 369–403.

Hashimoto, M., & Sasaki, H. (2019). Epiblast Formation by TEAD-YAP-Dependent Expression of Pluripotency Factors and Competitive Elimination of Unspecified Cells. *Developmental Cell*, *50*(2), 139-154.e5. https://doi.org/10.1016/j.devcel.2019.05.024

Hay, D. C., Sutherland, L., Clark, J., & Burdon, T. (2004). Oct-4 Knockdown Induces Similar Patterns of Endoderm and Trophoblast Differentiation Markers in Human and Mouse Embryonic Stem Cells. *Stem Cells*, *22*(2), 225–235. https://doi.org/10.1634/stemcells.22-2-225

Hayes, M. J., Rescher, U., Gerke, V., & Moss, S. E. (2004). Annexin-Actin interactions. *Traffic*, *5*(8), 571–576. https://doi.org/10.1111/j.1600-0854.2004.00210.x

Hildebrand, S., Hultin, S., Subramani, A., Petropoulos, S., Zhang, Y., Cao, X., Mpindi, J., Kalloniemi, O., Johansson, S., Majumdar, A., Lanner, F., & Holmgren, L. (2017). The E-cadherin/AmotL2 complex organizes actin filaments required for epithelial hexagonal packing and blastocyst hatching. *Scientific Reports*, *7*(1), 1–17. https://doi.org/10.1038/s41598-017-10102-w

Hirate, Y., Hirahara, S., Inoue, K. I., Suzuki, A., Alarcon, V. B., Akimoto, K., Hirai, T., Hara, T., Adachi, M., Chida, K., Ohno, S., Marikawa, Y., Nakao, K., Shimono, A., & Sasaki, H. (2013). Polarity-dependent distribution of angiomotin localizes hippo signaling in preimplantation embryos. *Current Biology*, *23*(13), 1181–1194. https://doi.org/10.1016/j.cub.2013.05.014

Hirose, M., Ishizaki, T., Watanabe, N., Uehata, M., Kranenburg, O., Moolenaar, W. H., Matsumura, F., Maekawa, M., Bito, H., & Narumiya, S. (1998). Molecular dissection of the Rho-associated protein kinase (p160ROCK)- regulated neurite remodeling in neuroblastoma N1E-115 cells. *Journal of Cell Biology*, *141*(7), 1625–1636. https://doi.org/10.1083/jcb.141.7.1625

Hogrebe, N. J., Augsornworawat, P., Maxwell, K. G., Velazco-Cruz, L., & Millman, J. R. (2020). Targeting the cytoskeleton to direct pancreatic differentiation of human pluripotent stem cells. *Nature Biotechnology*, *38*(4), 460–470. https://doi.org/10.1038/s41587-020-0430-6

Home, P., Ray, S., Dutta, D., Bronshteyn, I., Larson, M., & Paul, S. (2009). GATA3 is selectively expressed in the trophectoderm of peri-implantation embryo and directly regulates Cdx2 gene expression. *Journal of Biological Chemistry*, *284*(42), 28729–28737. https://doi.org/10.1074/jbc.M109.016840

Howard, B. A. (2008). The role of NRG3 in mammary development. *Journal of Mammary Gland Biology and Neoplasia*, *13*(2), 195–203. https://doi.org/10.1007/s10911-008-9082-8

Huang, H.-P., Liu, M., El-Hodiri, H. M., Chu, K., Jamrich, M., & Tsai, M.-J. (2000). Regulation of the Pancreatic Islet-Specific Gene BETA2 (neuroD) by Neurogenin 3. *Molecular and Cellular Biology*, *20*(9), 3292–3307. https://doi.org/10.1128/mcb.20.9.3292-3307.2000

Huang, H., Lu, F. I., Jia, S., Meng, S., Cao, Y., Wang, Y., Ma, W., Yin, K., Wen, Z., Peng, J., Thisse, C., Thisse, B., & Meng, A. (2007). Amotl2 is essential for cell movements in zebrafish embryo and regulates c-Src translocation. *Development*, *134*(5), 979–988. https://doi.org/10.1242/dev.02782

Huang, T. S., Li, L., Moalim-Nour, L., Jia, D., Bai, J., Yao, Z., Bennett, S. A. L., Figeys, D., & Wang, L. (2015). A regulatory network involving β-catenin, e-Cadherin, PI3k/Akt, and slug balances self-renewal and differentiation of human pluripotent stem cells in response to wnt signaling. *Stem Cells*, *33*(5), 1419–1433. https://doi.org/10.1002/stem.1944

Hultin, S., Subramani, A., Hildebrand, S., Zheng, Y., Majumdar, A., & Holmgren, L. (2017). AmotL2 integrates polarity and junctional cues to modulate cell shape. *Scientific Reports*, *7*(1), 1–10. https://doi.org/10.1038/s41598-017-07968-1

Hultin, S., Zheng, Y., Mojallal, M., Vertuani, S., Gentili, C., Balland, M., Milloud, R., Belting, H. G., Affolter, M., Helker, C. S. M., Adams, R. H., Herzog, W., Uhlen, P., Majumdar, A., & Holmgren, L. (2014). Amotl2 links ve-cadherin to contractile actin fibres necessary for aortic lumen

expansion. *Nature Communications*, *5*(May). https://doi.org/10.1038/ncomms4743

Hyslop, L., Stojkovic, M., Armstrong, L., Walter, T., Stojkovic, P., Przyborski, S., Herbert, M., Murdoch, A., Strachan, T., & Lako, M. (2005). Downregulation of NANOG Induces Differentiation of Human Embryonic Stem Cells to Extraembryonic Lineages. *Stem Cells*, *23*(8), 1035–1043. https://doi.org/10.1634/stemcells.2005-0080

James, D., Levine, A. J., Besser, D., & Hemmati-Brivanlou, A. (2005). TGFβ/activin/nodal signaling is necessary for the maintenance of pluripotency in human embryonic stem cells. *Development*, *132*(6), 1273–1282. https://doi.org/10.1242/dev.01706

Janssen, A. F. J., Breusegem, S. Y., & Larrieu, D. (2022). Current Methods and Pipelines for Image-Based Quantitation of Nuclear Shape and Nuclear Envelope Abnormalities. *Cells*, *11*(3). https://doi.org/10.3390/cells11030347

Jennings, R. E., Berry, A. A., Kirkwood-Wilson, R., Roberts, N. A., Hearn, T., Salisbury, R. J., Blaylock, J., Hanley, K. P., & Hanley, N. A. (2013). Development of the human pancreas from foregut to endocrine commitment. *Diabetes*, *62*(10), 3514–3522. https://doi.org/10.2337/db12-1479

Jennings, R. E., Berry, A. A., Strutt, J. P., Gerrard, D. T., & Hanley, N. A. (2015). Human pancreas development. *Development*, *142*(18), 3126–3137. https://doi.org/10.1242/dev.120063

Jeon, J., Correa-Medina, M., Ricordi, C., Edlund, H., & Diez, J. A. (2009). Endocrine cell clustering during human pancreas development. *Journal of Histochemistry and Cytochemistry*, *57*(9), 811–824. https://doi.org/10.1369/jhc.2009.953307

Johansson, K. A., Dursun, U., Jordan, N., Gu, G., Beermann, F., Gradwohl, G., & Grapin-Botton, A. (2007). Temporal Control of Neurogenin3 Activity in Pancreas Progenitors Reveals Competence Windows for the Generation of Different Endocrine Cell Types. *Developmental Cell*, *12*(3), 457–465. https://doi.org/10.1016/j.devcel.2007.02.010

Kantar, D., Mur, E. B., Mancini, M., Slaninova, V., Salah, Y. Ben, Costa, L., Forest, E., Lassus, P., Géminard, C., Boissière-Michot, F., Orsetti, B., Theillet, C., Colinge, J., Benistant, C., Maraver, A., Heron-Milhavet, L., & Djiane, A. (2021). MAGI1 inhibits the AMOTL2/p38 stress pathway and prevents luminal breast tumorigenesis. *Scientific Reports*, *11*(1), 1–20. https://doi.org/10.1038/s41598-021-85056-1

Khieu, M. L., Broadwater, D. R., Aden, J. K., Coviello, J. M., Lynch, D. T., & Hall, J. M. (2019). The Utility of Phosphohistone H3 (PHH3) in Follicular Lymphoma Grading: A Comparative Study with Ki-67 and H&E Mitotic Count. *American Journal of Clinical Pathology*, *151*(6), 542–550. https://doi.org/10.1093/ajcp/aqz003

Kim, M., Kim, M., Park, S., Lee, C., & Lim, D. (2016). Role of Angiomotin-like 2 mono-ubiquitination on YAP inhibition. *EMBO Reports*, *17*(1), 64–78. https://doi.org/10.15252/embr.201540809

Kroon, E., Martinson, L. A., Kadoya, K., Bang, A. G., Kelly, O. G., Eliazer, S., Young, H., Richardson, M., Smart, N. G., Cunningham, J., Agulnick, A. D., D'Amour, K. A., Carpenter, M. K., & Baetge, E. E. (2008). Pancreatic endoderm derived from human embryonic stem cells generates glucose-responsive insulin-secreting cells in vivo. *Nature Biotechnology*, *26*(4), 443–452. https://doi.org/10.1038/nbt1393

Kumar, V., Goutam, R. S., Park, S., Lee, U., & Kim, J. (2021). Functional Roles of FGF Signaling in Early Development of Vertebrate Embryos. *Cells*, *10*(8). https://doi.org/10.3390/cells10082148

Kushner, J. A., MacDonald, P. E., & Atkinson, M. A. (2014). Stem cells to insulin secreting cells: Two steps forward and now a time to pause? *Cell Stem Cell*, *15*(5), 535–536. https://doi.org/10.1016/j.stem.2014.10.012

Laowtammathron, C., Lorthongpanich, C., Jiamvoraphong, N., Srisook, P., Klaihmon, P., Kheolamai, P., Luanpitpong, S., & Issaragrisil, S. (2023). Role of YAP in hematopoietic differentiation and erythroid lineage specification of human-induced pluripotent stem cells. *Stem Cell Research and*

Therapy, *14*(1), 1–15. https://doi.org/10.1186/s13287-023-03508-z

Lee, H. J., Ewere, A., Diaz, M. F., & Wenzel, P. L. (2018). TAZ responds to fluid shear stress to regulate the cell cycle. *Cell Cycle*, *17*(2), 147–153. https://doi.org/10.1080/15384101.2017.1404209

Leung, C. Y., & Zernicka-Goetz, M. (2013). Angiomotin prevents pluripotent lineage differentiation in mouse embryos via Hippo pathway-dependent and-independent mechanisms. *Nature Communications*, *4*(2251). https://doi.org/10.1038/ncomms3251

Levenstein, M. E., Ludwig, T. E., Xu, R.-H., Llanas, R. A., VanDenHeuvel-Kramer, K., Manning, D., & Thomson, J. A. (2006). Basic Fibroblast Growth Factor Support of Human Embryonic Stem Cell Self-Renewal. *Stem Cells*, *24*(3), 568–574. https://doi.org/10.1634/stemcells.2005-0247

Li, J., Wang, G., Wang, C., Zhao, Y., Zhang, H., Tan, Z., Song, Z., Ding, M., & Deng, H. (2007). MEK/ERK signaling contributes to the maintenance of human embryonic stem cell self-renewal. *Differentiation*, *75*(4), 299–307. https://doi.org/10.1111/j.1432-0436.2006.00143.x

Li, L., Wang, B. H., Wang, S., Moalim-Nour, L., Mohib, K., Lohnes, D., & Wang, L. (2010). Individual cell movement, asymmetric colony expansion, Rho-associated kinase, and E-cadherin impact the clonogenicity of human embryonic stem cells. *Biophysical Journal*, *98*(11), 2442–2451. https://doi.org/10.1016/j.bpj.2010.02.029

Li, Z., Wang, Y., Zhang, M., Xu, P., Huang, H., Wu, D., & Meng, A. (2012). The Amotl2 gene inhibits Wnt/β-catenin signaling and regulates embryonic development in zebrafish. *Journal of Biological Chemistry*, *287*(16), 13005–13015. https://doi.org/10.1074/jbc.M112.347419

Liao, Y., Smyth, G. K., & Shi, W. (2014). FeatureCounts: An efficient general purpose program for assigning sequence reads to genomic features. *Bioinformatics*, *30*(7), 923–930. https://doi.org/10.1093/bioinformatics/btt656

Liu, H., Jiang, D., Chi, F., & Zhao, B. (2012). The Hippo pathway regulates stem cell proliferation, self-renewal, and differentiation. *Protein and Cell*, *3*(4), 291–304. https://doi.org/10.1007/s13238-012-2919-3

Love, M. I., Huber, W., & Anders, S. (2014). Moderated estimation of fold change and dispersion for RNA-seq data with DESeq2. *Genome Biology*, *15*(12), 1–21. https://doi.org/10.1186/s13059-014-0550-8

Lucci, V., Di Palma, T., D'Ambrosio, C., Scaloni, A., & Zannini, M. (2013). AMOTL2 interaction with TAZ causes the inhibition of surfactant proteins expression in lung cells. *Gene*, *529*(2), 300–306. https://doi.org/10.1016/j.gene.2013.07.015

Lv, J., Yi, Y., Qi, Y., Yan, C., Jin, W., Meng, L., Zhang, D., & Jiang, W. (2022). Mitochondrial homeostasis regulates definitive endoderm differentiation of human pluripotent stem cells. *Cell Death Discovery*, *8*(1), 1–13. https://doi.org/10.1038/s41420-022-00867-z

Madsen, R. R. (2020). PI3K in stemness regulation: From development to cancer. *Biochemical Society Transactions*, *48*(1), 301–315. https://doi.org/10.1042/BST20190778

Mana-Capelli, S., Paramasivam, M., Dutta, S., & McCollum, D. (2014). Angiomotins link F-actin architecture to Hippo pathway signaling. *Molecular Biology of the Cell*, *25*(10), 1676–1685. https://doi.org/10.1091/mbc.E13-11-0701

Mana-Capelli, Sebastian, & McCollum, D. (2018). Angiomotins stimulate LATS kinase autophosphorylation and act as scaffolds that promote Hippo signaling. *Journal of Biological Chemistry*, *293*(47), 18230–18241. https://doi.org/10.1074/jbc.RA118.004187

Marikawa, Y., & Alarcon, V. B. (2014). Creation of Trophectoderm, the First Epithelium, in Mouse Preimplantation Development. In J. Z. Kubiak (Ed.), *Mouse development - From oocyte to stem cells* (Vol. 58, Issue 1, pp. 165–184). https://doi.org/10.4081/ejh.2014.2369

Matin, M. M., Walsh, J. R., Gokhale, P. J., Draper, J. S., Bahrami, A. R., Morton, I., Moore, H. D., & Andrews, P. W. (2004). Specific Knockdown of Oct4 and β2-microglobulin Expression by RNA

Interference in Human Embryonic Stem Cells and Embryonic Carcinoma Cells. *Stem Cells*, *22*(5), 659–668. https://doi.org/10.1634/stemcells.22-5-659

Mcgrath, P. S., Watson, C. L., Ingram, C., Helmrath, M. A., & Wells, J. M. (2015). The Basic Helix-Loop-Helix Transcription Factor NEUROG3 Is Required for Development of the Human Endocrine Pancreas. *Diabetes*, *64*(January), 2497–2505. https://doi.org/10.2337/db14-1412

McLean, A. B., D'Amour, K. A., Jones, K. L., Krishnamoorthy, M., Kulik, M. J., Reynolds, D. M., Sheppard, A. M., Liu, H., Xu, Y., Baetge, E. E., & Dalton, S. (2007). Activin A Efficiently Specifies Definitive Endoderm from Human Embryonic Stem Cells Only When Phosphatidylinositol 3-Kinase Signaling Is Suppressed. *Stem Cells*, *25*(1), 29–38. https://doi.org/10.1634/stemcells.2006-0219

Meng, Z., Moroishi, T., & Guan, K. L. (2016). Mechanisms of Hippo pathway regulation. *Genes and Development*, *30*(1), 1–17. https://doi.org/10.1101/gad.274027.115

Meyer, K., Lammers, N. C., Bugaj, L. J., Garcia, H. G., & Weiner, O. D. (2023). Optogenetic control of YAP reveals a dynamic communication code for stem cell fate and proliferation. *Nature Communications*, *14*(1). https://doi.org/10.1038/s41467-023-42643-2

Mojallal, M., Zheng, Y., Hultin, S., Audebert, S., Van Harn, T., Johnsson, P., Lenander, C., Fritz, N., Mieth, C., Corcoran, M., Lembo, F., Hallström, M., Hartman, J., Mazure, N. M., Weide, T., Grandér, D., Borg, J. P., Uhlén, P., & Holmgren, L. (2014). AmotL2 disrupts apical-basal cell polarity and promotes tumour invasion. *Nature Communications*, *5*. https://doi.org/10.1038/ncomms5557

Morales, J. S., Raspopovic, J., & Marcon, L. (2021). From embryos to embryoids: How external signals and self-organization drive embryonic development. *Stem Cell Reports*, *16*(5), 1039–1050. https://doi.org/10.1016/j.stemcr.2021.03.026

Mullen, A. C., & Wrana, J. L. (2017). TGF-β family signaling in embryonic and somatic stem-cell renewal and differentiation. *Cold Spring Harbor Perspectives in Biology*, *9*(7), 1–32. https://doi.org/10.1101/cshperspect.a022186

Müller, P., Langenbach, A., Kaminski, A., & Rychly, J. (2013). Modulating the Actin Cytoskeleton Affects Mechanically Induced Signal Transduction and Differentiation in Mesenchymal Stem Cells. *PLoS ONE*, *8*(7), 1–8. https://doi.org/10.1371/journal.pone.0071283

Nair, G., & Hebrok, M. (2015). Islet formation in mice and men: Lessons for the generation of functional insulin-producing β-cells from human pluripotent stem cells. *Current Opinion in Genetics and Development*, *32*, 171–180. https://doi.org/10.1016/j.gde.2015.03.004

Narumiya, S., Ishizaki, T., & Uehata, M. (2000). Use and properties of ROCK-specific inhibitor Y-27632. *Methods in Enzymology*, *325*(1998), 273–284. https://doi.org/10.1016/s0076-6879(00)25449-9

Noisa, P., Ramasamy, T. S., Lamont, F. R., Yu, J. S. L., Sheldon, M. J., Russell, A., Jin, X., & Cui, W. (2012). Identification and Characterisation of the Early Differentiating Cells in Neural Differentiation of Human Embryonic Stem Cells. *PLoS ONE*, *7*(5). https://doi.org/10.1371/journal.pone.0037129

O'Reilly, M. S., Holmgren, L., Shing, Y., Chen, C., Rosenthal, R. A., Moses, M., Lane, W. S., Cao, Y., Sage, E. H., & Folkman, J. (1994). Angiostatin: A novel angiogenesis inhibitor that mediates the suppression of metastases by a lewis lung carcinoma. *Cell*, *79*(2), 315–328. https://doi.org/10.1016/0092-8674(94)90200-3

Olaniru, O. E., Kadolsky, U., Kannambath, S., Vaikkinen, H., Fung, K., Dhami, P., & Persaud, S. J. (2023). Single-cell transcriptomic and spatial landscapes of the developing human pancreas. *Cell Metabolism*, *35*(1), 184-199.e5. https://doi.org/10.1016/j.cmet.2022.11.009

Pagliari, S., Vinarsky, V., Martino, F., Perestrelo, A. R., Oliver De La Cruz, J., Caluori, G., Vrbsky, J., Mozetic, P., Pompeiano, A., Zancla, A., Ranjani, S. G., Skladal, P., Kytyr, D., Zdráhal, Z., Grassi,

G., Sampaolesi, M., Rainer, A., & Forte, G. (2021). YAP–TEAD1 control of cytoskeleton dynamics and intracellular tension guides human pluripotent stem cell mesoderm specification. *Cell Death and Differentiation*, *28*(4), 1193–1207. https://doi.org/10.1038/s41418-020-00643-5

Pagliuca, F. W., Millman, J. R., Gürtler, M., Segel, M., Van Dervort, A., Ryu, J. H., Peterson, Q. P., Greiner, D., & Melton, D. A. (2014). Generation of functional human pancreatic β cells in vitro. *Cell*, *159*(2), 428–439. https://doi.org/10.1016/j.cell.2014.09.040

Pan, F. C., & Wright, C. (2011). Pancreas organogenesis: From bud to plexus to gland. *Developmental Dynamics*, *240*(3), 530–565. https://doi.org/10.1002/dvdy.22584

Paramasivam, M., Sarkeshik, A., Yates, J. R., Fernandes, M. J. G., & McCollum, D. (2011). Angiomotin family proteins are novel activators of the LATS2 kinase tumor suppressor. *Molecular Biology of the Cell*, *22*(19), 3725–3733. https://doi.org/10.1091/mbc.E11-04-0300

Patten, J., & Wang, K. (2021). Fibronectin in development and wound healing. *Advanced Drug Delivery Reviews*, *170*, 353–368. https://doi.org/10.1016/j.addr.2020.09.005

Pavlakis, E., Chiotaki, R., & Chalepakis, G. (2011). The role of Fras1/Frem proteins in the structure and function of basement membrane. *International Journal of Biochemistry and Cell Biology*, *43*(4), 487–495. https://doi.org/10.1016/j.biocel.2010.12.016

Pera, M. F., & Rossant, J. (2021). The exploration of pluripotency space: Charting cell state transitions in peri-implantation development. *Cell Stem Cell*, *28*(11), 1896–1906. https://doi.org/10.1016/j.stem.2021.10.001

Petropoulos, S., Edsgärd, D., Reinius, B., Deng, Q., Panula, S. P., Codeluppi, S., Plaza Reyes, A., Linnarsson, S., Sandberg, R., & Lanner, F. (2016). Single-Cell RNA-Seq Reveals Lineage and X Chromosome Dynamics in Human Preimplantation Embryos. *Cell*, *165*(4), 1012–1026. https://doi.org/10.1016/j.cell.2016.03.023

Phadnis, S. M., Loewke, N. O., Dimov, I. K., Pai, S., Amwake, C. E., Solgaard, O., Baer, T. M., Chen, B., & Pera, R. A. R. (2015). Dynamic and social behaviors of human pluripotent stem cells. *Scientific Reports*, *5*, 1–12. https://doi.org/10.1038/srep14209

Piper, K., Brickwood, S., Turnpenny, L. W., Cameron, I. T., Ball, S. G., Wilson, D. I., & Hanley, N. A. (2004). Beta cell differentiation during early human pancreas development. *Journal of Endocrinology*, *181*(1), 11–23. https://doi.org/10.1677/joe.0.1810011

Plotnikov, A., Zehorai, E., Procaccia, S., & Seger, R. (2011). The MAPK cascades: Signaling components, nuclear roles and mechanisms of nuclear translocation. *Biochimica et Biophysica Acta - Molecular Cell Research*, *1813*(9), 1619–1633. https://doi.org/10.1016/j.bbamcr.2010.12.012

Portela-Gomes, G. M., Gayen, J. R., Grimelius, L., Stridsberg, M., & Mahata, S. K. (2008). The importance of chromogranin A in the development and function of endocrine pancreas. *Regulatory Peptides*, *151*(1–3), 19–25. https://doi.org/10.1016/j.regpep.2008.07.005

Qi, Y., Ye, Y., Wang, R., Yu, S., Zhang, Y., Lv, J., Jin, W., Xia, S., Jiang, W., Li, Y., & Zhang, D. (2022). Mitochondrial dysfunction by TFAM depletion disrupts self-renewal and lineage differentiation of human PSCs by affecting cell proliferation and YAP response. *Redox Biology*, *50*, 102248. https://doi.org/10.1016/j.redox.2022.102248

Qin, H., Blaschke, K., Wei, G., Ohi, Y., Blouin, L., Qi, Z., Yu, J., Yeh, R. F., Hebrok, M., & Ramalho-santos, M. (2012). Transcriptional analysis of pluripotency reveals the hippo pathway as a barrier to reprogramming. *Human Molecular Genetics*, *21*(9), 2054–2067. https://doi.org/10.1093/hmg/dds023

Quan, Y., Shan, X., Hu, M., Jin, P., Ma, J., Fan, J., Yang, J., Zhang, H., Fan, X., Gong, Y., Li, M., & Wang, Y. (2022). YAP inhibition promotes endothelial cell differentiation from pluripotent stem cell through EC master transcription factor FLI1. *Journal of Molecular and Cellular Cardiology*, *163*, 81–96. https://doi.org/10.1016/j.yjmcc.2021.10.004

Ralston, A., Cox, B. J., Nishioka, N., Sasaki, H., Chea, E., Rugg-Gunn, P., Guo, G., Robson, P., Draper, J. S., & Rossant, J. (2010). Gata3 regulates trophoblast development downstream of Tead4 and in parallel to Cdx2. *Development*, *137*(3), 395–403. https://doi.org/10.1242/dev.038828

Ralston, A., & Rossant, J. (2008). Cdx2 acts downstream of cell polarization to cell-autonomously promote trophectoderm fate in the early mouse embryo. *Developmental Biology*, *313*(2), 614–629. https://doi.org/10.1016/j.ydbio.2007.10.054

Rausch, T., Fritz, M. H. Y., Untergasser, A., & Benes, V. (2020). Tracy: Basecalling, alignment, assembly and deconvolution of sanger chromatogram trace files. *BMC Genomics*, *21*(1), 1–9. https://doi.org/10.1186/s12864-020-6635-8

Rezania, A., Bruin, J. E., Arora, P., Rubin, A., Batushansky, I., Asadi, A., O'Dwyer, S., Quiskamp, N., Mojibian, M., Albrecht, T., Yang, Y. H. C., Johnson, J. D., & Kieffer, T. J. (2014). Reversal of diabetes with insulin-producing cells derived in vitro from human pluripotent stem cells. *Nature Biotechnology*, *32*(11), 1121–1133. https://doi.org/10.1038/nbt.3033

Riedel, M. J., Asadi, A., Wang, R., Ao, Z., Warnock, G. L., & Kieffer, T. J. (2012). Immunohistochemical characterisation of cells co-producing insulin and glucagon in the developing human pancreas. *Diabetologia*, *55*(2), 372–381. https://doi.org/10.1007/s00125-011-2344-9

Riopel, M., Li, J., Fellows, G. F., Goodyer, C. G., & Wang, R. (2014). Ultrastructural and immunohistochemical analysis of the 8-20 week human fetal pancreas. *Islets*, *6*(4), 1–10. https://doi.org/10.4161/19382014.2014.982949

Rodda, D. J., Chew, J. L., Lim, L. H., Loh, Y. H., Wang, B., Ng, H. H., & Robson, P. (2005). Transcriptional regulation of Nanog by OCT4 and SOX2. *Journal of Biological Chemistry*, *280*(26), 24731–24737. https://doi.org/10.1074/jbc.M502573200

Rodriguez, R. T., Velkey, J. M., Lutzko, C., Seerke, R., Kohn, D. B., O'Shea, K. S., & Firpo, M. T. (2007). Manipulation of OCT4 levels in human embryonic stem cells results in induction of differential cell types. *Experimental Biology and Medicine*, *232*(10), 1368–1380. https://doi.org/10.3181/0703-RM-63

Rosen, B. P., & Gonza, F. (2016). *Genome Editing of Lineage Determinants in Human Pluripotent Stem Cells Reveals Mechanisms of Pancreatic Development and Diabetes Article Genome Editing of Lineage Determinants in Human Pluripotent Stem Cells Reveals Mechanisms of Pancreatic Development an*. 755–768. https://doi.org/10.1016/j.stem.2016.03.015

Rubio-Cabezas, O., Codner, E., Flanagan, S. E., Gómez, J. L., Ellard, S., & Hattersley, A. T. (2014). Neurogenin 3 is important but not essential for pancreatic islet development in humans. In *Diabetologia* (Vol. 57, Issue 11, pp. 2421–2424). https://doi.org/10.1007/s00125-014-3349-y

Rubio-Cabezas, O., Jensen, J. N., Hodgson, M. I., Codner, E., Ellard, S., Serup, P., & Hattersley, A. T. (2011). Permanent neonatal diabetes and enteric anendocrinosis associated with biallelic mutations in NEUROG3. *Diabetes*, *60*(4), 1349–1353. https://doi.org/10.2337/db10-1008

Rueden, C. T., Schindelin, J., Hiner, M. C., Dezonia, B. E., Walter, A. E., Arena, E. T., & Eliceiri, K. W. (2017). ImageJ2: ImageJ for the next generation of scientific image data. *BMC Bioinformatics*, *18*(529). https://doi.org/10.1186/s12859-017-1934-z

Russ, H. A., Parent, A. V, Ringler, J. J., Hennings, T. G., Nair, G. G., Shveygert, M., Guo, T., Puri, S., Haataja, L., Cirulli, V., Blelloch, R., Szot, G. L., Arvan, P., & Hebrok, M. (2015). Controlled induction of human pancreatic progenitors produces functional beta-like cells in vitro. *The EMBO Journal*, *34*(13), 1759–1772. https://doi.org/10.15252/embj.201591058

Salisbury, R. J., Blaylock, J., Berry, A. A., Jennings, R. E., De Krijger, R., Hanley, K. P., & Hanley, N. A. (2014). The window period of NEUROGENIN3 during human gestation. *Islets*, *6*(3). https://doi.org/10.4161/19382014.2014.954436

Sato, N., Meijer, L., Skaltsounis, L., Greengard, P., & Brivanlou, A. H. (2004). Maintenance of

pluripotency in human and mouse embryonic stem cells through activation of Wnt signaling by a pharmacological GSK-3-specific inhibitor. *Nature Medicine*, *10*(1), 55–63. https://doi.org/10.1038/nm979

Scavuzzo, M. A., Hill, M. C., Chmielowiec, J., Yang, D., Teaw, J., Sheng, K., Kong, Y., Bettini, M., Zong, C., Martin, J. F., & Borowiak, M. (2018). Endocrine lineage biases arise in temporally distinct endocrine progenitors during pancreatic morphogenesis. *Nature Communications*, *9*(1). https://doi.org/10.1038/s41467-018-05740-1

Schindelin, J., Arganda-Carreras, I., Frise, E., Kaynig, V., Longair, M., Pietzsch, T., Preibisch, S., Rueden, C., Saalfeld, S., Schmid, B., Tinevez, J.-Y., White, D. J., Hartenstein, V., Eliceiri, K., Tomancak, P., & Cardona, A. (2012). Fiji: an open-source platform for biological-image analysis. *Nature Methods*, *9*(7), 676–682. https://doi.org/10.1038/nmeth.2019

Seo, B. J., Yoon, S. H., & Do, J. T. (2018). Mitochondrial dynamics in stem cells and differentiation. *International Journal of Molecular Sciences*, *19*(12). https://doi.org/10.3390/ijms19123893

Sharon, N., Chawla, R., Mueller, J., Vanderhooft, J., Whitehorn, L. J., Rosenthal, B., Gürtler, M., Estanboulieh, R. R., Shvartsman, D., Gifford, D. K., Trapnell, C., & Melton, D. (2019). A Peninsular Structure Coordinates Asynchronous Differentiation with Morphogenesis to Generate Pancreatic Islets. *Cell*, *176*(4), 790–804. https://doi.org/10.1016/j.cell.2018.12.003

Sharon, N., Vanderhooft, J., Straubhaar, J., Mueller, J., Chawla, R., Zhou, Q., Engquist, E. N., Trapnell, C., Gifford, D. K., & Melton, D. A. (2019). Wnt Signaling Separates the Progenitor and Endocrine Compartments during Pancreas Development. *Cell Reports*, *27*(8), 2281-2291.e5. https://doi.org/10.1016/j.celrep.2019.04.083

Shi, X., Yin, Z., Ling, B., Wang, L., Liu, C., Ruan, X., Zhang, W., & Chen, L. (2017). Rho differentially regulates the hippo pathway by modulating the interaction between amot and Nf2 in the blastocyst. *Development (Cambridge)*, *144*(21), 3957–3967. https://doi.org/10.1242/dev.157917

Short, K., Wiradjaja, F., & Smyth, I. (2007). Let's stick together: The role of the Fras1 and Frem proteins in epidermal adhesion. *IUBMB Life*, *59*(7), 427–435. https://doi.org/10.1080/15216540701510581

Singh, A. M., Reynolds, D., Cliff, T., Ohtsuka, S., Mattheyses, A. L., Sun, Y., Menendez, L., Kulik, M., & Dalton, S. (2012). Signaling network crosstalk in human pluripotent cells: A Smad2/3-regulated switch that controls the balance between self-renewal and differentiation. *Cell Stem Cell*, *10*(3), 312–326. https://doi.org/10.1016/j.stem.2012.01.014

Sinha, S., Elbaz-Alon, Y., & Avinoam, O. (2022). Ca2+ as a coordinator of skeletal muscle differentiation, fusion and contraction. *FEBS Journal*, *289*(21), 6531–6542. https://doi.org/10.1111/febs.16552

Skory, R. M., Moverley, A. A., Ardestani, G., Alvarez, Y., Domingo-Muelas, A., Pomp, O., Hernandez, B., Tetlak, P., Bissiere, S., Stern, C. D., Sakkas, D., & Plachta, N. (2023). The nuclear lamina couples mechanical forces to cell fate in the preimplantation embryo via actin organization. *Nature Communications*, *14*(1). https://doi.org/10.1038/s41467-023-38770-5

Speir, M. L., Bhaduri, A., Markov, N. S., Moreno, P., Nowakowski, T. J., Papatheodorou, I., Pollen, A. A., Raney, B. J., Seninge, L., Kent, W. J., & Haeussler, M. (2021). UCSC Cell Browser: Visualize your single-cell data. *Bioinformatics*, *37*(23), 4578–4580. https://doi.org/10.1093/bioinformatics/btab503

Stamos, J. L., & Weis, W. I. (2013). The β-catenin destruction complex. *Cold Spring Harbor Perspectives in Biology*, *5*(1). https://doi.org/10.1101/cshperspect.a007898

Steiner, D. J., Kim, A., Miller, K., & Hara, M. (2010). Pancreatic islet plasticity: Interspecies comparison of islet architecture and composition. In *Islets* (Vol. 2, Issue 3). https://doi.org/10.4161/isl.2.3.11815

Stelzer, G., Rosen, N., Plaschkes, I., Zimmerman, S., Twik, M., Fishilevich, S., Stein, T. I., Nudel, R., Lieder, I., Mazor, Y., Kaplan, S., Dahary, D., Warshawsky, D., Guan-Golan, Y., Kohn, A.,

Rappaport, N., Safran, M., & Lancet, D. (2016). The GeneCards Suite: From Gene Data Mining to Disease Genome Sequence Analyses. *Curr. Protoc. Bioinform*, *54*, 1.30.1-1.30-33. https://doi.org/10.1002/cpbi.5

Stephenson, R. O., Rossant, J., & Tam, P. P. L. (2012). Intercellular interactions, position, and polarity in establishing blastocyst cell lineages and embryonic axes. *Cold Spring Harbor Perspectives in Biology*, *4*(11). https://doi.org/10.1101/cshperspect.a008235

Stirling, D. R., Swain-Bowden, M. J., Lucas, A. M., Carpenter, A. E., Cimini, B. A., & Goodman, A. (2021). CellProfiler 4: improvements in speed, utility and usability. *BMC Bioinformatics*, *22*(1), 1–11. https://doi.org/10.1186/s12859-021-04344-9

Stronati, E., Giraldez, S., Huang, L., Abraham, E., McGuire, G. R., Hsu, H. T., Jones, K. A., & Estarás, C. (2022). YAP1 regulates the self-organized fate patterning of hESC-derived gastruloids. *Stem Cell Reports*, *17*, 211–220. https://doi.org/10.1016/j.stemcr.2021.12.012

Strumpf, D., Mao, C. A., Yamanaka, Y., Ralston, A., Chawengsaksophak, K., Beck, F., & Rossant, J. (2005). Cdx2 is required for correct cell fate specification and differentiation of trophectoderm in the mouse blastocyst. *Development*, *132*(9), 2093–2102. https://doi.org/10.1242/dev.01801

Sturn, A., & Quackenbush, J. (2002). Genesis: cluster analysis ofmicroarray data. *Bioinformatics (Oxford, England)*, *18*(1), 207–208. https://doi.org/10.1093/bioinformatics/18.1.207

Subramani, A., Cui, W., Zhang, Y., Friman, T., Zhao, Z., Huang, W., Fonseca, P., Lui, W., Narayanan, V., Bobrowska, J., Lekka, M., Yan, J., Conway, D. E., & Holmgren, L. (2023). Modulation of E-Cadherin Function through the AmotL2 Isoforms Promotes Ameboid Cell Invasion. *Cells*, *12*(1682), 1–24. https://doi.org/https:// doi.org/10.3390/cells12131682

Takahashi, K., Tanabe, K., Ohnuki, M., Narita, M., Ichisaka, T., Tomoda, K., & Yamanaka, S. (2007). Induction of Pluripotent Stem Cells from Adult Human Fibroblasts by Defined Factors. *Cell*, *131*(5), 861–872. https://doi.org/10.1016/j.cell.2007.11.019

Thompson, J. D., Higgins, D. G., & Gibson, T. J. (1994). CLUSTAL W: Improving the sensitivity of progressive multiple sequence alignment through sequence weighting, position-specific gap penalties and weight matrix choice. *Nucleic Acids Research*, *22*(22), 4673–4680. https://doi.org/10.1093/nar/22.22.4673

Thomson, J. A., Itskovitz-Eldor, J., Shapiro, S. S., Waknitz, M. A., Swiergiel, J. J., Marshall, V. S., & Jones, J. M. (1998). Embryonic stem cell lines derived from human blastocysts. *Science*, *282*(5391), 1145–1147. https://doi.org/10.1126/science.282.5391.1145

Toledano, S., Nir-Zvi, I., Engelman, R., Kessler, O., & Neufeld, G. (2019). Class-3 semaphorins and their receptors: Potent multifunctional modulators of tumor progression. *International Journal of Molecular Sciences*, *20*(3). https://doi.org/10.3390/ijms20030556

Troyanovsky, B., Levchenko, T., Månsson, G., Matvijenko, O., & Holmgren, L. (2001). Angiomotin: An angiostatin binding protein that regulates endothelial cell migration and tube formation. *Journal of Cell Biology*, *152*(6), 1247–1254. https://doi.org/10.1083/jcb.152.6.1247

Vallier, L., Alexander, M., & Pedersen, R. A. (2005). Activin/Nodal and FGF pathways cooperate to maintain pluripotency of human embryonic stem cells. *Journal of Cell Science*, *118*(19), 4495–4509. https://doi.org/10.1242/jcs.02553

Vallier, L., Mendjan, S., Brown, S., Ching, Z., Teo, A., Smithers, L. E., Trotter, M. W. B., Cho, C. H. H., Martinez, A., Rugg-Gunn, P., Brons, G., & Pedersen, R. A. (2009). Activin/Nodal signalling maintains pluripotency by controlling Nanog expression. *Development*, *136*(8), 1339–1349. https://doi.org/10.1242/dev.033951

Vallier, L., Touboul, T., Brown, S., Cho, C., Bilican, B., Alexander, M., Cedervall, J., Chandran, S., Ährlund-Richter, L., Weber, A., & Pedersen, R. A. (2009). Signaling pathways controlling pluripotency and early cell fate decisions of human induced pluripotent stem cells. *Stem Cells*, *27*(11), 2655–2666. https://doi.org/10.1002/stem.199

Vallier, L., Touboul, T., Chng, Z., Brimpari, M., Hannan, N., Millan, E., Smithers, L. E., Trotter, M., Rugg-Gunn, P., Weber, A., & Pedersen, R. A. (2009). Early cell fate decisions of human embryonic stem cells and mouse epiblast stem cells are controlled by the same signalling pathways. *PLoS ONE*, *4*(6). https://doi.org/10.1371/journal.pone.0006082

van Gurp, L., Muraro, M. J., Dielen, T., Seneby, L., Dharmadhikari, G., Gradwohl, G., van Oudenaarden, A., & de Koning, E. J. P. (2019). A transcriptomic roadmap to α- and β-cell differentiation in the embryonic pancreas. *Development (Cambridge)*, *146*(12). https://doi.org/10.1242/dev.173716

Varelas, X., Sakuma, R., Samavarchi-Tehrani, P., Peerani, R., Rao, B. M., Dembowy, J., Yaffe, M. B., Zandstra, P. W., & Wrana, J. L. (2008). TAZ controls Smad nucleocytoplasmic shuttling and regulates human embryonic stem-cell self-renewal. *Nature Cell Biology*, *10*(7), 837–848. https://doi.org/10.1038/ncb1748

Velazco-Cruz, L., Song, J., Maxwell, K. G., Goedegebuure, M. M., Augsornworawat, P., Hogrebe, N. J., & Millman, J. R. (2019). Acquisition of Dynamic Function in Human Stem Cell-Derived β Cells. *Stem Cell Reports*, *12*(2), 351–365. https://doi.org/10.1016/j.stemcr.2018.12.012

Wadkin, L. E., Elliot, L. F., Neganova, I., Parker, N. G., Chichagova, V., Swan, G., Laude, A., Lako, M., & Shukurov, A. (2017). Dynamics of single human embryonic stem cells and their pairs: A quantitative analysis. *Scientific Reports*, *7*(1), 1–12. https://doi.org/10.1038/s41598-017-00648-0

Wang, Chao, Zhu, X., Feng, W., Yu, Y., Jeong, K., Guo, W., Lu, Y., & Mills, G. B. (2016). Verteporfin inhibits YAP function through up-regulating 14-3-3σ sequestering YAP in the cytoplasm. *American Journal of Cancer Research*, *6*(1), 27–37.

Wang, Chenji, An, J., Zhang, P., Xu, C., Gao, K., Wu, D., Wang, D., Yu, H., Liu, J. O., & Yu, L. (2012). The Nedd4-like ubiquitin E3 ligases target angiomotin/p130 to ubiquitin-dependent degradation. *Biochemical Journal*, *444*(2), 279–289. https://doi.org/10.1042/BJ20111983

Wang, G., Zhang, H., Zhao, Y., Li, J., Cai, J., Wang, P., Meng, S., Feng, J., Miao, C., Ding, M., Li, D., & Deng, H. (2005). Noggin and bFGF cooperate to maintain the pluripotency of human embryonic stem cells in the absence of feeder layers. *Biochemical and Biophysical Research Communications*, *330*(3), 934–942. https://doi.org/10.1016/j.bbrc.2005.03.058

Wang, J., Cortina, G., Wu, S. V., Tran, R., Cho, J.-H., Tsai, M.-J., Bailey, T. J., Jamrich, M., Ament, M. E., Treem, W. R., Hill, I. D., Vargas, J. H., Gershman, G., Farmer, D. G., Reyen, L., & Martín, M. G. (2006). Mutant Neurogenin-3 in Congenital Malabsorptive Diarrhea. *New England Journal of Medicine*, *355*(3), 270–280. https://doi.org/10.1056/nejmoa054288

Wang, W., Huang, J., & Chen, J. (2011). Angiomotin-like proteins associate with and negatively regulate YAP1. *Journal of Biological Chemistry*, *286*(6), 4364–4370. https://doi.org/10.1074/jbc.C110.205401

Wang, W., Li, N., Li, X., Tran, M. K., Han, X., & Chen, J. (2015). Tankyrase Inhibitors Target YAP by Stabilizing Angiomotin Family Proteins. *Cell Reports*, *13*(3), 524–532. https://doi.org/10.1016/j.celrep.2015.09.014

Wang, Y., Li, Z., Xu, P., Huang, L., Tong, J., Huang, H., & Meng, A. (2011). Angiomotin-like2 gene (amotl2) is required for migration and proliferation of endothelial cells during angiogenesis. *Journal of Biological Chemistry*, *286*(47), 41095–41104. https://doi.org/10.1074/jbc.M111.296806

Wang, Z., Oron, E., Nelson, B., Razis, S., & Ivanova, N. (2012). Distinct lineage specification roles for NANOG, OCT4, and SOX2 in human embryonic stem cells. *Cell Stem Cell*, *10*(4), 440–454. https://doi.org/10.1016/j.stem.2012.02.016

Warmflash, A., Sorre, B., Etoc, F., Siggia, E. D., & Brivanlou, A. H. (2014). A method to recapitulate early embryonic spatial patterning in human embryonic stem cells. *Nature Methods*, *11*(8), 847–854. https://doi.org/10.1038/nMeth.3016

Watanabe, K., Ueno, M., Kamiya, D., Nishiyama, A., Matsumura, M., Wataya, T., Takahashi, J. B., Nishikawa, S., Nishikawa, S. I., Muguruma, K., & Sasai, Y. (2007). A ROCK inhibitor permits survival of dissociated human embryonic stem cells. *Nature Biotechnology*, *25*(6), 681–686. https://doi.org/10.1038/nbt1310

Weng, C., Xi, J., Li, H., Cui, J., Gu, A., Lai, S., Leskov, K., Ke, L., Jin, F., & Li, Y. (2020). Single-cell lineage analysis reveals extensive multimodal transcriptional control during directed beta-cell differentiation. *Nature Metabolism*, *2*(12), 1443–1458. https://doi.org/10.1038/s42255-020-00314-2

Willems, E., Leyns, L., & Vandesompele, J. (2008). Standardization of real-time PCR gene expression data from independent biological replicates. *Analytical Biochemistry*, *379*(1), 127–129. https://doi.org/10.1016/j.ab.2008.04.036

Xiao, L., Yuan, X., & Sharkis, S. J. (2006). Activin A Maintains Self-Renewal and Regulates Fibroblast Growth Factor, Wnt, and Bone Morphogenic Protein Pathways in Human Embryonic Stem Cells. *Stem Cells*, *24*(6), 1476–1486. https://doi.org/10.1634/stemcells.2005-0299

Xu, C., Rosler, E., Jiang, J., Lebkowski, J. S., Gold, J. D., O'Sullivan, C., Delavan-Boorsma, K., Mok, M., Bronstein, A., & Carpenter, M. K. (2005). Basic Fibroblast Growth Factor Supports Undifferentiated Human Embryonic Stem Cell Growth Without Conditioned Medium. *Stem Cells*, *23*(3), 315–323. https://doi.org/10.1634/stemcells.2004-0211

Xu, R. H., Sampsell-Barron, T. L., Gu, F., Root, S., Peck, R. M., Pan, G., Yu, J., Antosiewicz-Bourget, J., Tian, S., Stewart, R., & Thomson, J. A. (2008). NANOG Is a Direct Target of TGFβ/Activin-Mediated SMAD Signaling in Human ESCs. *Cell Stem Cell*, *3*(2), 196–206. https://doi.org/10.1016/j.stem.2008.07.001

Yamamoto, Y., Miyazaki, S., Maruyama, K., Kobayashi, R., Le, M. N. T., Kano, A., Kondow, A., Fujii, S., & Ohnuma, K. (2018). Random migration of induced pluripotent stem cell-derived human gastrulation-stage mesendoderm. *PLoS ONE*, *13*(9), 1–13. https://doi.org/10.1371/journal.pone.0201960

Yan, L., Yang, M., Guo, H., Yang, L., Wu, J., Li, R., Liu, P., Lian, Y., Zheng, X., Yan, J., Huang, J., Li, M., Wu, X., Wen, L., Lao, K., Li, R., Qiao, J., & Tang, F. (2013). Single-cell RNA-Seq profiling of human preimplantation embryos and embryonic stem cells. *Nature Structural and Molecular Biology*, *20*(9), 1131–1139. https://doi.org/10.1038/nsmb.2660

Yang, Y. H. C., Manning Fox, J. E., Zhang, K. L., MacDonald, P. E., & Johnson, J. D. (2013). Intraislet SLIT-ROBO signaling is required for beta-cell survival and potentiates insulin secretion. *Proceedings of the National Academy of Sciences of the United States of America*, *110*(41), 16480–16485. https://doi.org/10.1073/pnas.1214312110

Yiangou, L., Grandy, R. A., Morell, C. M., Tomaz, R. A., Osnato, A., Kadiwala, J., Muraro, D., Garcia-Bernardo, J., Nakanoh, S., Bernard, W. G., Ortmann, D., McCarthy, D. J., Simonic, I., Sinha, S., & Vallier, L. (2019). Method to Synchronize Cell Cycle of Human Pluripotent Stem Cells without Affecting Their Fundamental Characteristics. *Stem Cell Reports*, *12*(1), 165–179. https://doi.org/10.1016/j.stemcr.2018.11.020

Yu, J. S. L., & Cui, W. (2016). Proliferation, survival and metabolism: The role of PI3K/AKT/ mTOR signalling in pluripotency and cell fate determination. *Development (Cambridge)*, *143*(17), 3050–3060. https://doi.org/10.1242/dev.137075

Yu, J., Vodyanik, M. A., Smuga-Otto, K., Antosiewicz-Bourget, J., Frane, J. L., Tian, S., Nie, J., Jonsdottir, G. A., Ruotti, V., Stewart, R., Slukvin, I. I., & Thompson, J. A. (2007). Induced pluripotent stem cell lines derived from human somatic cells. *Science*, *318*(5858), 1917–1920. https://doi.org/10.1126/science.1151526

Zaehres, H., Lensch, M. W., Daheron, L., Stewart, S. A., Itskovitz-Eldor, J., & Daley, G. Q. (2005). High-Efficiency RNA Interference in Human Embryonic Stem Cells. *Stem Cells*, *23*(3), 299–305. https://doi.org/10.1634/stemcells.2004-0252

Zaltsman, Y., Masuko, S., Bensen, J. J., & Kiessling, L. L. (2019). Angiomotin Regulates YAP Localization during Neural Differentiation of Human Pluripotent Stem Cells. *Stem Cell Reports*, *12*(5), 869–877. https://doi.org/10.1016/j.stemcr.2019.03.009

Zeevaert, K., Goetzke, R., Elsafi Mabrouk, M. H., Schmidt, M., Maaßen, C., Henneke, A. C., He, C., Gillner, A., Zenke, M., & Wagner, W. (2023). YAP1 is essential for self-organized differentiation of pluripotent stem cells. *Biomaterials Advances*, *146*(September 2022). https://doi.org/10.1016/j.bioadv.2023.213308

Zerbino, D. R., Achuthan, P., Akanni, W., Ridwan Amode, M., Barrell, D., Bhai, J., Billis, K., Cummins, C., Gall, A., García, C., Gir´girón, G., Gil, L., Gordon, L., Haggerty, L., Haskell, E., Hourlier, T., Izuogu, O. G., Janacek, S. H., Juettemann, T., … Flicek, P. (2018). Ensembl 2018. *Nucleic Acids Research*, *46*(D1), D754–D761. https://doi.org/10.1093/nar/gkx1098

Zernicka-Goetz, M., Morris, S. A., & Bruce, A. W. (2009). Making a firm decision: Multifaceted regulation of cell fate in the early mouse embryo. *Nature Reviews Genetics*, *10*(7), 467–477. https://doi.org/10.1038/nrg2564

Zhang, X., McGrath, P. S., Salomone, J., Rahal, M., McCauley, H. A., Schweitzer, J., Kovall, R., Gebelein, B., & Wells, J. M. (2019). A Comprehensive Structure-Function Study of Neurogenin3 Disease-Causing Alleles during Human Pancreas and Intestinal Organoid Development. *Developmental Cell*, *50*(3), 367-380.e7. https://doi.org/10.1016/j.devcel.2019.05.017

Zhao, B., Li, L., Lu, Q., Wang, L. H., Liu, C. Y., Lei, Q., & Guan, K. L. (2011). Angiomotin is a novel Hippo pathway component that inhibits YAP oncoprotein. *Genes and Development*, *25*(1), 51–63. https://doi.org/10.1101/gad.2000111

Zhu, Z., González, F., & Huangfu, D. (2014). The iCRISPR platform for rapid genome editing in human pluripotent stem Cells. In *Methods in Enzymology* (Vol. 546, Issue C). https://doi.org/10.1016/B978-0-12-801185-0.00011-8

Zollinger, A. J., & Smith, M. L. (2017). Fibronectin, the extracellular glue. *Matrix Biology*, *60–61*, 27–37. https://doi.org/10.1016/j.matbio.2016.07.011